

AD-A154 435

ENHANCED THERMAL COUPLING BY A REPETITIVELY PULSED
LASER(U) AIR FORCE INST OF TECH WRIGHT-PATTERSON AFB OH
SCHOOL OF ENGINEERING J R COVICK MAR 85

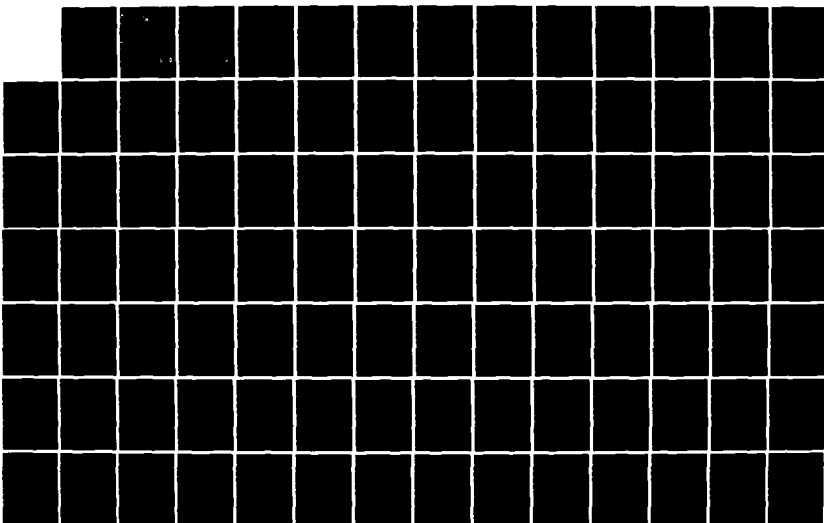
172

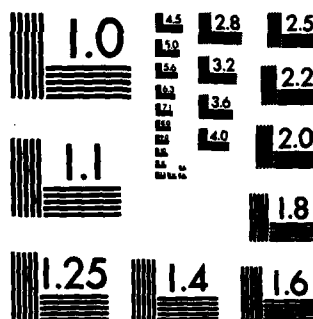
UNCLASSIFIED

AFIT/GAE/AA/85M-3

F/G 20/13

NL





MICROCOPY RESOLUTION TEST CHART
NATIONAL BUREAU OF STANDARDS-1963-A

AD-A154 435



ENHANCED THERMAL COUPLING BY A
REPETITIVELY PULSED LASER

THESIS

Jerry R. Couick
First Lieutenant, USAF

AFIT/GAE/AA/85M-3

Access

NTIS

DTIC T

Unanno

Justif

This document has been approved
for public release and sale in
distribution is unlimited.

DEPARTMENT OF THE AIR FORCE
AIR UNIVERSITY

AIR FORCE INSTITUTE OF TECHNOLOGY

Wright-Patterson Air Force Base, Ohio

85

REPRODUCED AT GOVERNMENT EXPENSE

DTIC

SELECTE

JUN 4 1985

E

AFIT/GAE/AA/85M-3

(1)

DTIC
SELECTED
JUN 4 1985
E D

ENHANCED THERMAL COUPLING BY A
REPETITIVELY PULSED LASER

THESIS

Jerry R. Couick
First Lieutenant, USAF

AFIT/GAE/AA/85M-3

Accession For		
NTIS GRA&I <input checked="" type="checkbox"/>		
DTIC TAB <input checked="" type="checkbox"/>		
Unannounced <input type="checkbox"/>		
Justification		
By		
Distribution/		
Availability Codes		
Dist	Avail and/or Special	
A/		

DTIC
COPY
INSTRUMENT
3

Approved for public release; distribution unlimited

AFIT/GAE/AA/85M-3

ENHANCED THERMAL COUPLING BY A
REPETITIVELY PULSED LASER

THESIS

Presented to the Faculty of the School of Engineering
of the Air Force Institute of Technology

Air University

In Partial Fulfillment of the
Requirements for the Degree of
Master of Science in Aeronautical Engineering

Jerry R. Couick, B.S.
First Lieutenant, USAF

March 1985

Approved for public release; distribution unlimited

Preface

In developing the analytical relations and writing this thesis I have received a great deal of help from others. I am deeply indebted to my faculty advisor, Lt Col Eric J. Jumper, for his continuing patience and assistance in times of need. I am deeply grateful to Dr. John P. Jackson, of the KAMAN Sciences Corporation, Colorado Springs, Colorado, for his valuable comments on the subject of vapor condensation and for providing me with a copy of the hydrocode. I wish to thank Maj Leslie L. McKee, III, of the Engineering Physics Department, for his valuable comments concerning the laser-surface interaction. Also, I wish to thank Dr. James E. Hitchcock of the Department of Aeronautics and Astronautics for his guidance in developing the heat transfer relations. I wish to thank Lt Col Phil E. Nielsen of the Air Force Weapons Laboratory, Kirtland AFB, New Mexico, for providing documentation of the hydrocode. Also, I wish to thank Mr. Nick Miller, of the Air Force Institute of Technology Computer Resources Department, for his assistance in the operation of the computer facilities. Finally, I wish to thank my wife, Janie, for her continual support and longsuffering during the countless hours that I spent performing this work.

Jerry R. Couick

Table of Contents

	<u>Page</u>
Preface.....	ii
List of Figures.....	iv
List of Tables.....	vi
Abstract.....	vii
I. Introduction.....	1
II. The Experiment.....	7
III. The Hydrocode.....	18
IV. Convection Heat Transfer.....	51
V. Vapor Condensation.....	70
VI. Radiation Heat Transfer.....	77
VII. Results.....	82
VIII. Conclusions.....	96
Appendix A: Thermodynamic and Transport Properties of High-Temperature Air.....	98
Appendix B: Listing of Hydrocode.....	107
Appendix C: Listing of Convection Heat Transfer Code	129
Appendix D: Listing of Vapor Condensation Code.....	132
Bibliography.....	135
Vita.....	138

List of Figures

<u>Figure</u>		<u>Page</u>
3.1	Cylindrical Laser Beam Impinging on a Metal Target.....	18
3.2	Control Volume Used for Derivation of the Hydrodynamic Flow Equations.....	19
3.3	Axial Mesh Used by the Hydrocode.....	27
3.4	Radial Mesh Used by the Hydrocode.....	27
3.5	Schematic of the Lax-Wendroff Two-Step Technique.....	31
3.6	Schematic of Cell-Centered Pressure-Differencing.....	34
3.7	Schematic of Laser Attenuation and Energy Deposition.....	42
1.	Hall's Absorbed Energy Density Profile.....	8
2.	Normalized Power (Flux) as a Function of Time for Halls 9.3 J Pulse.....	11
3.	Laser Beam Energy as a Function of Time for Hall's 9.3 J Pulse.....	13
4.	Normalized Laser Flux as a Function of Radius	15
5.	Radial Velocity Component as a Function of Radius, With Time as a Parameter.....	53
6.	Boundary Layer Similarity Solutions as a Function of the Similarity Variable.....	58
7.	Stagnation Flow Constant as a Function of Time.....	60
8.	Temperature Profile at the Target Surface as a Function of Radius With Time as a Parameter	64
9.	Heat Flux into the Target Due to Convection Heat Transfer as a Function of Radius with Time as a Parameter.....	83
10.	Projected Heat Flux into the Target Due to Convection Heat Transfer as a Function of Radius for Times up to 10 microseconds.....	85

11.	Energy Flux into the Target Due to Vapor Condensation as a Function of Radius With Time as a Parameter.....	87
12.	Projected energy Flux into the Target Due to Vapor Condensation as a Function of Radius for Times up to 10 microseconds.....	88
13.	Energy Absorbed by the Target Per Unit Area as a Function of Radius.....	90
14.	Depth of Laser Induced Target Vaporization as a Function of Radius With Time as a Parameter...	93
A.1	Compressibility Factor of High-Temperature Air as a Function of Temperature With Pressure as a Parameter.....	100
A.2	Mass Specific Enthalpy of High-Temperature Air As a Function of Temperature with Pressure as a Parameter.....	101
A.3	Mass Specific Heat at Constant Pressure of High-Temperature Air as a Function of Temperature With Pressure as a Parameter.....	102
A.4	Ratio of Specific Heats of High-Temperature Air as a Function of Temperature With Pressure as a Parameter.....	103
A.5	Thermal Conductivity of High-Temperature Air as a Function of Temperature With Pressure as a Parameter.....	104
A.6	Dynamic Viscosity of High-Temperature Air as a Function of Temperature With Pressure as a Parameter.....	105
A.7	Prandtl Number of High-Temperature Air as a Function of Temperature With Pressure as a Parameter.....	106

List of Tables

<u>Table</u>	<u>Page</u>
I. Estimate of Bremsstrahlung Plasma Reradiation.....	92

Abstract

The purpose of this study was to determine the effects of convection heat transfer, target vapor condensation, and radiation heat transfer on the observed enhanced thermal coupling of a pulsed laser to an Aluminum target. The need for this study is to develop a base from which the laser parameters needed to most efficiently couple laser energy to a metal target may be predicted.

An attempt was made to analytically duplicate a set of experimental data in which enhanced thermal coupling was observed. Analytical relations were developed to compute the heat flux, into the surface of an Aluminum species, due to convection heat transfer, target vapor condensation, and plasma reradiation. From these relations, the most significant coupling mechanism was identified to be vapor condensation. Convection heat transfer was found to have a less significant effect on enhanced coupling, and plasma reradiation was found to be negligible. The calculations were performed by a three-dimensional Lagrangian hydrocode. The results of this work are somewhat inconclusive due to the extensive computer resources used by the hydrocode; however, the relations presented here do seem to give promising results. The work should be continued to investigate the effects of laser and target parameters on enhanced thermal coupling.

ENHANCED THERMAL COUPLING BY A REPETITIVELY PULSED LASER

I. Introduction

Much work has been done in past years, primarily by researchers at the United States Air Force Weapons Laboratory, in studying the effects of high-power lasers on metallic surfaces. In particular, much research has been directed towards studying the thermal coupling of lasers to metals. The amount of thermal coupling is a direct indication of how efficiently laser energy is being delivered to the target.* In most practical applications of laser energy, it is sometimes desirable to deliver the most energy to the target for the least investment, in terms of total laser energy; thus, it is desirable to maximize the amount of "thermal" coupling. Experimental data, though the amount is relatively limited, is available on the subject. What is needed, however, is a theoretical explanation of how the amount of thermal coupling may be increased. Since such an explanation is not currently available, a natural "starting point" for its development is an attempt to analytically duplicate a set of experimental data. Such a model, due to the fact that it is derived from a given set of experimental data, will not be expected to yield accurate

* The words target, metal, and surface will be used synonymously in this document.

results for all experimental conditions; however, in theory, it can be modified to include the effect of experimental parameters. Once the model is fully developed, it will then be possible to predict the laser parameters needed to maximize the amount of thermal coupling to a particular type of target.

It is known [1] that, under certain conditions, the thermal coupling of a pulsed laser (with average intensity I) to a target is an order of magnitude greater than that of a continuous wave laser (with intensity I). For example, Hall [2]** reports that the coupling of a 10.6 micron continuous wave (CW) CO₂ laser to cold Aluminum is about 3%; whereas, the coupling of a pulsed CO₂ laser of the same wavelength is about 17.5% for a 9.3 J pulse. The as yet unanswered question is then, "why does the enhancement occur?" It is generally accepted that the overall reason for the enhancement is that much higher intensities are attainable when a laser is operated in a pulsed mode, as opposed to a continuous wave mode. Furthermore, it has been observed [3] that a prerequisite for enhancement is the ignition of an air breakdown plasma called - laser supported detonation wave (LSD). It appears, therefore, that the phenomenon of enhanced thermal coupling is due to the presence of an LSD.

** Hall's experimental data is the background for this research, and is discussed in detail in Section II.

The LSD is a highly absorptive plasma front, considered to be optically thick. For this reason, it has been acknowledged [4, 5, 6] that the enhancement is due to the efficient transfer of energy from the plasma to the target by convection and radiation heat transfer. Approximate heat transfer calculations, however, have been made and they fail to match experimental data. For example, Stamm, Nielsen, and Jackson [7] report that radiation is not the cause of the enhancement. Also, Jumper and Jackson [8] report that convection heat transfer is probably not responsible for the enhancement. There is, then, a large discrepancy between experimental data and approximate heat transfer calculations.

When a laser pulse of sufficient intensity strikes a target, boiling and vaporization of the target may occur. If a LSD is ignited, it propagates up the laser beam and, as it passes by a region of target vapor, the high pressures associated with the LSD force the target vapor back onto the surface where it flows out radially and condenses. Jumper [9] has suggested that this condensation may be responsible for the enhancement and he has shown [10] that sufficient energy resides in the condensing vapor to account for observed values of enhanced coupling. This theory is worthy of further investigation since the vapor, when it condenses, gives up not only the latent heat of vaporization required to vaporize it, but also the energy

it gains while in the vapor state. Therefore, it appears that if a LSD forces target vapor onto the surface and if some or all the vapor condenses, the final energy residing in the target will be greater and thus the amount of thermal coupling will be enhanced.

The foremost object of this research effort was to perform detailed calculations of the convection heat transfer taking place at the surface of an aluminum species, under the presence of a LSD. The results of the heat transfer calculations were compared to Hall's experimental data [2], in order that the role of convection heat transfer on enhanced coupling could be determined. The second object of this research was to examine the role of vapor condensation on enhanced coupling. The vapor condensation calculations were performed in more detail than those made by Jumper and Jackson [10]. The third and final object of this research was to predict the role of plasma radiation on enhanced coupling. It was projected that these calculations would identify the most important cause of enhanced thermal coupling for Hall's 9.3 J pulse. The effect of beam parameters on coupling was not studied here; however, it is hoped that the models developed here might eventually be extended to include these parameters. Future study in this area is needed.

The calculations needed for this study were performed numerically by a three-dimensional Lagrangian hydrocode,

given by Nielsen [11]. The hydrocode is explained in detail in Section III and it suffices to say here that the hydrocode solves the inviscid "control volume" equations for the conservation of mass, momentum, and energy, augmented with the perfect gas equations of state for air and target vapor. The hydrocode gives the following time-dependent flow properties for air, through which a time-varying, spatial-varying laser beam is propagating: pressure, total density, vapor density, energy density, components of momentum (velocity) in all spatial directions of interest, and temperature. The hydrocode may be modified to include the presence of a target and, of course, since this problem is a laser-target interaction problem, the presence of a target was assumed.

The reader is informed that the results of this study are somewhat inconclusive, as the amount of numerical data for analysis was limited. This was due to the fact that the hydrocode, because of its size and multi-dimensionality, requires massive amounts of computer time and computer resources; whereas the amount of computer time allocated to this study was limited. The large computer time requirement arises due to the fact that this study was one of boundary layer effects and, in order to accurately predict the properties at the edge of a boundary layer, of unknown thickness, the numerical grid size must be quite small. With a small grid size and the small steps in time

needed for stability of the solution, the numerical calculations for Hall's 9.3 J pulse only went out to about one third of the pulse time. This is even with the maximum allotted amount of computer resources. Nevertheless, it is felt that the data obtained provides fairly accurate results since the most intense laser energy is provided very early during the laser pulse (during the "spike of the pulse").

In summary, this study was directed towards examining the effects of convection heat transfer, radiation heat transfer, and vapor condensation on the thermal coupling of a pulsed, CO₂ laser to a "cold" Aluminum surface. The experimental background is Hall's 9.3 J pulse [2], and the results are based on a limited amount of numerical data.

II. The Experiment

The experimental background for this research is Hall's famous 9.3 J pulse experiment, in which he noticed that the thermal coupling of a CO₂ laser to an Aluminum target increased from about 3%, for a cold target at CW intensities, to about 17.5%, for the same target exposed to a 9.3 J pulse. The documentation for this experiment is found in reference [2]. This reference lists the results of several experiments, one of which is the thermal coupling measurement being studied here. The experiments were performed at the Boeing Aerospace Laboratory under contract to the the United States Air Force Weapons Laboratory. The laser used for the experiments was a Marx Double Bank CO₂ laser of 10.6 micron wavelength radiation, operated in a pulsed mode, with a focal length of 28 centimeters, and a focused spot radius of 0.126 centimeters at the target surface. The irradiated target was a 2024-T3 Aluminum alloy disc of 5 centimeters diameter, and a thickness of 0.028 centimeters.

The back surface temperature of the target was monitored with a 0.005 inch diameter chromel-alumel thermocouple spot-welded to the target. From this measured data, Hall was able to find the absorbed energy density of the target as a function of radial position from the center of the irradiated area (Fig. 1). By integrating over the

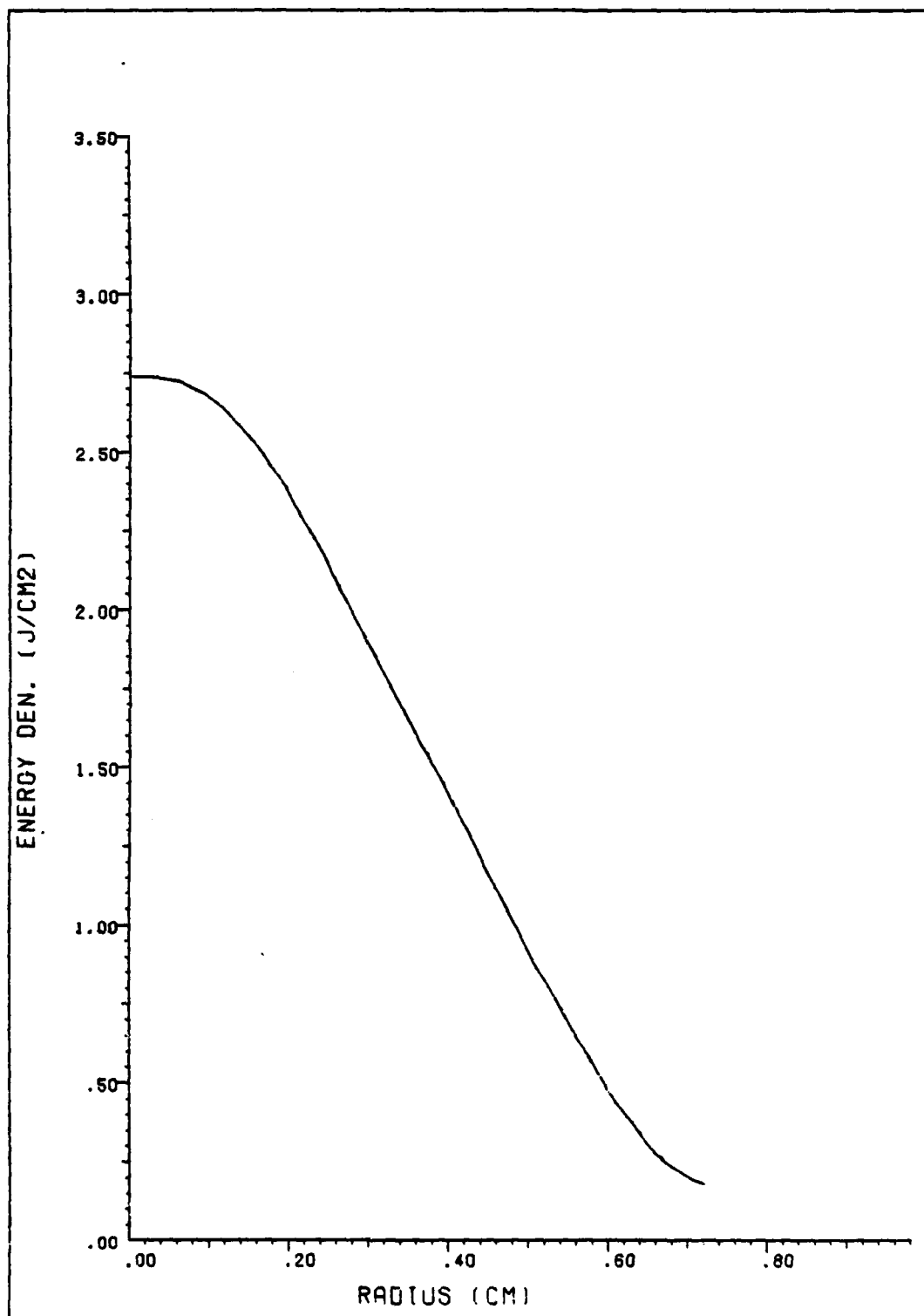


FIG. 1: HALL'S ABSORBED ENERGY DENSITY PROFILE

area, he determined that the total laser energy residing in the target was 1.63 J, or 17.5% of the incident beam energy, 9.3 J. By following the above procedure, one includes in a thermal coupling calculation only that portion of laser energy which resides in the target after irradiation, such that the temperature of the target is increased. As such, impulsive forces delivered to the target by pressure relaxation are not included in a thermal coupling calculation; rather, they are referred to as mechanical coupling phenomena.

In order to duplicate Hall's data numerically, it is necessary to know: the temporal variation of the beam, the spatial variation of the beam, and the peak flux, or intensity, of the beam. Hall presents a plot of the normalized power* of the laser used versus time. The hydrocode, as explained later, needs to know the normalized flux as a function of time but, since flux is just power per unit area, the two functions are the same. To obtain a functional expression for the normalized flux, Hall's plot was traced onto graph paper and the resulting curve was fit using the method of least squares as given by Book [13]. The following curve fit was obtained and, though it is tedious, it agrees almost exactly with Hall's plot:

* Normalized to the peak value.

$$\begin{aligned}
& 0, & t = 0 \\
& 0.07339 + 1.6579t - 1.2480t^2 \\
& \quad + 0.3845t^3, & 0 < t \leq 1.5 \\
p(t)/p^* = & 0.8483 + 0.1765t - 0.05158t^2, & 1.5 < t \leq 3 \\
& 1.5577 - 0.2599 + 0.01508t^2, & 3 < t \leq 8 \quad (1) \\
& -0.025t + 0.6432, & 8 < t \leq 25.73 \\
& 0, & t \geq 25.73
\end{aligned}$$

where p^* is the maximum power in the pulse, t is in microseconds, and the pulse time is 25.73 microseconds. Equation (1) is plotted in Fig. 2. The remaining needed parameters, spatial beam variation and peak flux, are not given explicitly by Hall, though he does say that the beam is Gaussian with a spot radius of 0.126 centimeters, and that the total energy in the beam is 9.3 J.

The peak power, p^* , may be found from equation (1) and the total beam energy. Since energy is power integrated over time,

$$E = 9.3 \text{ J} = p^* \int_0^{\tau_p} p(t)/p^* dt, \quad (2)$$

where τ_p is the pulse time of the laser, given above. By solving equation (2), p^* was found to be 0.976121 MW. Also, the energy in the beam at time t is given by:

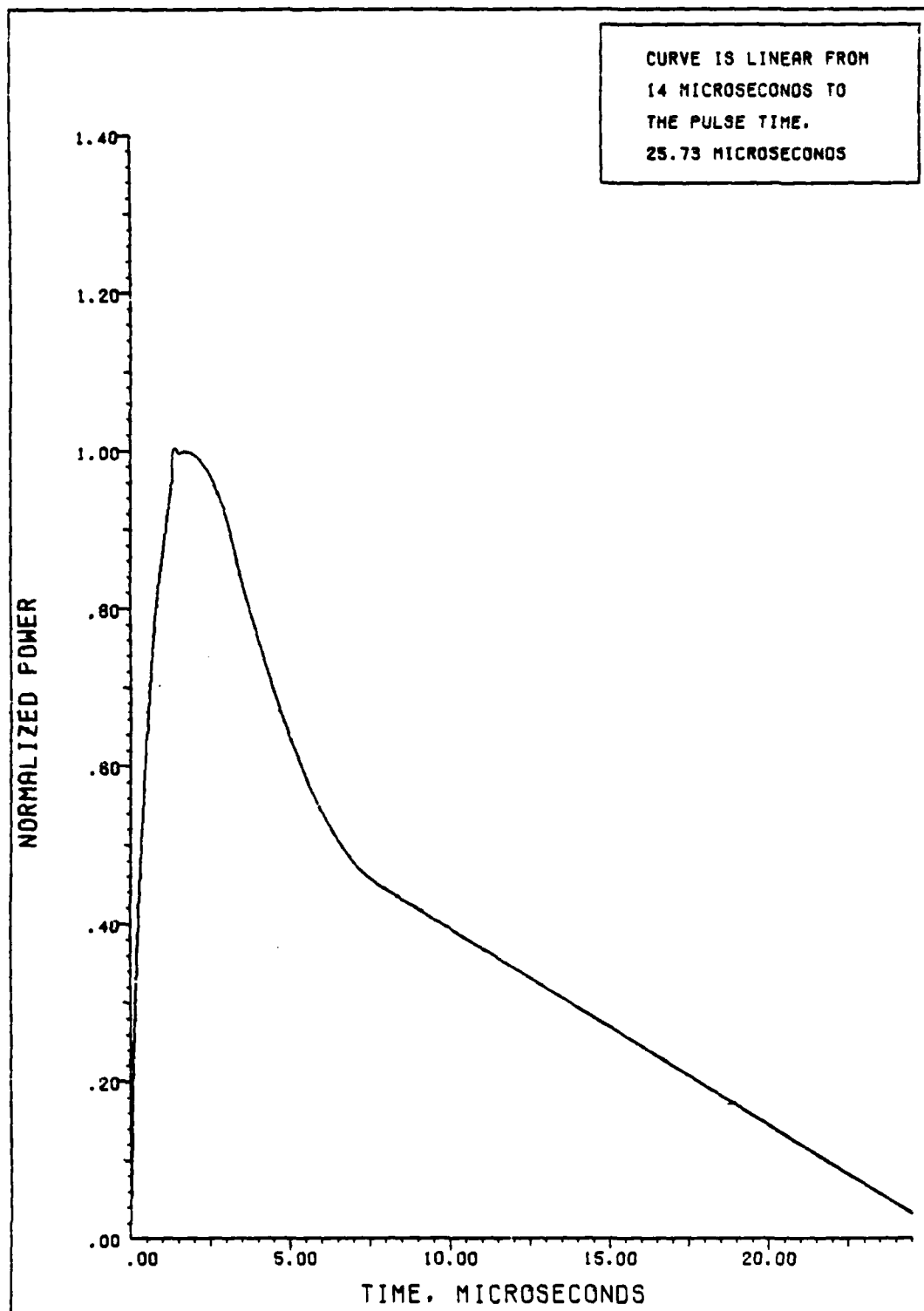


FIG. 2: NORMALIZED POWER (FLUX) FOR HALL'S PULSE

$$E(t) = p^* \int_0^t p(\tau)/p^* d\tau, \quad (3)$$

where τ is now only a dummy integration variable. Equation (3) is plotted in Fig. 3.

As stated above, the beam is Gaussian with a spot radius of 0.126 centimeters. The spatial form of such a beam is given by Ready [12] to be:

$$ENV(r) = \exp(-ar^2), \quad (4)$$

where $ENV(r)$ is the ratio of the flux at radius, r , to its peak value at the center of the beam ($r = 0$), and a is a constant related to the spot radius. The spot radius is known, but there are two common definitions of the spot radius for a Gaussian beam: (a) the radius at which the flux is equal to $\exp(-1)$ times its peak value and; (b) the radius at which the flux is equal to $\exp(-2)$ times its peak value. It is necessary, therefore, to determine which definition Hall uses in his report. He states that the Gaussian width of his calculated absorbed energy density profile is 4.38 millimeters, and by referring to Fig. 1, one sees that this radius corresponds to definition (a) above. It is assumed, then, that the same definition applies to the beam spot radius. From equation (4) and

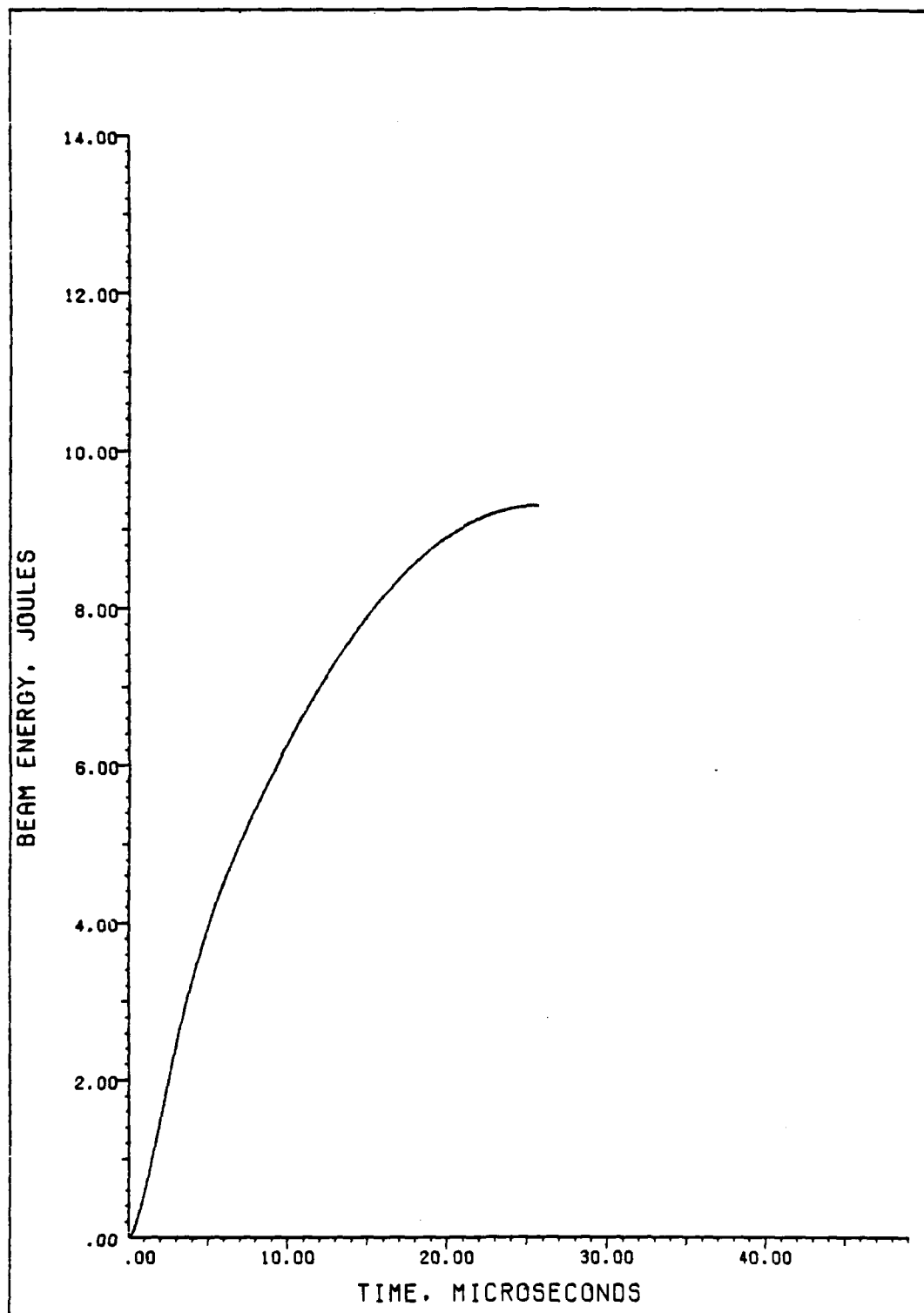


FIG. 3: BEAM ENERGY OF HALL'S 9.3 JOULE PULSE

definition (a),

$$\text{ENV}(0.126) = \exp \{-a(0.126)^2\} = \exp(-1).$$

Thus, $a = 1/(0.126)^2 = 62.988 \approx 63$. The spatial variation of the beam becomes,

$$\text{ENV}(r) = \exp(-63r^2). \quad (5)$$

Equation (5) is plotted in Fig. 4.

The only beam parameter, needed by the hydrocode, which remains to be found is the peak laser flux. As mentioned previously, this value is not given by Hall. It is found by assuring that the laser flux, integrated over space and time, is equal to the total beam energy of 9.3 J. At a given time, the flux incident on the mesh is given by equation (1) to be,

$$I(t) = \text{IMAX}p(t)/p^*, \quad (6)$$

where IMAX is the peak laser intensity. From equation (5), the flux varies spacially as:

$$I(r,t) = \text{IMAX}(p(t)/p^*) \exp(-63r^2). \quad (7)$$

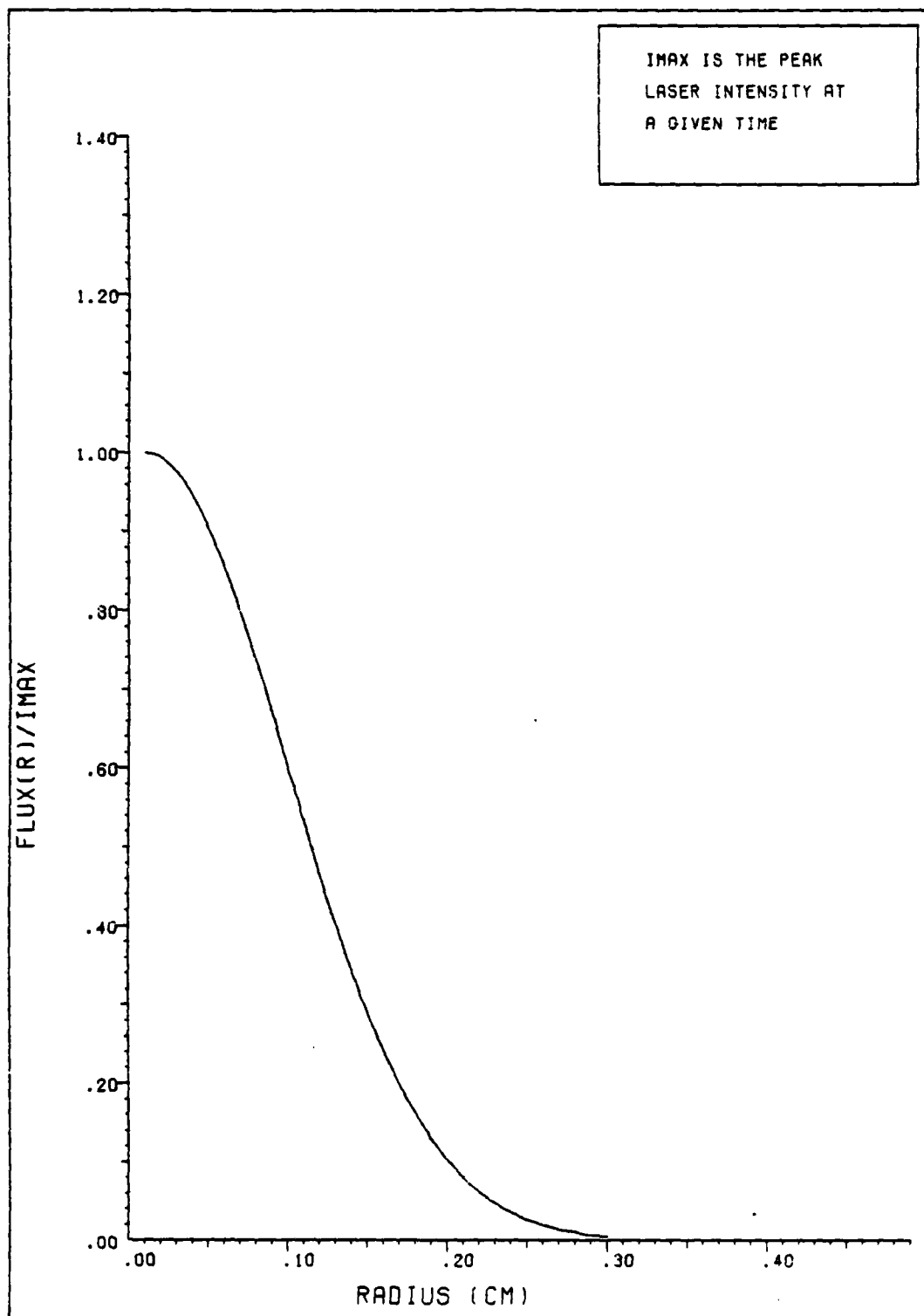


FIG. 4: RADIAL VARIATION OF LASER FLUX

The integral of equation (7), over all space and time, must equal the total beam energy of 9.3 J. Therefore,

$$\int_0^{\infty} \int_0^{\tau_p} \int_0^{2\pi} I(r,t) d\theta dt dr = 9.3 \text{ J.} \quad (8)$$

Since $I(r,t)$ is not a function of the angle, θ , and $IMAX$ is a constant, equation (8) reduces to:

$$2\pi IMAX \int_0^{\infty} \int_0^{\tau_p} p(t)/p^* r \exp(-63r^2) dt dr = 9.3 \text{ J.} \quad (9)$$

By solving equation (9), $IMAX$ is found to be 19.571 megawatts per square centimeter, which is approximately 20 megawatts per square centimeter.

In summary, the hydrocode needs to know three beam parameters in order to determine the laser energy deposited above the target. It needs to know the peak laser flux, the temporal variation of the beam, and the radial variation of the beam. Should the reader be concerned, the axial variation of the beam is determined by the hydrocode, as explained in Section III. In this section, the above parameters were derived from Hall's report. The temporal variation is given by equation (1), the spatial variation is given by equation (5), and the peak flux is

taken to be 20 megawatts per square centimeter. Equations (1) and (5) are plotted, respectively, in Fig. 2 and Fig. 4.

III. The Hydrocode

It was stated in the introduction that the numerical calculations needed for this study are performed by a three-dimensional hydrocode. Henceforth, the hydrocode shall be known simply as HYDRO. In this section, HYDRO is explained in detail and all of its equations are derived. The version of HYDRO used (and modified) by the author was obtained from Jackson*. It differs some from the original version which is briefly explained by Nielsen [11].

HYDRO solves the unsteady inviscid flow equations, yielding flow properties outside the boundary layer. The laser beam is assumed to be cylindrical and the flow is assumed to be axisymmetric about the beam axis, as shown in Fig. 3.1.

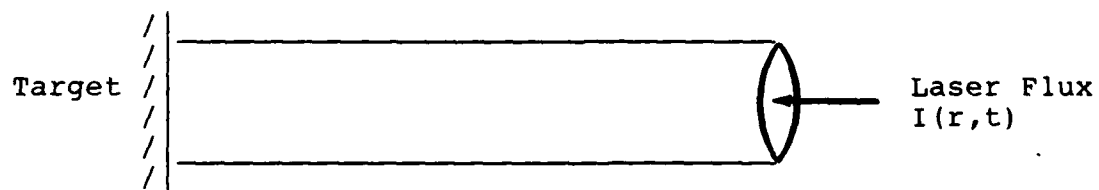


Fig 3.1 Cylindrical laser beam impinging on a metal target.

The equations solved are the "control volume" equations for the conservation of mass, momentum, and energy. In

* Research Scientist, KAMAN Sciences Corp.

deriving these equations, the control volume of interest is a cylindrical shell, as shown in Fig. 3.2.



Depth = dz

Fig. 3.2 Control volume used for derivation of the hydrodynamic flow equations.

Following the method outlined by Reynolds and Perkins [30], the equations may be derived in the following manner:

(a) Mass: $\sum \dot{M}_o - \sum \dot{M}_i = - \partial M / \partial t)_{cv}$, where

the subscript, i, means "in"

the subscript, o, means "out",

$\sum \dot{M}$ is the net mass flow rate, and

$\partial M / \partial t)_{cv}$ is the time rate-of-change of mass in the control volume.

(b) Momentum: $\sum \dot{M}_o - \sum \dot{M}_i + \partial \underline{M} / \partial t)_{cv} = \sum \underline{F}$, where

the subscript, i, means "in",

the subscript, o, means "out",

$\sum \dot{M}$ is the net linear momentum flow rate,

$\sum \underline{F}$ is the net external force, and

$\partial \underline{M} / \partial t)_{cv}$ is the time rate-of-change of linear momentum in the control volume.

(c) Energy: $\sum \dot{W}_i + \sum \dot{Q}_i + \sum \dot{M}_i (h+ke+pe)_i$
 $= \sum \dot{W}_o + \sum \dot{Q}_o + \sum \dot{M}_o (h+ke+pe)_o +$
 $\partial \tilde{E} / \partial t)_{cv}$, where

the subscript, i, means "in",

the subscript, o, means "out",

$\sum \dot{W}$ is the net rate of work done by external forces,

$\sum \dot{Q}$ is the net rate of heat input (or output),

h is the mass specific enthalpy,

ke is the mass specific kinetic energy,

pe is the mass specific potential energy, and

$\partial \tilde{E} / \partial t)_{cv}$ is the time rate-of-change of energy in the control volume.

As stated previously, the flow is assumed to be axisymmetric about the beam axis; therefore, there is no angular (θ) dependence in the hydrodynamic equations. Using the manner outlined above, the flow equations are now derived.

Conservation of Mass:

$$\sum \dot{M}_0 - \sum \dot{M}_1 = - \partial M / \partial t) cv. \quad (1a)$$

Referring to Fig. 3.2,

$$\sum \dot{M}_1 = \rho u_r r d\theta dz + \rho u_z r d\theta dr. \quad (2a)$$

Using a first order Taylor series expansion about the inlet conditions,

$$\begin{aligned} \sum \dot{M}_0 = & \rho u_r r d\theta dz + \partial / \partial r (\rho u_r r d\theta dz) dr + \\ & \rho u_z r d\theta dr + \partial / \partial z (\rho u_z r d\theta dr) dz. \end{aligned} \quad (3a)$$

Since mass is density times volume,

$$\partial M / \partial t) cv = \partial / \partial t (\rho r dr d\theta dz). \quad (4a)$$

Substituting equations (2a) through (4a) into equation (1a) yields:

$$1/r \{ \partial / \partial r (\rho r u_r) + \partial / \partial z (\rho r u_z) \} = - \partial \rho / \partial t. \quad (5a)$$

Now, the axisymmetric divergence operator, in cylindrical coordinates is:

$$\text{div} (\underline{X}) = 1/r \partial / \partial r (r X_r) + \partial / \partial z (X_z).$$

With this identity, equation (5a) becomes:

$$\partial / \partial t = -\text{div} (\rho \underline{v}), \quad (10)$$

where the velocity, \underline{v} , equals $u_r \underline{e}_r + u_z \underline{e}_z$.

Conservation of Momentum:

$$\sum \dot{\underline{M}}_0 - \sum \dot{\underline{M}}_i + \partial \underline{M} / \partial t \text{ cv} = \sum \underline{F}. \quad (1b)$$

Consider first the linear momentum in the radial direction.

$$\sum \dot{\underline{M}}_i = \sum \dot{M}_{iR} = \rho u_r^2 r d\theta dz + \rho u_r u_z r d\theta dr. \quad (2b)$$

Likewise,

$$\begin{aligned} \sum \dot{\underline{M}}_0 = & \rho u_r^2 r d\theta dz + \partial / \partial r (\rho u_r^2 r d\theta dz) dr + \\ & \rho u_r u_z r d\theta dr + \partial / \partial z (\rho u_r u_z r d\theta dr) dz. \end{aligned} \quad (3b)$$

Also,

$$\partial \underline{M} / \partial t)_{cv} = \partial / \partial t (M u_r) = \partial / \partial t (\rho u_r r dr d\theta dz). \quad (4b)$$

Finally, for no body forces,

$$\sum \underline{F} = p r d\theta dz - (p + \partial p / \partial r dr) r d\theta dz. \quad (5b)$$

Substituting equations (2b) through (5b) into equation (1b) yields:

$$\begin{aligned} \partial(\rho u_r) / \partial t = & -1/r \{ \partial / \partial r (\rho r u_r^2) + \partial / \partial z (\rho r u_r u_z) \} \\ & - \partial p / \partial r. \end{aligned} \quad (6b)$$

Using the definition of the divergence operator, equation (6b) becomes:

$$\partial(\rho u_r) / \partial t = -\text{div}(\rho u_r \underline{v}) - \partial p / \partial r. \quad (11)$$

Similarly, consideration of the linear momentum in the axial direction yields:

$$\partial(\rho u_z) / \partial t = -\text{div}(\rho u_z \underline{v}) - \partial p / \partial z. \quad (12)$$

Conservation of Energy:

$$\sum \dot{W}_i + \sum \dot{Q}_i + \sum \dot{M}_i (h+ke+pe)_i = \sum \dot{W}_o + \sum \dot{Q}_o + \sum \dot{M}_o (h+ke+pe)_o + \partial \tilde{E} / \partial t)_{cv}. \quad (1c)$$

Since there is no shaft work and no viscous work, the work terms are zero. Assuming that the change in potential energy is very small,

$$\tilde{Q} = \partial \tilde{E} / \partial t)_{cv} + \sum \dot{M}_o (h+ke)_o - \sum \dot{M}_i (h+ke)_i, \quad (2c)$$

where \tilde{Q} is the net heat input per unit time.

$$\sum \dot{M}_i (h+ke)_i = \rho u_r r d\theta dz (h+v^2/2) + \rho u_z r d\theta dr (h+v^2/2). \quad (3c)$$

Using a first order Taylor series expansion about the inlet conditions,

$$\begin{aligned} \sum \dot{M}_o (h+ke)_o &= \rho u_r r d\theta dz (h+v^2/2) + \\ &\quad \partial / \partial r [\rho u_r r d\theta dz (h+v^2/2)] dr + \rho u_z r d\theta dr (h+v^2/2) + \\ &\quad \partial / \partial z [\rho u_z r d\theta dr (h+v^2/2)] dz. \end{aligned} \quad (4c)$$

Now,

$$\partial \tilde{E} / \partial t)_{cv} = \partial / \partial t [\rho (e+v^2/2) r dr d\theta dz], \quad (5c)$$

where e is the mass specific internal energy. Substituting equations (2c) through (5c) into equation (1c) yields:

$$\begin{aligned} \tilde{Q}/rdrd\theta dz = & 1/r \partial/\partial r [\rho r u_r (h+v^2/2)] + \\ & 1/r \partial/\partial z [\rho r u_z (h+v^2/2)] + \partial/\partial t [\rho (e+v^2/2)]. \end{aligned} \quad (6c)$$

Now, $rdrd\theta dz$ is the volume and if Q is the net heat input per unit mass, per unit time,

$$\tilde{Q}/rdrd\theta dz = \rho Q. \quad (7c)$$

To be consistent with Nielsen's [11] documentation, the following definition is made:

$$E = \rho(e+v^2/2). \quad (8c)$$

By definition, $h = e + p/\rho$; therefore,

$$h + v^2/2 = 1/\rho (E+p). \quad (9c)$$

Substituting equations (7c) through (9c) into equation (6c) yields:

$$\partial E/\partial t = -1/r \partial/\partial r [r u_r (E+p)] - \partial/\partial z [u_z (E+p)] + \rho Q. \quad (10c)$$

Using the definition of the divergence operator, equation (10c) becomes:

$$\partial E/\partial t = -\text{div}[(E+p)\underline{v}] + \rho Q. \quad (13)$$

The "control volume" conservation equations are:

$$\partial \rho / \partial t = -\text{div}(\rho \underline{v}), \quad (10)$$

$$\partial(\rho u_r) / \partial t = -\text{div}(u_r \rho \underline{v}) - \partial p / \partial r, \quad (11)$$

$$\partial(\rho u_z) / \partial t = -\text{div}(u_z \rho \underline{v}) - \partial p / \partial z, \quad (12)$$

$$\partial E / \partial t = -\text{div}[(E+p)\underline{v}] + \rho Q. \quad (13)$$

There are only four equations in the five unknowns, ρ , u_r , u_z , E , and p . An additional equation is needed in order to simultaneously find the five unknowns. The equation used is the perfect gas equation of state for air, $p = \rho RT$. Assuming that the gas is calorically perfect, $R = c_p - c_v = c_v(\gamma - 1)$, where γ is the ratio of specific heats. Also, for the same assumptions, $e = c_v T$; therefore, $p = \rho e(\gamma - 1)$. Since $E = \rho(e + v^2/2)$,

$$p = (E - v^2/2)(\gamma - 1), \quad (14)$$

where $v = (u_r^2 + u_z^2)^{1/2}$. Equation (14) augments equations (10) through (13). The hydrodynamic equations solved by HYDRO are thus derived.

Equations (10) through (14) are solved by HYDRO, using finite difference techniques. Before the difference equations are derived, a suitable mesh or grid must be established. The mesh used by HYDRO corresponds with the control volume shown in Fig. 3.2. The axial mesh is set up

such that the axial cells have a constant thickness, Δz , in the axial direction, as shown in Fig. 3.3 below. The radial mesh is set up such that the cylindrical cells have a constant thickness, Δr , in the radial direction, as shown in Fig. 3.4 below. For simplicity $\Delta z = \Delta r = \Delta x$.

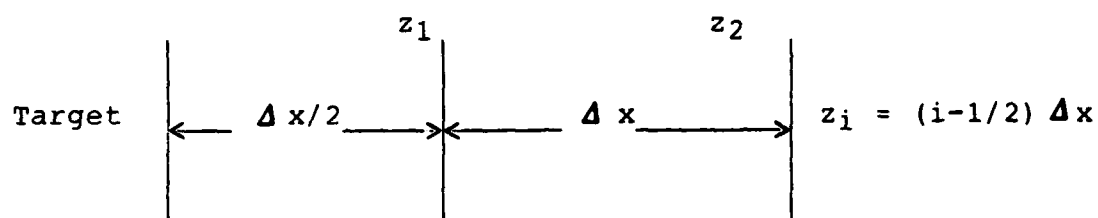


Fig. 3.3 Schematic of axial mesh.

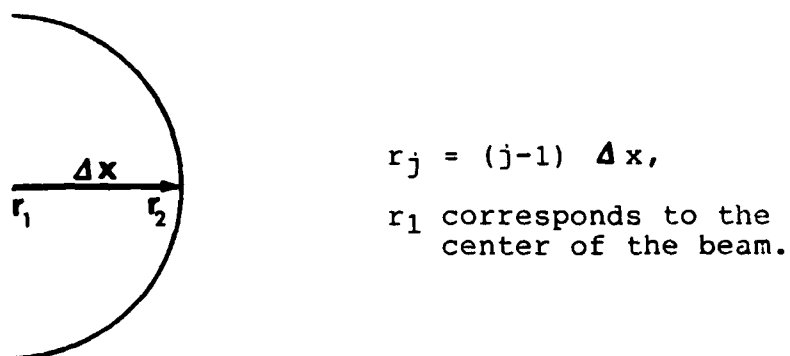


Fig. 3.4 Schematic of radial mesh.

To derive the difference equations for a flux-divergent quantity q , such that $dq/dt = -\text{div} \underline{f}$, Gauss' divergence theorem is used. The theorem is stated as:

$$\iiint_V \text{div} \underline{f} \, dV = \iint_S \underline{f} \, d\underline{A}.$$

For a differential volume element, the theorem reduces to:

$$\text{div} \underline{f}(V) = f_o A_o - f_i A_i \text{ where}$$

V is the volume of the element,

$f_o A_o$ is the amount of q leaving the element per unit time, and

$f_i A_i$ is the amount of q entering the element per unit time.

Consider first the divergence of a quantity, q , in the radial direction. The volume element is a cylindrical shell of height Δx , inner radius r , and outer radius $r + \Delta x$. By Gauss' theorem,

$$\text{div} \underline{f} = \frac{f(r + \Delta x) 2\pi(r + \Delta x) \Delta x - f(r) 2\pi r \Delta x}{[\pi(r + \Delta x)^2 - \pi r^2] \Delta x}$$

This equation reduces to:

$$\text{div} \underline{f} = 1/\Delta x (1 + \Delta x/2r)^{-1} [(1 + \Delta x/r) f(r + \Delta x) - f(r)].$$

For a flux-divergent quantity, q , $dq/dt = -\text{div} \underline{f}$; therefore,

$$dq/dt = -1/\Delta x [1 + \Delta x/(2r)]^{-1} [(1 + \Delta x/r)f(r + \Delta x) - f(r)]. \quad (15)$$

Consider now the divergence of q in the axial direction. This case is simpler since $V = A \Delta x$, and Gauss' theorem yields;

$$dq/dt = -1/\Delta x [f(z + \Delta x) - f(z)]. \quad (16)$$

Equations (15) and (16) may be combined into a single equation by defining a parameter l , such that $l = 1$ corresponds to the axial direction and $l = 2$ corresponds to the radial direction. The combined equation is:

$$dq_l/dt = -1/\Delta x [1 + ((l-1)\Delta x)/(2x_l)]^{-1} \times \\ \{ [1 + ((l-1)\Delta x)/x_l] f(x_l + \Delta x) - f(x_l) \}. \quad (17)$$

Equation (17) does not, however, apply to the radial flux of quantities from the first radial cell. The center of this cell is at the center of the beam; therefore, there is only one boundary through which quantities are transported. For this cell, Gauss' theorem yields;

$$\text{div} \underline{f} \pi (\Delta x)^2/4 = \pi \Delta x f_{3/2}. \quad (18)$$

Equations (17) and (18) are used by the difference method to update hydrodynamic quantities as they vary with both time and spatial position in the mesh.

The numerical method used to update quantities is the Lax-Wendroff two-step technique, which is accurate to order $(\Delta t / \Delta x)^2$. A detailed explanation of this method may be found in reference [14]. Here, the method is explained only to the extent that the interested reader will be able to understand how HYDRO does the differencing. The two steps employed are:

$$(1) \quad q_{n+1/2}^{t+1/2} = q_{n+1/2}^t + dq_n / dt (\Delta t / 2), \text{ and}$$

$$(2) \quad q_n^{t+1} = q_n^t + dq_{n-1/2} / dt (\Delta t).$$

In these equations, q_n^t is the value of a flux-divergent quantity at spatial position n and time step (cycle) t , and f_n^t is the corresponding flux component in the direction of interest. Also, $q_{n+1/2}$ is defined to be the arithmetic mean of q_n^t and q_{n+1}^t . Fig. 3.5 on the following page will help the reader visualize the notation used above.

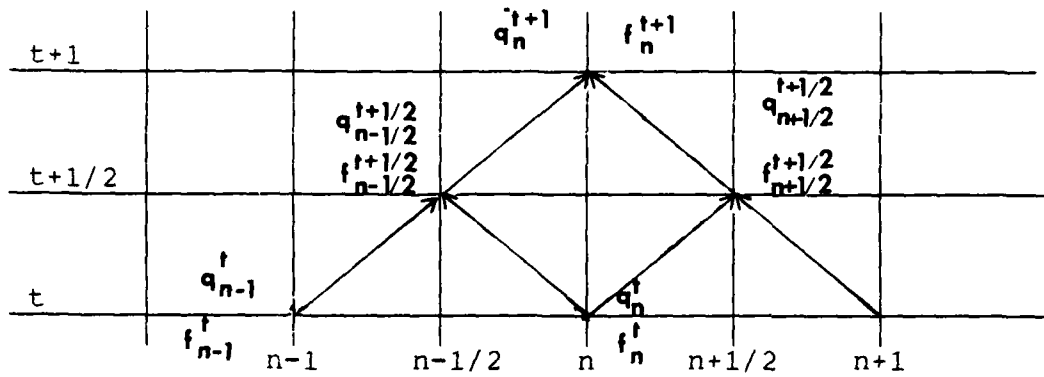


Fig. 3.5 Schematic of Lax-Wendroff two-step technique.

Without going through the algebra, the two Lax-Wendroff steps, with dq_n/dt given by equations (17) and (18), become:

$$q_{n+1/2}^{t+1/2} = (q_n^t + q_{n+1}^t)/2 - (\Delta t/2 \Delta x) [1 + (1-1)/(2(n-1))]^{-1} \{ [1 + (1-1)/(n-1)] f_{n+1}^t - f_n^t \}, \quad (19)$$

$$q_n^{t+1} = q_n^t - [\Delta t/\Delta x] [1 + (1-1)/(2n-3)]^{-1} \{ [1 + (1-1)/(n-3/2)] f_{n+1/2}^{t+1/2} - f_{n-1/2}^{t+1/2} \}, \quad (20)$$

for all cells except the first radial cell, and

$$q_{3/2}^{t+1/2} = 1/2 [q_1^t + q_2^t - (2 \Delta t/\Delta x) f(\Delta x)], \quad (21)$$

$$q_1^{t+1} = q_1^t - (\Delta t/\Delta x) 4 f_{3/2}^{t+1/2}, \quad (22)$$

for the first radial cell.

Equations (19) through (22) are used to update density, energy density, and the axial component of the momentum. The radial component of the momentum is troublesome, though, because it contains a gradient term, $-\partial p / \partial r$, and must be handled differently. This term is handled by assuming that $\partial p / \partial r$ is approximately equal to $\Delta p / \Delta r$. With this assumption, the two Lax-Wendroff steps become, for $q = \rho u_r$:

$$q_{n+1/2}^{t+1/2} = (q_{n+1/2}^{t+1/2})_{f-d} - \Delta t / (2 \Delta x) (p_{n+1}^t - p_n^t), \quad (19a)$$

$$q_n^{t+1} = (q_n^{t+1})_{f-d} - \Delta t / \Delta x (p_{n+1/2}^{t+1/2} - p_{n-1/2}^{t+1/2}), \quad (20a)$$

$$q_{3/2}^{t+1/2} = (q_{3/2}^{t+1/2})_{f-d} - \Delta t / (2 \Delta x) (p_2^t - p_1^t), \quad (21a)$$

$$q_1^{t+1} = (q_1^{t+1})_{f-d} - \Delta t / \Delta x (p_{3/2}^{t+1/2} - p_{1/2}^{t+1/2}). \quad (22a)$$

In equations (19a) through (22a), the subscript, "f-d", refers to the flux-divergent term given by equations (19) through (22).

According to Nielsen [11], it is sometimes convenient to difference pressure, instead of energy, as an independent variable. This is done to avoid negative pressures and temperatures near the target when laser-induced boiling is taking place. In pressure-differencing, equation (13) is

transformed by using the perfect gas equation of state (equation (14)), the mass continuity equation (equation (10)), and Euler's equation in vector form. Euler's equation is stated as:

$$\partial \underline{v} / \partial t = -(\underline{v} \cdot \nabla) \underline{v} - \nabla p / \rho .$$

With this transformation, equation (13) is replaced by:

$$\partial p / \partial t = -\text{div}(\rho \underline{v}) - (\gamma - 1) p \text{div} \underline{v} + (\gamma - 1) \rho Q. \quad (23)$$

To make equation (23) consistent with the flux-divergent form, $dq/dt = -\text{div} \underline{f}$, the following adaption is made:

$$\partial p / \partial t = -\text{div} (p + (\gamma - 1) p_c) \underline{v} + (\gamma - 1) \rho Q, \quad (24)$$

where p_c is a constant pressure evaluated at the center of a cell, taken to be the arithmetic mean of the pressures at the boundaries of the cell. Fig. 3.6 helps clarify the meaning of p_c . One of the advantages of the flux-divergent equations is that the flux of a quantity out of one cell is the flux of that quantity into the next cell. Due to the presence of p_c in equation (24), one sees that the "pressure flux" out of a cell will not be the "pressure flux" into the next cell. HYDRO handles this problem by multiplying the flux out of a cell by a "correction factor,"

such that it approximates the flux into the next cell. The correction factor is described below.

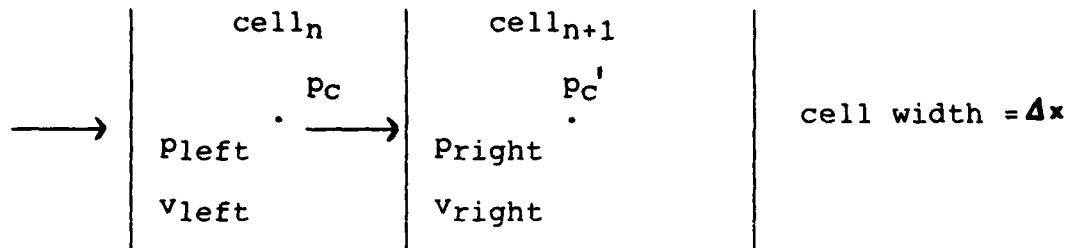


Fig. 3.6 Schematic of cell-centered pressure-differencing.

If the pressure flux at the left-hand boundary and that at the right-hand boundary are given respectively by,

$$f_l = (p_l + (\gamma - 1)p_c)v_l \text{ and } f_r = (p_r + (\gamma - 1)p_c)v_r,$$

one sees that the flux-divergent part of $dp/dt \approx -f(f_r - f_l)/\Delta x$. As stated above, $f_{rn} \neq f_{ln+1}$; therefore, f_{rn} is multiplied by a "correction factor" such that it will approximate f_{ln+1} . there are two of these correction factors: one for space-interval steps and one for time-interval steps. Referring to Fig. 3.6, it is evident that the space-interval factor is given by,

$$CF = (p_r + (\gamma - 1)p'_c) / (p_r + (\gamma - 1)p_c). \quad (25)$$

In equation (25), $P_C = (p_r + p_l)/2$ and $p_C' = (p_{n+2} + p_r)/2$, where the subscripts r and l mean "right" and "left", respectively. Also $p_r = p_{n+1}$ and $p_l = p_n$, where n is the cell number. Correction factors for both the radial and axial directions are found by equation (25); however, the time-interval correction factor is handled somewhat differently. It is defined by equation (25), but p_C' is now zero since no "time-pressures" have been found past time t ,

$p_r = p_{n+1/2}^{t+1/2}$, extrapolated from $p_n^{t+1/2}$, and

$p_l = p_{n-1/2}^{t+1/2}$, known from previous calculations. The time-

interval correction factor is thus given by,

$$CF = \frac{p_{n+1/2}^{t+1/2}}{p_{n+1/2}^{t+1/2}} + 0.5(\gamma - 1) \left(\frac{p_{n+1/2}^{t+1/2}}{p_{n+1/2}^{t+1/2}} + \frac{p_{n-1/2}^{t+1/2}}{p_{n-1/2}^{t+1/2}} \right). \quad (26)$$

For pressure-differencing, equation (24), augmented with the correction factors given by equations (25) and (26), replaces equation (13) of the hydrodynamic flow equations. In order to difference either energy or pressure with the same code, the variable NDIF is introduced. If NDIF = 0, pressure is differenced, and if NDIF = 1, energy is differenced. Formulas which differ in the two cases are written in the form,

$X = (\text{energy formula}) \times \text{NDIF} + (\text{pressure formula}) \times (1 - \text{NDIF})$.

As stated previously, when a laser of sufficient intensity strikes a target surface, boiling and vaporization of the target may occur. Consider a control volume (as shown in Fig. 3.2) near the target surface, consisting of air and target vapor. If one assumes that the mixture is dilute, the species mass conservation equation for target vapor yields*,

$$\partial \rho_v / \partial t = -\text{div}(\rho_v \underline{v}_v). \quad (27)$$

The development of equation (27) may be found in Vincenti and Kruger [15]. According to the approach taken by Anisimov [16], conservation of energy in the control volume yields,

$$v_d = f_b / [\rho_o (L + CT_v)], \quad (28)$$

where v_d is the velocity of the vaporization front into the target, f_b is the incident laser flux, and ρ_o , L , C , and T_v are the target density, latent heat of vaporization, specific heat, and vaporization temperature. To determine T_v self-consistently at the elevated recoil pressure of the blow-off vapor, equation (28) is augmented by,

$$V_d = C_s \exp(-L/CT_v), \quad (29)$$

* In this development, the subscript, v , denotes target vapor.

where C_s is the speed of sound in the target material. Steady-state conservation of mass at the target surface requires that $\rho_v v_v = \rho_o v_d$, where v_d is given by equation (28). Thus ρ_v is found to be,

$$\rho_v = f_b / [v_v (L + CT_v)]. \quad (30)$$

Substitution of equation (29) into equation (28) yields,

$$f_b / [\rho_o (L + CT_v)] = C_s \exp(-L/CT_v). \quad (31)$$

From equation (31), CT_v is expressed by the transcendental equation,

$$CT_v = L / \ln [\rho_o C_s (L + CT_v) / f_b]. \quad (32)$$

Assuming that the blow-off vapor is a perfect gas, both calorically and thermally,

$$p_v = (\gamma - 1) \rho_v e_v = \rho_v CT_v (\gamma - 1).$$

Now,

$$p_v = \rho_v v_v^2,$$

so that

$$v_v = (p_v / \rho_v)^{1/2} = (\gamma - 1)^{1/2} (CT_v)^{1/2}.$$

Substituting this result into equation (30) yields,

$$\rho_v = f_b / [\Omega (\gamma - 1)^{1/2} (CT_v)^{1/2}], \quad (33)$$

where $\Omega \equiv L + CT_v$. The total energy in the vapor is,

$$E_v = \rho_v (e_v + v_v^2 / 2) = 0.5 \rho_v CT_v (\gamma + 1). \quad (34)$$

Substitution of equation (33) into equation (34) yields,

$$E_v = f_b (\gamma - 1) / (2 \Omega) [CT_v / (\gamma - 1)]^{1/2}. \quad (35)$$

The mass flux at the surface is,

$$\dot{M}_s = \rho_v v_v = f_b / \Omega. \quad (36)$$

One sees, therefore, that the evolution of target vapor is governed by the following equations:

$$\rho_v = f_b / [\Omega (\gamma - 1)^{1/2} (CT_v)^{1/2}], \quad (33)$$

$$E_v = f_b (\gamma + 1) / (2 \Omega) [CT_v / (\gamma - 1)]^{1/2}, \quad (35)$$

$$\rho_v v_v = f_b / \Omega. \quad (36)$$

With the velocity of the vaporization front into the target given by equation (28), it is possible to determine the depth to which the laser has penetrated the target at time, t . Denoting this depth by $\text{CHEW}(r,t)$,

$$\text{CHEW}(r,t) = \int_0^t v_d d\tau \approx \sum_i f_b(r,t) / (\rho_0 \alpha) \Delta t. \quad (36a)$$

The extent to which CHEW is advancing in time is an indication of how plasma effects are shielding the surface from laser radiation. One can therefore determine the time at which a surface-shielding LSD is formed.

Two key assumptions are implicit in the derivation of equations (33) through (36). First, it is assumed that the fraction of incident laser radiation (α) absorbed by the target is unity, although in general the derivation of the equations need not have a value of unity. According to Schwirzke [23], a critical density sublayer of plasma is formed at the target surface in the nanosecond range and the mechanism of unipolar arcing assures that $\alpha = 1$ once this sublayer is formed. The time frame of the laser pulse under study is in the microsecond range; therefore, α should approach 1 rapidly. When a LSD is ignited, α actually decreases due to dissipation of the critical density sublayer. However, the amount of laser attenuation, as discussed below, assures that the flux incident on the surface rapidly decreases as the LSD forms. For these

reasons, it is felt that the first assumption is valid for the problem under study. The second assumption is that the radial and axial conduction of heat into the target surface is negligible over the time of the pulse. From dimensional analysis of the one-dimensional heat conduction equation, the diffusion time required for radial conduction may be estimated as $t_r \approx r_s^2/\kappa$, where r_s is the laser spot radius and κ is the thermal diffusivity of the target material. Hall [2] gives r_s and κ to be 0.126 cm and 0.54 cm²/sec, respectively. Thus, $t_r \approx 30,000$ microseconds which is about three orders of magnitude larger than the laser pulse time of about 26 microseconds. This may also be compared to the characteristic time in the direction into the target. By the same reasoning this relaxation time, $t_z \approx d^2/\kappa$, where d is the target thickness (.028 cm), is $t_z \approx 1450$ microseconds. It is felt, then, that the second assumption is valid.

As a laser beam propagates through a gaseous medium, some of the laser energy is deposited in the medium. The amount of energy deposited depends on the absorption coefficient of the medium. Two absorption coefficients are used by HYDRO; a "cold" absorption coefficient representing absorption in molecular bands of the target vapor, and a "free-free" coefficient representing inverse bremsstrahlung absorption by electrons. These coefficients are defined as follows:

$$k_{cold} = C_1 \rho_v, \quad (37)$$

$$k_{ff} = C_2 n_e^2 / (kT)^{3/2},$$

where n_e is the electron equilibrium number density. The constant, C_1 , is chosen such that $C_1 \rho_o$ is the absorption coefficient of the bulk solid. The constant, C_2 , is given by Zeldovich and Raizer [17] to be,

$$C_2 = 4/3 (2\pi/3m)^{1/2} e^6 h^2 / [mc(h\nu)^2] \approx 4.05 \times 10^{-53}, \quad (38)$$

where m is the electronic mass, c is the speed of light, h is Planck's constant, e is the electronic charge, and ν is the laser frequency. The temperature in a cell, needed by equation (37) is found using the ideal gas equation of state, given by $p_i = \rho_i kT/m_i$ for species i , where m_i is the molecular weight of the i^{th} species. By Daltons Law of partial Pressures, $p = p_1 + p_2$, where the subscript 1 corresponds to air and the subscript 2 corresponds to target vapor. Therefore,

$$kT = m_1 m_2 p / (\rho_1 m_2 + \rho_2 m_1). \quad (39)$$

Equation (39) is the equation of state used by the original version of HYDRO. In order to account for high temperatures and pressures, this equation was modified by the author to

include the compressibility factor for air. The compressibility factor, Z , is defined by $p = \rho Z kT/m$. With the inclusion of Z , equation (39) becomes,

$$kT = m_1 m_2 p / (\rho_1 m_2 Z + \rho_2 m_1). \quad (40)$$

Now, p , ρ_1 , and ρ_2 are found from the hydrodynamic flow equations. The temperature may be found by an iterative process, such that equation (40) is satisfied. Once the temperature is found, the absorption coefficients given by equation (37) are determined.

Laser attenuation and energy deposition are illustrated by Fig. 3.7 below.

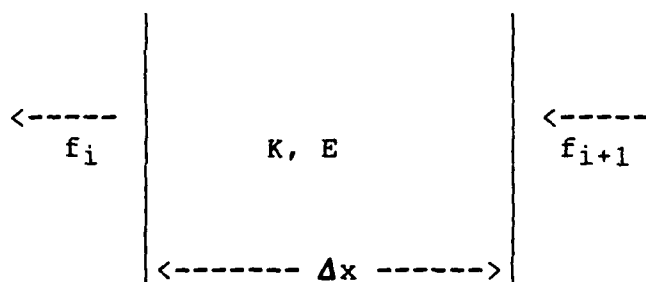


Fig. 3.7 Schematic of laser attenuation and energy deposition.

In Fig. 3.7, f_{i+1} is the laser flux entering the i th cell and f_i is the flux leaving the cell. Also, K is the total absorption coefficient in the cell and E is the rate of energy deposition in the cell. Using a first order

Taylor series expansion about the cell entrance, the flux leaving an arbitrary cell may be expressed by,

$$f_{out} = f + (\partial f / \partial x)dx, \quad (41)$$

where f is the flux entering the cell. Now, part of the flux, f , passes through the cell unattenuated; whereas, part of it is absorbed while in the cell. If the amount absorbed is given by $K_i f dx$, then the following equation must be true:

$$f_{out} + K_i f dx = f. \quad (42)$$

Substituting equation (41) into equation (42), one sees that

$$f = f + (\partial f / \partial x)dx + K_i f dx. \quad (43)$$

The f 's in equation (43) cancel each other and the resulting differential equation is separable. By separating the variables, one obtains,

$$df/f = -K_i dx \quad (44)$$

Equation (44) may be integrated from the inlet condition, cell $i+1$, to the exit condition, cell i . The result of the integration, when rearranged is,

$$f_i = f_{i+1} \exp(-K_i \Delta x). \quad (45)$$

Thus, the amount of laser attenuation is determined by equation (45), where K_i is taken to be the sum of K_{eff} and K_{cold} , given by equation (37). With f_i known, the time rate-of-change of energy density in the cell, due to laser deposition, is simply $\partial f / \partial x$, which is approximately $(f_{i+1} - f_i) / \Delta x$. Therefore,

$$\dot{E}_i = (f_{i+1} - f_i) / \Delta x. \quad (46)$$

In order to solve equations (45) and (46), the equilibrium electron number density, n_e , must be calculated. The calculation of n_e is done using a two material Saha equation that allows only single ionization. For single ionization only, there are five species present in equilibrium: A, B, A⁺, B⁺, and e⁻. The corresponding concentrations are N_A , N_B , N_A^+ , N_B^+ , AND n_e . Note that, as the final result of this development will show, it does not matter which species (air or target vapor) is denoted by A or B. The local equilibrium equations are:

$$N_A n_e R_I(A) = N_A^+ n_e^2 R_R(A), \quad (47)$$

$$N_B n_e R_I(B) = N_B^+ n_e^2 R_R(B), \quad (48)$$

where R_I is the ionization rate and R_R is the recombination rate. Equations (47) and (48) are subject to the "atom conservation" equations, given by:

$$N_A^+ + N_A = n_A, \quad (49)$$

$$N_B^+ + N_B = n_B, \quad (50)$$

$$N_A^+ + N_A = n_e, \quad (51)$$

where n_i is the number density of the i^{th} species.

Substitution of equations (49) and (50) into equations (47) and (48) yields:

$$n_A - N_A^+ = N_A^+ n_e R_R(A) / R_I(A), \quad (52)$$

$$n_B - N_B^+ = N_B^+ n_e R_R(B) / R_I(B), \quad (53)$$

Addition of equations (52) and (53) yields:

$$n_A + n_B - (N_A^+ + N_B^+) = n_e [N_A^+ R_R(A) / R_I(A) + N_B^+ R_R(B) / R_I(B)]. \quad (54)$$

By substituting equation (51) into equation (54), one obtains,

$$n - n_e = n_e [N_A^+ R_R(A) / R_I(A) + N_B^+ R_R(B) / R_I(B)] \quad (55)$$

where $n = n_A + n_B$. Equation (55), expressed in terms of n_A and n_B becomes:

$$n - n_e = n_e \left[\frac{n_A(n_e + S_B) + n_B(n_e + S_A)}{(n_e + S_A)(n_e + S_B)} \right], \quad (56)$$

where S_i is defined as R_i/R_R for the i th species. Equation (56) is a cubic equation in n_e . By letting $n_e = x - (S_A + S_B)/3$, one arrives at the following equation for x :

$$x^3 + ax + b = 0 \quad (57)$$

$$a = S_A S_B - n_A S_A - n_B S_B - 1/3 (S_A + S_B)^2, \quad (58)$$

$$b = 1/27 \left[2(S_A + S_B)^3 - 9(S_A + S_B)(S_A S_B - n_A S_A - n_B S_B) \right] - n S_A S_B. \quad (59)$$

Before equations (57) through (59) can be solved, S_A and S_B must be found. According to Zeldovich and Raizer [17], they are determined by the following relations:

$$S_A = G(kT)^{3/2} \exp(-I_A/kT), \quad (60)$$

$$S_B = G(kT)^{3/2} \exp(-I_B/kT), \quad (61)$$

where I_A and I_B are the ionization potentials of species A and B, and the constant, G , has the value, 2.98×10^{39} , when kT is expressed in ergs. With S_A and S_B determined by equations (60) and (61), the solution of equation (57) has been found by trial and error to be:

$$x = 2(-a/3)^{1/2} \cos(\phi/3), \quad (61)$$

where

$$\cos \phi = -b/2a(27/-a)^{1/2}. \quad (62)$$

With x given by equations (61) and (62), n_e is determined by the relation, $n_e = x - (S_A + S_B)/3$. The free-free absorption coefficient is determined by equation (37), and once K_{ff} is known, the energy deposition rate is given by equation (46). The total amount of laser energy deposition in the mesh is therefore approximated by:

$$E = \sum_i \sum_t (f_{i+1} - f_i) \Delta t / \Delta x (V_i), \quad (63)$$

where the first summation is over all axial cells, the second summation is over time, and V_i is the volume of the i th cell.

HYDRO is equipped to compute the mechanical effects of a LSD on the surface, and even though they are not of interest

in this study, they are discussed briefly in order that the reader may be able to understand how HYDRO operates. First, the total impulse delivered to the target may be approximated by:

$$I(t) \approx \sum_t \sum_j (p_j - p_{\text{ambient}}) A_j \Delta t, \quad (64)$$

where p_j is the pressure in the j^{th} radial cell at the target surface and A_j is the corresponding area of the cell. In equation (64), the first summation is over time and the second summation is over all radial cells at the surface. The spot impulse is defined as the impulse delivered over the irradiated area only and is found by equation (64), except that the second summation is now over all radial cells out to the cell at which laser radiation is effectively zero.

The time increment, Δt , has been mentioned several times thus far, but it has not been defined. It is important to note that, due to the presence of a LSD, Δt cannot be chosen arbitrarily or the LAX-Wendroff technique becomes unstable; rather, it must be chosen such that stability of the solution is assured. This is done by locating the maximum mass specific energy in the mesh and defining Δt by,

$$\Delta t = \beta \Delta x / (E / \rho)_{\text{max}}^{1/2}, \quad (65)$$

where E/ρ is defined by equation (8c). The factor, β , known as the "courant number" is normally taken to be 0.1. One sees, therefore, that equation (65) assures that a disturbance propagates no further than one tenth of a cell size during Δt . For further discussion of accuracy and stability criteria, the reader is referred to reference [14].

There are, however, two types of instabilities which will be discussed here. The first arises when the pressure gradient and velocity are in the same direction. This situation may occur near the surface in the presence of highly ionized target vapor. HYDRO is modified to handle this problem and the modification is discussed in detail by Nielsen [11]. It suffices to say here that the effect of the modification is to prevent the Lax-Wendroff technique from giving negative pressures and temperatures in the cell previous to the LSD front. The other instability arises due to the fact that HYDRO is inviscid in nature, and no dissipative mechanisms are used in solving the flow equations. With this approach, the LSD front is a numerical discontinuity, and modification in the neighborhood of the front is necessary. HYDRO does the modification by introducing an "artificial diffusion" factor, discussed in detail in reference [11]. Briefly, stated, the diffusion factor has the effect of spreading the LSD front over several cells, while assuring that the

Rankine-Hugoniot equations {18} are satisfied on either side of these cells.

In summary, HYDRO solves the inviscid flow equations for a mixture of air and target vapor, through which laser energy is propagating. In this section, these equations were derived for the cylindrical control volume of interest. The finite-difference technique used to solve the equations was discussed and the difference equations were derived. Finally, the topics of laser-target interaction and laser attenuation were discussed.

IV. Convection Heat Transfer

As stated in the introduction, the first object of this study was to perform detailed calculations of the convection heat transfer taking place at the target surface, under the presence of a LSD. In this section, the method used to perform these calculations is discussed in detail. Numerous relations exist, by which one can compute the amount of convective heat transfer to a surface, over which a fluid is flowing. The relation that one chooses to use depends on the particular flow situation. A flow field may be considered to consist of an inviscid, far region, or external flow field, and a viscous, near region, or boundary layer. Resistance to the transfer of heat between a surface and a fluid is confined to the boundary layer. In this region the physical processes are governed by the viscous flow and energy equations.

The external flow field is provided by HYDRO, as described in Section III. For the problem at hand, the field closely resembles that of axisymmetric three-dimensional stagnation flow. As given by Schlichting [19], the radial velocity component for such a flow is,

$$u_r = ar, \quad (66)$$

where a is a constant and r is the radius from the axis of

symmetry. The radial velocity is plotted in Fig. 5, from which one sees that the flow, out to the LSD front, is closely approximated by equation (66). There exists an exact solution to the Navier-Stokes equations for 3-D stagnation flow. This solution is given by Schlichting, but is rederived here for completeness. The Navier-Stokes equations for axisymmetric flow are:

$$u \frac{\partial u}{\partial r} + w \frac{\partial u}{\partial z} = (-1/\rho) \frac{\partial p}{\partial r} + \nu \left[\frac{\partial^2 u}{\partial r^2} + (1/r) \frac{\partial u}{\partial r} - u/r^2 + \frac{\partial^2 u}{\partial z^2} \right], \quad (67)$$

$$u \frac{\partial w}{\partial r} + w \frac{\partial w}{\partial z} = (-1/\rho) \frac{\partial p}{\partial z} + \nu \left[\frac{\partial^2 w}{\partial r^2} + (1/r) \frac{\partial w}{\partial r} + \frac{\partial^2 w}{\partial z^2} \right], \quad (68)$$

$$\frac{\partial u}{\partial r} + u/r + \frac{\partial w}{\partial z} = 0 \quad (69)$$

where $\underline{v} = u\underline{e}_r + w\underline{e}_z$. The boundary conditions are:

$$\text{at } z = 0, \quad u = 0 \text{ and } w = 0, \quad (67a)$$

$$\text{at } z = \infty, \quad u = U, \quad (68a)$$

where U is the velocity of the external flow field. Note that equations (67) through (69) are for steady-state, incompressible flow with no body forces. Neglecting the effect of gravity, there are no body forces for the problem under study. The assumptions of steady, incompressible flow are, strictly speaking, incorrect for this problem;

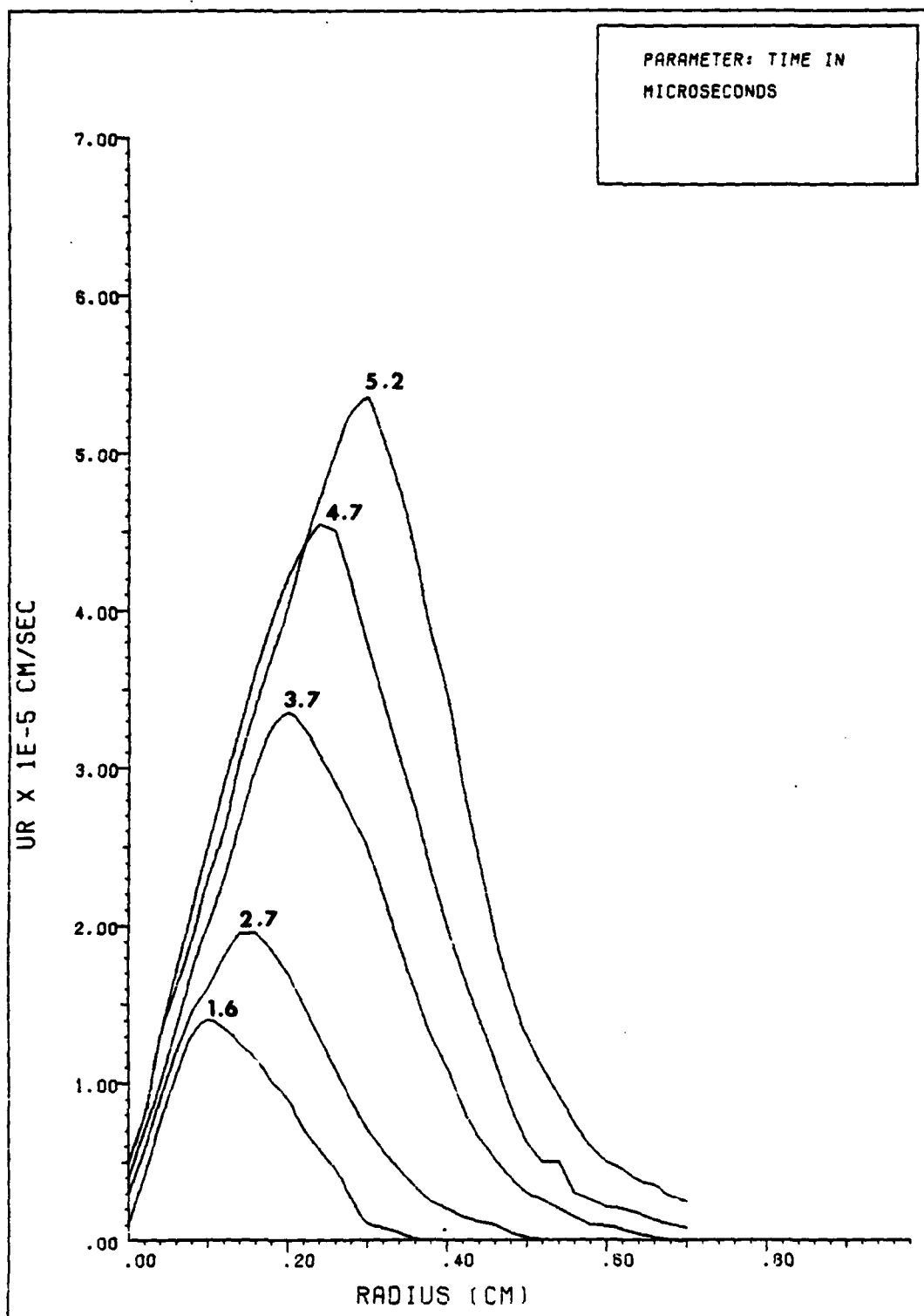


FIG. 5: RADIAL VELOCITY COMPONENT GIVEN BY HYDRO

however, it is felt that the information provided with these assumptions will be qualitatively correct and quite useful in the analysis which follows. These ideas are discussed in more detail later.

In ideal 3-D stagnation flow, the stagnation pressure is related to the local pressure by,

$$p_0 = p + \rho/2(v^2) = p + \rho/2(a^2)(r^2 + 4z^2), \quad (70)$$

where p_0 is the pressure at the stagnation point, p is the local pressure, z is the axial distance from the stagnation point opposite the direction of the impinging flow, and the external velocity, $\underline{U} = ar\underline{e}_r - 2az\underline{e}_z$. Here, a and r are the same as in equation (66). For the viscous boundary layer flow, the following forms of the solutions for the velocity and pressure distributions are assumed:

$$u = rf'(z), \quad (71)$$

$$w = -2f(z), \quad (72)$$

$$p_0 - p = \rho a^2/2(r^2 + F(z)). \quad (73)$$

Substitution of equations (71) through (73) into equations (67) through (69) yields:

$$f'^2(z) - 2f(z)f''(z) = a^2 + \nu f'''(z), \quad (74)$$

$$2f(z)f'(z) = a^2F'(z)/4 - \nu f''(z). \quad (75)$$

The boundary conditions given by equations (67a) and (68a) become:

$$\text{at } z = 0, f = 0, f' = 0, \text{ and } F = 0, \quad (74a)$$

$$\text{at } z = \infty, f' = a. \quad (75a)$$

Using the similarity transformation, $\xi = (a/\nu)^{1/2}z$ and $f(z) = (a\nu)^{1/2}\phi(\xi)$, equation (74) reduces to,

$$\phi'''' + 2\phi\phi'' - \phi'^2 + 1 = 0, \quad (76)$$

with the boundary conditions given by,

$$\text{at } \xi = 0, \phi = 0 \text{ and } \phi' = 0, \quad (76a)$$

$$\text{at } \xi = \infty, \phi' = 1. \quad (76b)$$

Equation (76) is handily solved by classical Runge-Kutta methods. Following the method outlined by Hornbeck [20], let $x_1 = \phi$, $x_2 = x_1'$, and $x_3 = x_2'$. By doing so, equations (76), (76a), and (76b) are transformed to the following matrix system:

$$X' = H(\xi, X), \quad (77)$$

$$H(\xi, X) = [x_2 \quad x_3 \quad -2x_1x_3 + x_2^2 - 1]^T, \quad (78)$$

$$X(0) = X_0 = [0 \quad 0 \quad K]^T, \quad (79)$$

where K must be found such that $\phi'(\infty) = x_2(\infty) = 1$.

The algorithm used consists of the following steps:

- (1) Guess a value for K ,
- (2) Compute $X^* = X_n + \Delta \xi / 2H(\xi_n, X_n)$,
- (3) Compute $M^* = H(\xi_n + \Delta \xi / 2, X^*)$,
- (4) Compute $X^{**} = X_n + \Delta \xi / 2M^*$,
- (5) Compute $M^{**} = H(\xi_n + \Delta \xi / 2, X^{**})$,
- (6) Compute $X^{***} = X_n + \Delta \xi M^{**}$,
- (7) Compute $M^{***} = H(\xi_n + \Delta \xi, X^{***})$,
- (8) Compute $M = 1/6 [H(\xi_n, X_n) + 2M^* + 2M^{**} + M^{***}]$,
- (9) Compute $X_{n+1} = X_n + \Delta \xi M$,
- (10) Perform steps (2) through (9) until ξ sufficiently approaches infinity,
- (11) If $x_2(\xi \infty)$ is sufficiently close to 1, the calculation is complete,
- (12) If step (11) is not satisfied, guess a new value for K and perform the above steps again.

For the solution of equation (76), it was assumed that $\xi = 10$ is sufficiently close to infinity, and X_0 is given by equation (79). Using $\Delta \xi = 0.01$, K was found to be 1.312. The calculated values of ϕ , ϕ' , and ϕ'' are plotted in

Fig. 6. The above method is a fourth order method, which is to say that it is accurate to the order of $(\Delta \xi)^4$.

The boundary layer thickness, δ , is traditionally defined as the value of z at which the velocity is equal to 0.99 times the free stream value, U . In terms of the quantities plotted in Fig. 6, $\phi' = u/U$, and from the Runge-Kutta solution, the value of ξ at which $u/U = 0.99$ is about 1.98. From the definition of ξ , one sees that,

$$(a/\nu)^{1/2} \delta = 1.98. \quad (80)$$

Knowing the stagnation flow constant, a , and the kinematic viscosity, ν , the boundary layer thickness may be calculated from equation (80). The kinematic viscosity is known for each cell from the dynamic viscosity, given in Appendix A, and the fluid density, available from HYDRO. The constant, a , however, is somewhat troublesome as it is not actually constant; rather, it changes with time. Equation (80) is a steady-state equation which indicates that there may be a conflict with using the stagnation flow solution. It is felt by the author and others [3] that the problem may be treated as pseudo-steady, yielding qualitatively good results, if the following conditions are met:

- (1) the "constant," a , settles down with time,
- (2) the time required to establish the boundary layer is small compared to the laser pulse time.

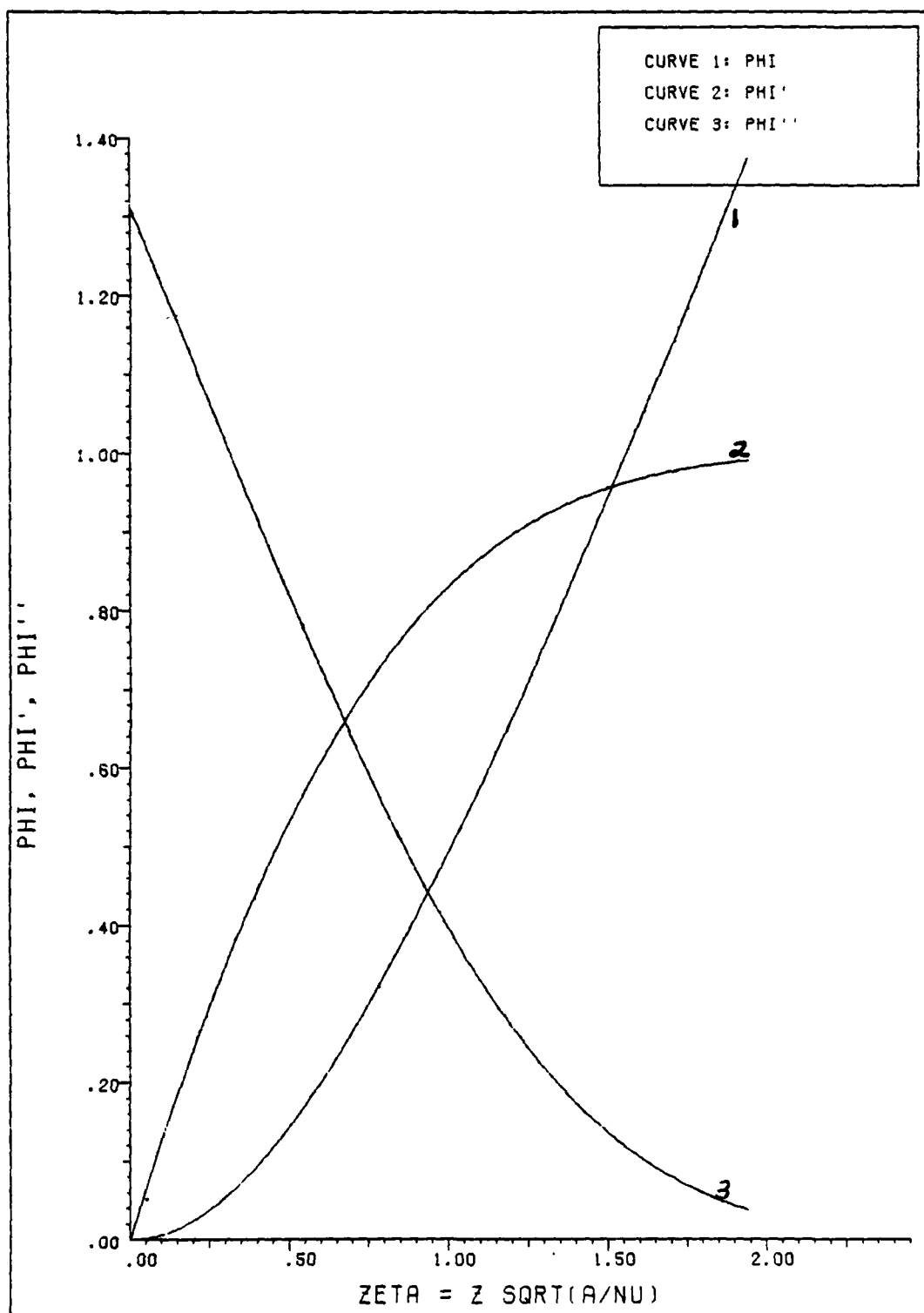


FIG. 6: BOUNDARY LAYER SIMILARITY SOLUTIONS

Even though the pseudo-steady solution is an approximation, it should identify the relative role of convective heat transfer on enhanced thermal coupling. This is especially true since the amount of numerical data available for analysis is limited to about one third of the pulse time, and many results are projected from trends during latter times of the data.

The time-dependent constant, a , was determined from the data plotted in Fig. 5. The curves in this plot show that, prior to the LSD front, the radial velocity component is closely approximated by equation (66). The slope of the linear portion of a curve for time, t , is $a(t)$. By looking at the data for twelve representative times (from 1.59 microseconds to 8.2 microseconds), $a(t)$ was determined and plotted in Fig. 7. The reason only twelve times were considered is that, in order to limit the amount of output, HYDRO was modified to output data at every 20th time step (cycle), and due to limited computer resources, only twelve sets of output were possible. Referring to Fig. 7, curve 1 is the computed numerical data and, though the data goes only to 8.2 microseconds, the following trend was noticed: $a(7.5) \approx 1/2a(7.0)$, $a(7.9) \approx 1/2a(7.5)$, and $a(8.2) \approx 1/2a(7.9)$. Based on this trend, it was projected that $a(t)$, for the entire pulse time, may go something like curve 1. Curve 2 is a forced fit to curve 1, chosen so as

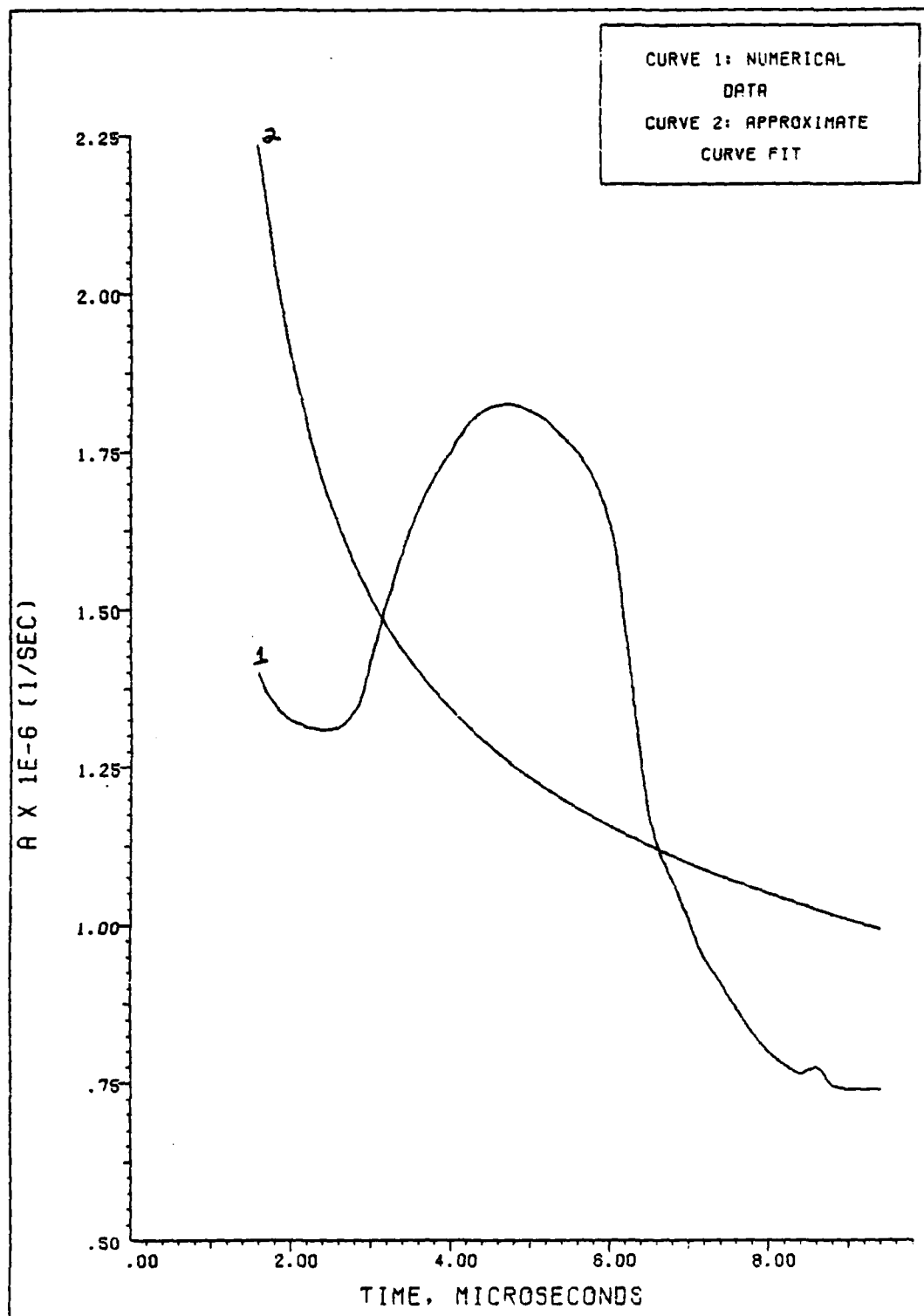


FIG. 7: STAGNATION FLOW FIELD "CONSTANT"

to approximate the general trend of $a(t)$. The equation of curve 2 is:

$$a(t) \times 10^{-6} = 0.76 \exp(0.35915 - 0.02339t + 1.2118/t), \quad (81)$$

for times less than 18 microseconds, and,

$$a(t) \times 10^{-6} = 0.76, \quad (82)$$

for times greater than 18 microseconds. In equation (81), t is in microseconds. The time-average value of $a(t)$ was found from the definition:

$$\bar{a} = 1/\tau_p \int_0^{\tau_p} a(t) dt, \quad (83)$$

where τ_p is the laser pulse time and \bar{a} is the time-averaged value of $a(t)$. From equations (81) through (83), \bar{a} was found to be about $0.95 \times 10^6 \text{ sec}^{-1}$. It is felt, then, that by replacing a , in the steady-state equations, with \bar{a} , the steady-state equations will yield qualitatively good results for the unsteady flow. Also, if the projection of $a(t)$ at latter times, in Fig. 7, approximates the true behavior (which is unknown due to lack of data), then condition (1) of the pseudo-steady requirements discussed earlier is satisfied, in that $a(t)$ does indeed settle down with time.

The boundary layer thickness is given by equation (80). The temperature in the LSD front, at the target surface, is about 11,000 degrees Kelvin. From Appendix A, the dynamic viscosity at this temperature is about 2.25×10^{-3} gm/(cm-sec), and the density, taken from HYDRO, is about 0.95×10^{-4} . The kinematic viscosity, ν , is about 23.7 (cm²/sec), and, from equation (80), δ is about 1.0×10^{-2} cm. The time required to establish a boundary layer of thickness, δ , may be approximated by the relation given by Schlichting [19] as: $t \approx \delta^2/4\nu$. It is interesting to note that, according to equation (80), the time required to establish a boundary layer in 3-D stagnation flow is independent of flow properties; rather, it is fully determined by the stagnation flow constant defined by equation (66). Using this relation, the time required to establish the boundary layer is about one microsecond, which is about four percent of the pulse time, 25.73 microseconds. Thus, condition (2) of the pseudo-steady requirements is satisfied, in that the time required to establish the boundary layer is short compared to the laser pulse time.

With the above fundamental boundary layer concepts in hand, and with the confidence that the solution may be treated as pseudo-steady, the convection heat transfer may now be calculated. In the presence of a LSD, fluid temperatures are sufficiently high that chemical

dissociation occurs. Consequently, the thermodynamic and transport properties of the fluid (air, in this case) vary greatly across the boundary layer. For these types of problems, Eckert [22] has recommended use of the reference enthalpy technique in computing heat transfer. Eckert reports [22] that this technique yields fairly accurate results (to within $\pm 20\%$ of experimentally measured values), even in the presence of compressibility, fluid property variation, and chemical dissociation. The reference enthalpy technique is, however, a steady-state technique. Therefore, before using it to calculate the convection heat transfer for a particular flow situation, one must verify that the flow may be approximated as being steady.

The radial temperature distribution at the target surface, as given by HYDRO, in the presence of the LSD ignited by Hall's 9.3 J pulse, is plotted in Fig. 8. Referring to this plot, one sees that temperatures on the order of 11,000 degrees Kelvin are present; therefore, the reference enthalpy technique was chosen to perform the convection heat transfer calculations. It is felt that use of the method is justified, in view of previous arguments that the boundary layer flow is pseudo-steady in nature. Using this technique, the convection heat transfer coefficient is defined by:

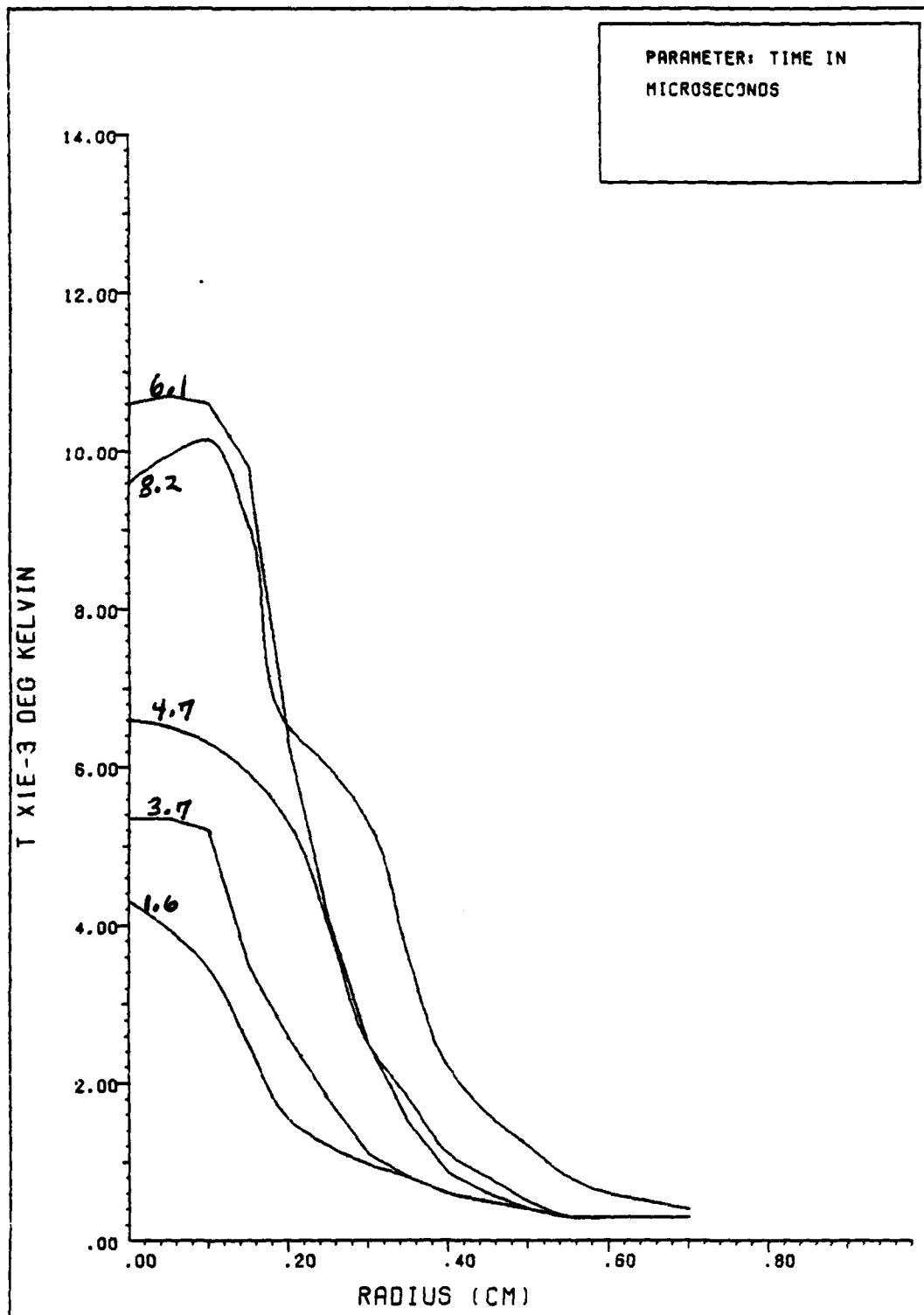


FIG. 8: TEMPERATURE PROFILE GIVEN BY HYDRO

$$\dot{q} = -Ah_i (i_w - i_r), \quad (84)$$

where q is the rate of heat addition to the target, A is the area over which the heat addition is taking place, h_i is the convection heat transfer coefficient, i_w is the mass specific enthalpy of the fluid at the target surface, and i_r is the recovery enthalpy of the fluid at the edge of the boundary layer. According to Eckert [22], the recovery enthalpy, in the neighborhood of a 3-D stagnation point, is given by,

$$i_r = i_e + 1/2 Pr^{1/2} u_e^2, \quad (85)$$

where i_e is the mass specific enthalpy at the edge of the boundary layer, u_e is the corresponding fluid velocity and Pr , the Prandtl number, is present as a recovery factor for high speed flow. Thus, one sees that, if h_i is known, the amount of convection heat transfer per unit area is easily determined by equation (84), with i_r given by equation (85). The problem, therefore, consists primarily of finding h_i . According to Eckert [22], if the external flow field is that of 3-D stagnation flow, h_i may be found from the following expression:

$$Nu_i = 0.763 (Pr_i)^{0.4} (Re_i)^{0.5}, \quad (86)$$

where Nu_i is the Nusselt number, Pr_i is the Prandtl number, and Re_i is the Reynolds number. In equations (84) and (86), the subscript, i , denotes that the properties must be evaluated at the reference enthalpy temperature (T_{ref}) which is determined from the following relation:

$$i_{ref} = i_e + 0.5(i_w - i_e) + 0.22(i_r - i_e), \quad (87)$$

where i_{ref} is the reference enthalpy. The nondimensional numbers appearing in equation (86) are defined as follows:

$$Nu_i = c_{p_i} h_i r / k_i, \quad (88)$$

$$Pr_i = \mu_i c_{p_i} / k_i, \quad (89)$$

$$Re_i = u_e r / \nu_i, \quad (90)$$

where r is the radius from the axis of symmetry. Note that the definition of the Nusselt number in equation (88) differs from the traditional definition by the factor, c_{p_i} . This is due to the fact that h_i is defined in terms of enthalpy differences rather than temperature differences. From equation (66), $u_e = \bar{a}r$, where a has been replaced by the time-average value of $a(t)$, found previously. With this result, equations (85) and (90) become:

$$i_r = i_e + 1/2 \text{Pr}^{1/2} (\bar{a}r)^2, \quad (91)$$

$$\text{Re}_i = \bar{a}r^2 / \nu_i. \quad (92)$$

Substitution of equations (88), (89), and (92) into equation (86) yields:

$$h_i = 0.763 (\bar{a})^{1/2} \rho_i^{1/2} \mu_i^{-0.1} (k_i / c_{p_i})^{0.6}, \quad (93)$$

where $\bar{a} = 0.95 \times 10^6 \text{ sec}^{-1}$.

The algorithm for computing the convection heat transfer is now complete and consists of the following steps:

- (1) Obtain T and pressure from HYDRO,
- (2) Compute i_e from the curve fit given in Appendix A,
- (3) Compute i_r from equation (91),
- (4) Compute i_{ref} from equation (87),
- (5) Compute T_{ref} by iteration, such that the curve fit yields i_{ref} ,
- (6) Compute μ_i , k_i , ρ_i and c_{p_i} at T_{ref} , using the curve fits given in Appendix A,
- (7) Compute h_i from equation (93),
- (8) Compute \dot{q}/A from equation (84).

The above algorithm is used to compute the heat transfer out to the radius at which the temperature is approximately equal to the ambient temperature, taken to be the standard temperature of 0°C. The target temperature is taken to be the same standard temperature. The last assumption is not correct since, if target vaporization is taking place, the surface temperature in these regions is essentially at the vaporization temperature appropriate for the local pressure; this will always be much higher than 0°C. Therefore, the heat transfer obtained with the assumption should be higher than the true value. Also, it is important to note that in front of the LSD, where flow velocities are small, the actual values of the local edge velocity given by HYDRO are used in computing the heat transfer. This correction to the above algorithm is necessary since u_e , as defined by equation (66), is valid only to the LSD front.

Due to limited computer resources, the heat transfer calculations are done by a separate program, for which the input data is the output from HYDRO. This program is listed in Appendix C.

In summary, it is necessary to assess the flow situation and to predict a few fundamental boundary layer quantities before one chooses a method by which to compute the amount of convection heat transfer taking place. The determination of whether the boundary layer flow may or may

not be approximated as steady-state is of particular importance, as most known solutions are for steady flow. Also, it is important to predict the effect of compressibility on the boundary layer, as flow properties may change drastically across the boundary layer. In this section, it was deduced from the hydrodynamic data that the external flow field for the problem under study closely resembles that of three-dimensional axisymmetric stagnation flow. The boundary layer thickness and the time required to establish the boundary layer were estimated from the compressible, steady flow boundary layer solutions. From these considerations, it was concluded that the boundary layer flow may be treated as pseudo-steady. High fluid temperatures and the possible effects of compressibility and property variations on the heat transfer solution led to the choice of Eckert's reference enthalpy technique as the method used to compute the heat transfer, since this technique is known to give fairly good results in the presence of such factors. Finally, the algorithm used to compute the heat transfer was presented. The results of these calculations are presented in Section VII.

V. Vapor Condensation

As stated in the introduction, the second object of this study is to examine the role of vapor condensation on enhanced coupling. In this section, the method used to calculate the amount of thermal energy imparted to the target by condensing target vapor is discussed in detail. The motivation for performing these calculations was stated in the introduction and is not repeated here. It is noted, however, that the presence of a high-pressure LSD is required for vapor condensation to take place because it is the high pressures associated with the LSD that force the evolved target vapor back onto the surface. In this section, therefore, the presence of a LSD is inherently assumed.

When a mixture of air and target vapor passes over a surface, the vapor species is deposited so as to remove energy, mass, and momentum from the flow. According to Jackson [24, 25], these quantities are determined from simple Maxwell-Boltzmann statistics. The Maxwellian velocity distribution function is given by Vincenti and Kruger [15] to be:

$$f(C_i) = (m/2\pi kT)^{3/2} \exp[-m/2kT(C_1^2 + C_2^2 + C_3^2)], \quad (94)$$

where m is the mass of the vapor particles, T is the temperature of the vapor particles, C_1 is the radial velocity component, C_2 is the velocity component in the angular direction, and C_3 is the axial velocity component. Equation (94) gives the probability that a given molecule chosen at random will have velocity in the range C_1, C_2, C_3 to $C_1 + dC_1, C_2 + dC_2, C_3 + dC_3$. It is assumed that, for this problem, vapor particles immediately above the target surface impinge upon the surface with the instantaneous velocity, C_3 , relative to the surface. Furthermore, it is assumed that all vapor particles which come into contact with the surface will be attached to it where they will condense and return to the target the energy required to vaporize them as well as the thermal kinetic energy gained while in the vapor state. The last assumption needs verification and, according to Levine and Gyftopoulos [26], virtually every particle which comes into contact with the surface does attach to the surface, where it condenses.

With the above assumptions, the flux of quantity, F_j , into the target surface may be calculated from the following relations:

$$F_j = n \int_0^\infty \int_{-\infty}^\infty \int_{-\infty}^\infty \bar{F}_j f(C_1) C_3 dC_2 dC_1 dC_3, \quad (95)$$

where n is the particle number density, \bar{F}_j is the quantity imparted to the surface by vapor collisions, $f(C_i)$ is given by equation (94), and the axial velocity goes from zero to $-\infty$ since it is zero at the surface and the impingement is in the negative axial direction. The F_j and \bar{F}_j in equation (95) are given by:

$$F_1 = \text{mass flux, } \dot{m},$$

$$F_2 = \text{energy flux, } \dot{q},$$

$$F_3 = \text{normal momentum flux, } \dot{M}_3,$$

$$F_4 = \text{radial momentum flux, } \dot{M}_4,$$

$$\bar{F}_1 = \text{mass, } m,$$

$$\bar{F}_2 = \text{kinetic energy, } mC^2/2,$$

$$\bar{F}_3 = \text{normal momentum component, } mC_3,$$

$$\bar{F}_4 = \text{radial momentum component, } mC_1,$$

where $C^2 = C_1^2 + C_2^2 + C_3^2$.

Therefore,

$$\dot{m} = n \int_0^\infty \int_{-\infty}^\infty \int_{-\infty}^\infty mC_3 f(C_i) dC_2 dC_1 dC_3, \quad (96)$$

$$\dot{q} = n \int_0^\infty \int_{-\infty}^\infty \int_{-\infty}^\infty (mC^2/2 + mL_v) C_3 f(C_i) dC_2 dC_1 dC_3, \quad (97)$$

$$\dot{M}_3 = n \int_0^\infty \int_{-\infty}^\infty \int_{-\infty}^\infty mC^2 f(C_i) dC_2 dC_1 dC_3, \quad (98)$$

$$\dot{M}_4 = n \int_0^\infty \int_{-\infty}^\infty \int_{-\infty}^\infty mC_1 C_3 f(C_i) dC_2 dC_1 dC_3. \quad (99)$$

The appearance of the latent heat of vaporization, L_v , in equation (97) is due to the fact that condensing particles must return the energy originally required to vaporize them. The mass flux of particles is calculated by inserting equation (94) into equation (96),

$$\dot{m} = n \int_0^{\infty} (m/2 \pi kT)^{3/2} m C_3^2 \exp(-m C_3^2/2kT) dC_3 I_1^2, \quad (96a)$$

where $I_1 = \int_{-\infty}^{\infty} \exp(-mx^2/2kT) dx^*$. I_1 is given by Vincenti and Kruger [15] to be $(2 \pi kT/m)^{1/2}$. Equation (96a) becomes,

$$\dot{m} = mn(2 \pi kT/m) (m/2 \pi kT)^{3/2} \int_0^{\infty} C_3 \exp(-m C_3^2/2kT) dC_3. \quad (96b)$$

Performing the integration, equation (96b) becomes,

$$\dot{m} = mn(2 \pi kT/m) (m/2 \pi kT)^{3/2} kT/m. \quad (96c)$$

The term, mn , is defined to be the vapor density; thus, the mass flux is given by:

$$\dot{m} = \rho_v (kT/2 \pi m)^{1/2}. \quad (100)$$

* In this section, x and y are dummy integration variables.

The energy flux imparted to the surface by condensing vapor particles is determined by inserting equation (94) into equation (97),

$$\begin{aligned} \dot{q} = & A \int_0^{\infty} \int_{-\infty}^{\infty} \int_{-\infty}^{\infty} \frac{1}{2} C_3^3 \exp[B(C_1^2 + C_2^2 + C_3^2)] dC_2 dC_1 dC_3 + \\ & 2A \int_0^{\infty} \int_{-\infty}^{\infty} \int_{-\infty}^{\infty} \frac{1}{2} C_3 x^2 \exp[B(x^2 + y^2 + C_3^2)] dy dx dC_3 + \\ & AL_v \int_0^{\infty} \int_{-\infty}^{\infty} \int_{-\infty}^{\infty} C_3 \exp[B(x^2 + y^2 + C_3^2)] dy dx dC_3, \end{aligned} \quad (97a)$$

where $A = mn(m/2\pi kT)^{3/2} = \rho_v(m/2\pi kT)^{3/2}$ and $B = -m/2kT$.

Denoting the first triple integral in equation (97a) by

I_2 ,

$$I_2 = A/2 \int_0^{\infty} C_3^3 \exp(BC_3^2) dC_3 I_3^2, \quad (97b)$$

where $I_3 = \int_{-\infty}^{\infty} \exp(Bx^2) dx$. I_3 is given by Vincenti and Kruger [15] to be $(2\pi kT/m)^{1/2}$. Equation (97b) becomes,

$$I_2 = A(2\pi kT/m)/2 \int_0^{\infty} C_3^3 \exp(BC_3^2) dC_3. \quad (97c)$$

The integral in equation (97c) is given [15] to be

$1/2B^2$. Thus, with the insertion of A and B, equation (97c) becomes,

$$I_2 = A/(4\pi^2) (2\pi kT/m)^3. \quad (97d)$$

Denoting the second triple integral in equation (97a) by I_4 ,

$$I_4 = I_3 I_5 / 2 \int_0^{\infty} A C_3 \exp(B C_3^2) dC_3, \quad (97e)$$

where $I_5 = \int_{-\infty}^{\infty} x^2 \exp Bx^2 dx$, given [15] to be $1/(2\pi)(2\pi kT/m)^{3/2}$. Evaluating the integral in equation (97e) and inserting the above values for I_3 , I_5 , A , and B , equation (97) becomes,

$$I_4 = A / (4\pi^2) (2\pi kT/m)^3. \quad (97f)$$

The third triple integral in equation (97a) is simply $\dot{m}L_V$; therefore, the energy flux is determined to be,

$$\dot{q} = \dot{m}(2kT/m + L_V). \quad (101)$$

An approach similar to that taken above shows that \dot{M}_3 and \dot{M}_4 are, respectively, $\rho_V/2$ (kT/m) and zero. The derivation is not included here, however, since the amount of thermal coupling is determined completely by equations (100) and (101).

In summary, it is felt that vapor particles passing over the target surface will become attached to it; thereby imparting the flux of mass, energy, and momentum to the

target. The energy contained by the particles is believed to be greater at the time of condensation than at the time of evolution due to the fact that they gain kinetic energy while in the vapor state. In this section, simple Maxwell-Boltzmann kinetic theory is used to evaluate the amount of mass, energy, and momentum imparted to the surface by the condensing particles. The fluid properties needed for the calculations are available from HYDRO and the results of these calculations are presented in Section VII.

VI. Radiation Heat Transfer

The third and final object of this study is to estimate the effect of plasma radiation on enhanced coupling. When a LSD is ignited at the target surface, it propagates up the laser beam and, due to its high absorptivity, it absorbs practically all of the incident laser radiation. It is assumed that some or all of this absorbed radiation will be radiated away from the plasma by various mechanisms. This process is referred to as plasma reradiation. The problem is to describe which processes are responsible for plasma reradiation and to estimate the amount of energy imparted to the target by these processes.

According to Dawson (27), there are two regimes of plasma reradiation: bremsstrahlung radiation and blackbody radiation. At a given point in space and time, the type of radiation present is determined by the absorption length of the plasma. The absorption length, l , is by definition the inverse of the free-free absorption coefficient given by equation (37) of Section III. According to Dawson, if l is less than the plasma radius (or thickness for a planar plasma) the radiation is blackbody and, if l is greater than the plasma radius (or thickness) the radiation is bremsstrahlung.

For bremsstrahlung radiation, the volumetric rate of radiation is given by Dawson (27) to be,

$$\epsilon = 4.86 \times 10^{-31} Z n_e^2 T^{1/2} \quad (102)$$

where ϵ is the volumetric rate in watts per cubic centimeter, Z is the degree of ionization, n_e is the electron number density, and T is the temperature in kiloelectron volts. The maximum temperature in the numerical mesh, as given by HYDRO, is only about 0.002 kiloelectron volts for the problem under study; therefore, the degree of ionization is assumed to be one. Actually, this assumption is implicit in that HYDRO uses the Saha equation for singly ionized species in the derivation of the electron number density. With this assumption, equation (102) becomes,

$$\epsilon = 1.427 \times 10^{-34} n_e^2 T^{1/2}. \quad (103)$$

where T is now in degrees Kelvin. Inserting equation (37) into equation (103) yields:

$$\epsilon = 5.715 \times 10^{-6} K_{ff} T^2. \quad (104)$$

Assuming that the LSD front is planar, its volume is simply its thickness times its cross-sectional area. From HYDRO, it appears that the thickness of the LSD is on the order of 0.1 centimeters. Actually, the thickness is expected to be less than that deduced from HYDRO due to the fact that the artificial diffusion has the effect of spreading the front such that it appears to be thicker than it really is. It is felt, therefore, that using the thickness predicted by HYDRO yields the maximum radiation possible. With the above assumption, the heat flux leaving the plasma due to bremsstrahlung radiation is,

$$\dot{q} = 5.715 \times 10^{-7} k_{ff} T^2, \quad (105)$$

where \dot{q} is the heat flux in watts per square centimeter. It is not expected that all of the radiation which leaves the plasma will reach the target surface; thus, the inclusion of a radiation shape factor, as discussed by Holman [21], should be made in equation (105). Furthermore, it is not expected that all of the radiation incident on the target surface will be absorbed; therefore, the inclusion of a surface absorptivity should be made in equation (105). As discussed in Section III, the absorptivity of the surface may be assumed to be unity in very early times due to the mechanism of unipolar arcing. However, once a LSD is formed, the absorptivity of the surface rapidly decreases.

Based on these ideas, it is felt by the author that the heat flux absorbed by the surface due to bremsstrahlung radiation is greatly overestimated by equation (105). In fact, it is suspected that the predicted value may be an order of magnitude greater than the true value. Thus, equation (105) should yield the maximum possible value of thermal coupling due to bremsstrahlung radiation from the LSD front. It is noted that the above model neglects reradiation from bound electrons and from recombination but, according to Dawson [27], these processes are unimportant for plasma temperatures below the order of one hundred electron volts. Since the maximum temperature for this problem is on the order of two electron volts, it is felt that these processes do not contribute to the plasma radiation.

According to Dawson, [27], blackbody radiation is negligible for plasma temperatures below the order of several hundred electron volts; therefore, it is not addressed in this study.

In summary, the type of plasma reradiation present is determined by the absorption length of the LSD front. The model presented by Dawson [27] was used to estimate the heat flux absorbed by the target due to bremsstrahlung radiation from the plasma, given by equation (105). It is felt that this equation will greatly overestimate the

amount of radiation absorbed, due to the absence of a surface absorptivity and a radiation shape factor in the equation. Blackbody radiation is, according to Dawson [27], negligible for the problem under study. The results of the bremsstrahlung radiation estimates are presented in Section VII.

VII. Results

In this section, the results of the calculations discussed in the previous sections are presented. It is of utmost importance to note that the results of this study are based on a limited amount of numerical data, as stated in the introduction. Nevertheless, the author feels that the results are qualitatively correct and that the relative roles of convection heat transfer, vapor condensation, and radiation heat transfer on enhanced coupling are accurately predicted from these results.

The amount of convection heat transfer taking place at the target surface under the presence of a LSD was calculated from the algorithm given in Section IV. The resulting heat flux into the surface is plotted, as a function of radius from the axis of symmetry with time as a parameter, in Fig. 9. Referring to Fig. 9, one sees that at early times, prior to the ignition of a LSD, the convection heat transfer is quite small. This result is consistent with the theory that it is the presence of the LSD which facilitates enhanced coupling. After the LSD is ignited (at about 5 microseconds, as discussed later), one sees from Fig. 9 that the convection heat transfer increases by a factor of about 7. As time progresses, however, one sees that the convection heat transfer appears to converge to a radial distribution with no dependence on

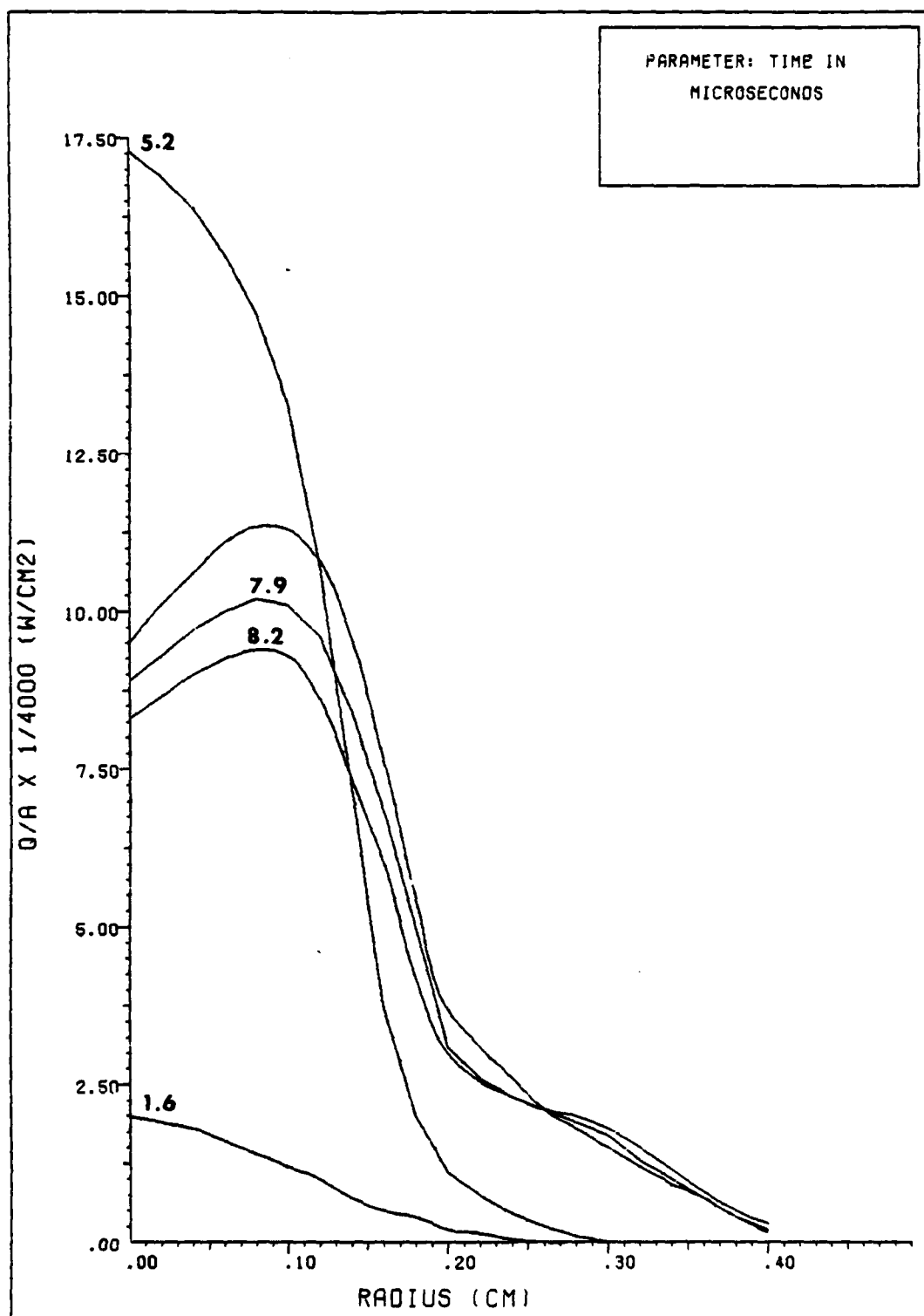


FIG. 9: HEAT FLUX DUE TO CONVECTION HEAT TRANSFER

time. The time for this convergence is at about 7 microseconds. Based on these observations, it is projected that the convection heat transfer may be approximated by a single radial distribution for all times up to 8.2 microseconds, which is taken to be about 10 microseconds. This distribution is plotted in Fig. 10. From Fig. 10, one sees that the projected heat flux overestimates the early-time curves of Fig. 9, underestimates the middle-time curves of Fig. 9, and approximates the late-time curves of Fig. 9. To obtain the energy imparted to the surface per unit area, the heat flux curve of Fig. 10 was integrated over time, up to 10 microseconds. Since the curve is independent of time, the integration amounts to simply multiplying the curve by 10 microseconds. Looking ahead, the result is plotted as curve 2 in Fig. 13 (p. 90), from which one sees that: (a) the amount of energy absorbed by the target due to convection heat transfer in 10 microseconds is much less than that measured by Hall (curve 1), and (b) the radial distribution of the energy absorbed due to convection heat transfer is not the same as for curve 1 (Fig. 13 p. 90). The thermal coupling coefficient, at a given time, is simply the thermal energy residing in the target at that time divided by the energy in the laser beam at that time. Therefore, the thermal coupling due to convection heat transfer, at 10 microseconds, is curve 2 (Fig. 13 p. 90) integrated over the area, divided by the

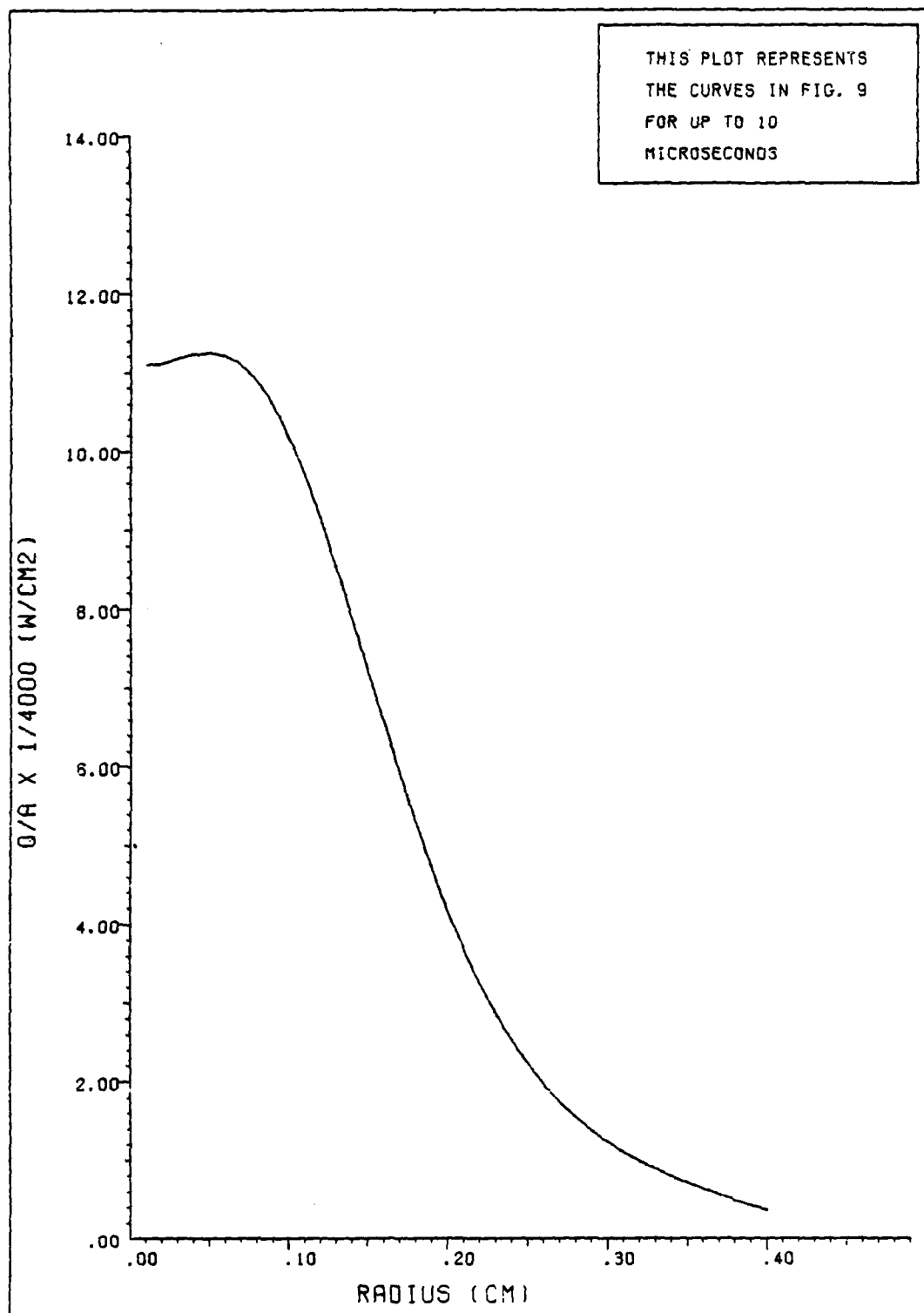


FIG. 10: PROJECTED HEAT FLUX DUE TO HEAT TRANSFER

beam energy at 10 microseconds. Curve 2 was (Fig. 13 p. 90) approximated by the following curve fit,

$$E/A = 0.444 \exp[a(r)], \quad (106)$$

where E/A is the energy per unit area and,

$$a(r) = 30.7r^2 - 641r^3 + 2231r^4 - 2405r^5. \quad (107)$$

The total energy absorbed by the target is,

$$E_t \approx 2\pi \int_0^{0.4} E/A \, r dr. \quad (108)$$

Equation (108) was integrated numerically by the trapezoid rule using $\Delta r = 0.0004$, with the result that $E_t = 0.0558$ J. From Fig. 3, the beam energy at 10 microseconds is about 5 J; therefore, the thermal coupling due to convection heat transfer at 10 microseconds is only about 0.011.

The energy flux carried into the target by condensing vapor particles was calculated from equation (101) of Section V. This energy flux is plotted, as a function of radius from the axis of symmetry with time as a parameter, in Fig. 11. Note that the curves in Fig. 11 are plotted only for times after the ignition of the LSD (about 5 microseconds) since equation (101) assumes that all vapor

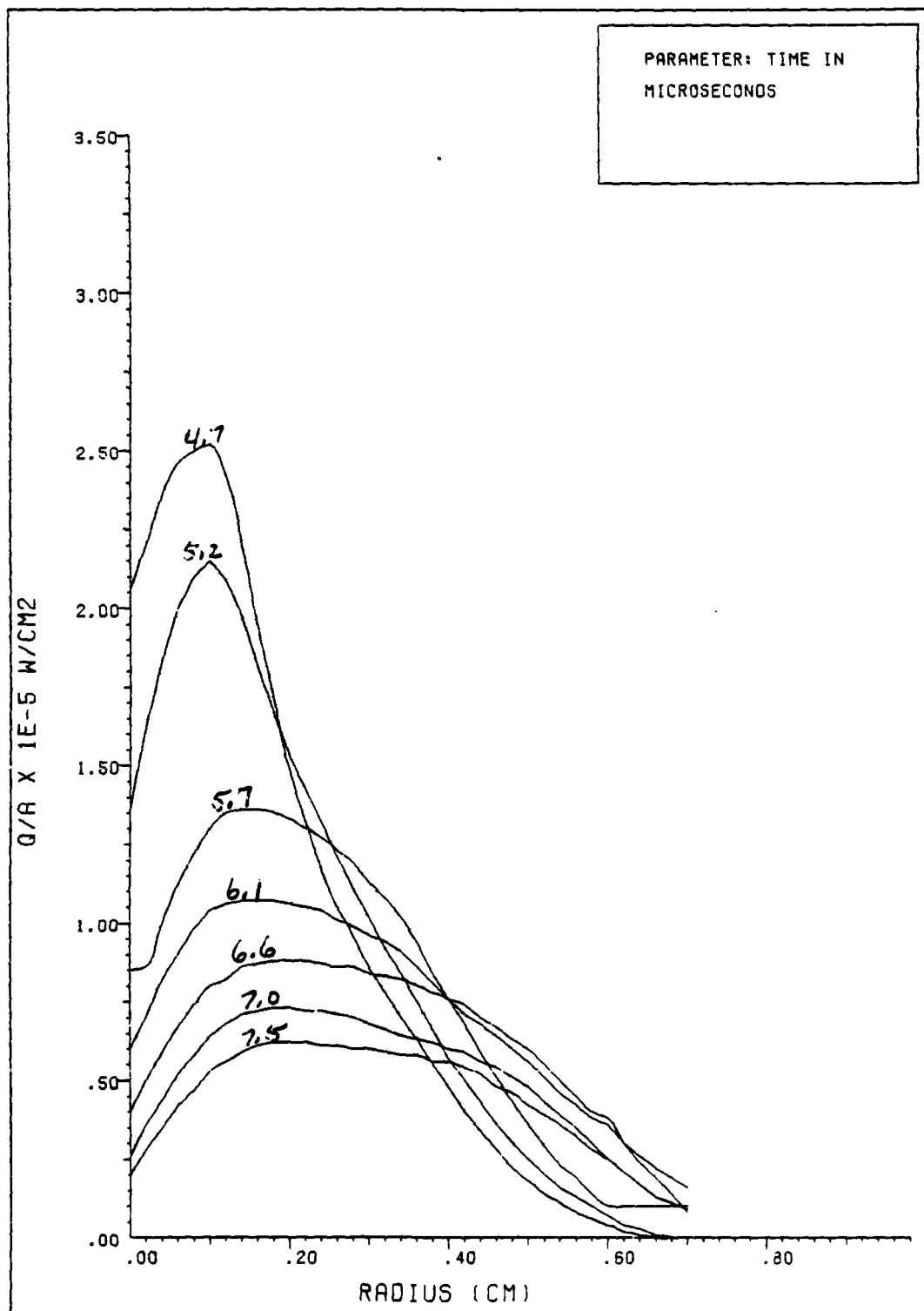


FIG. 11: ENERGY FLUX DUE TO VAPOR RECONDENSATION

UNCLASSIFIED

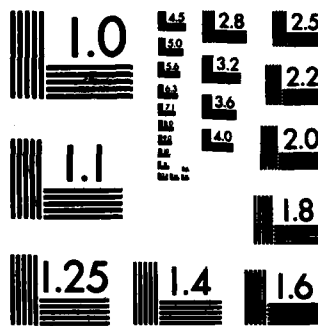
AFIT/GAE/AA/85M-3

2/2

F/G 20/13

NL

6. Results



MICROCOPY RESOLUTION TEST CHART
NATIONAL BUREAU OF STANDARDS-1963-A

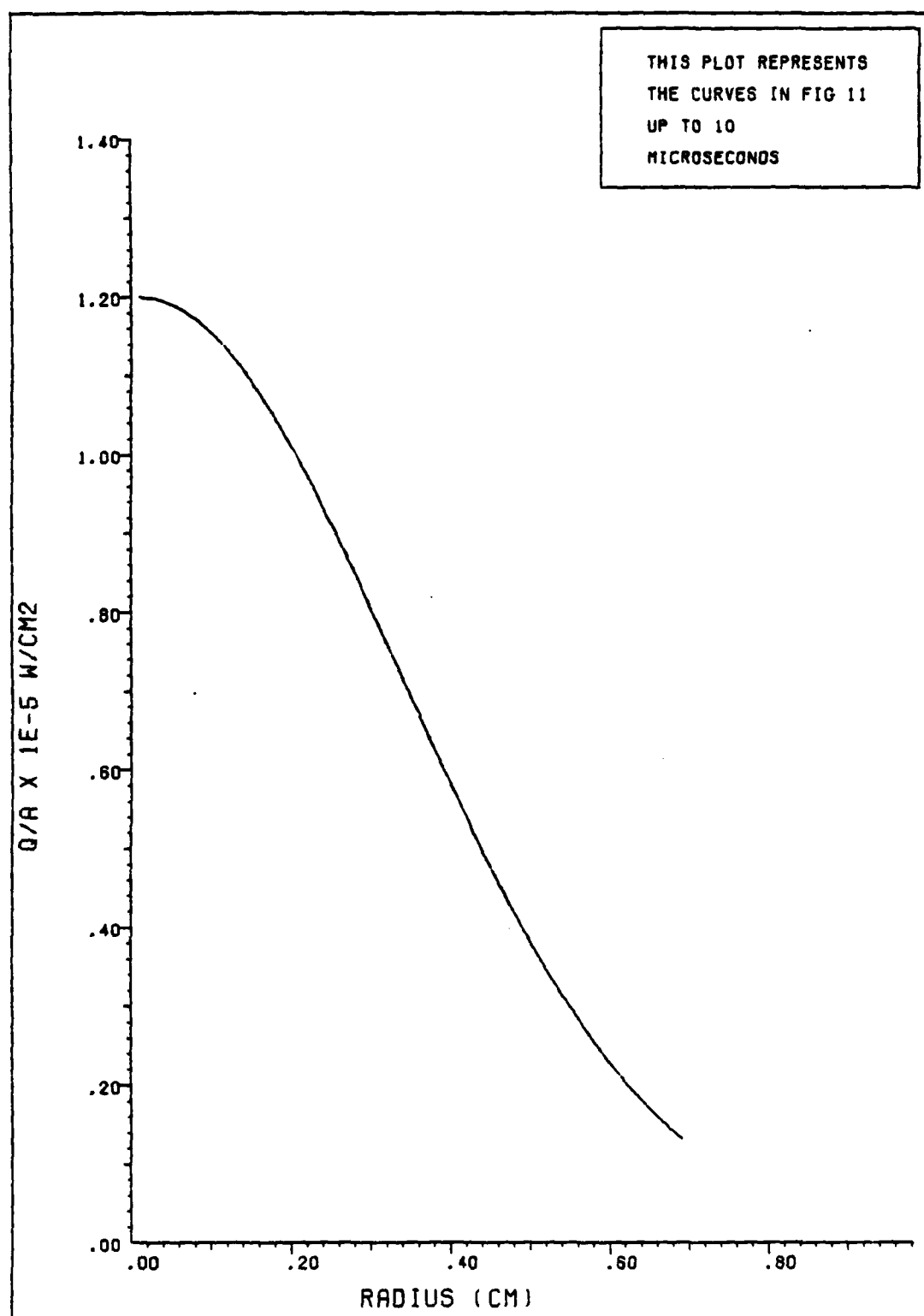


FIG. 12: PROJECTED ENERGY FLUX DUE TO CONDENSATION

particles which come into contact with the surface condense and this is not true prior to formation of the LSD, due to the fact that surface vaporization takes place until the LSD forms. From Fig. 11, one sees that the energy flux into the surface due to vapor condensation decreases with time and, as in the case of convection heat transfer, the flux appears to converge to a radial distribution with no time dependence by about 7 microseconds. It is projected, then, that the energy flux may be approximated by a single radial distribution, independent of time, for all times up to about 10 microseconds. This distribution is plotted in Fig. 12, from which one sees that the projected energy flux underestimates the early-time curves of Fig. 11, approximates the middle-time curves of Fig. 11, and overestimates the late-time curves of Fig. 11. To obtain the energy imparted to the target per unit area, the energy flux of Fig. 12 was integrated over time up to 10 microseconds. As before, the integration amounts to simply multiplying the curve in Fig. 12 by 10 microseconds. The result is plotted as curve 3 in Fig. 13, from which one sees that: (a) the energy imparted to the target by vapor condensation is much greater than the energy imparted to the target by convection heat transfer, (curve 2) and (b) the measured radial distribution of the energy imparted to the target per unit area (curve 1) is more closely matched by the condensation curve than by the heat transfer curve.

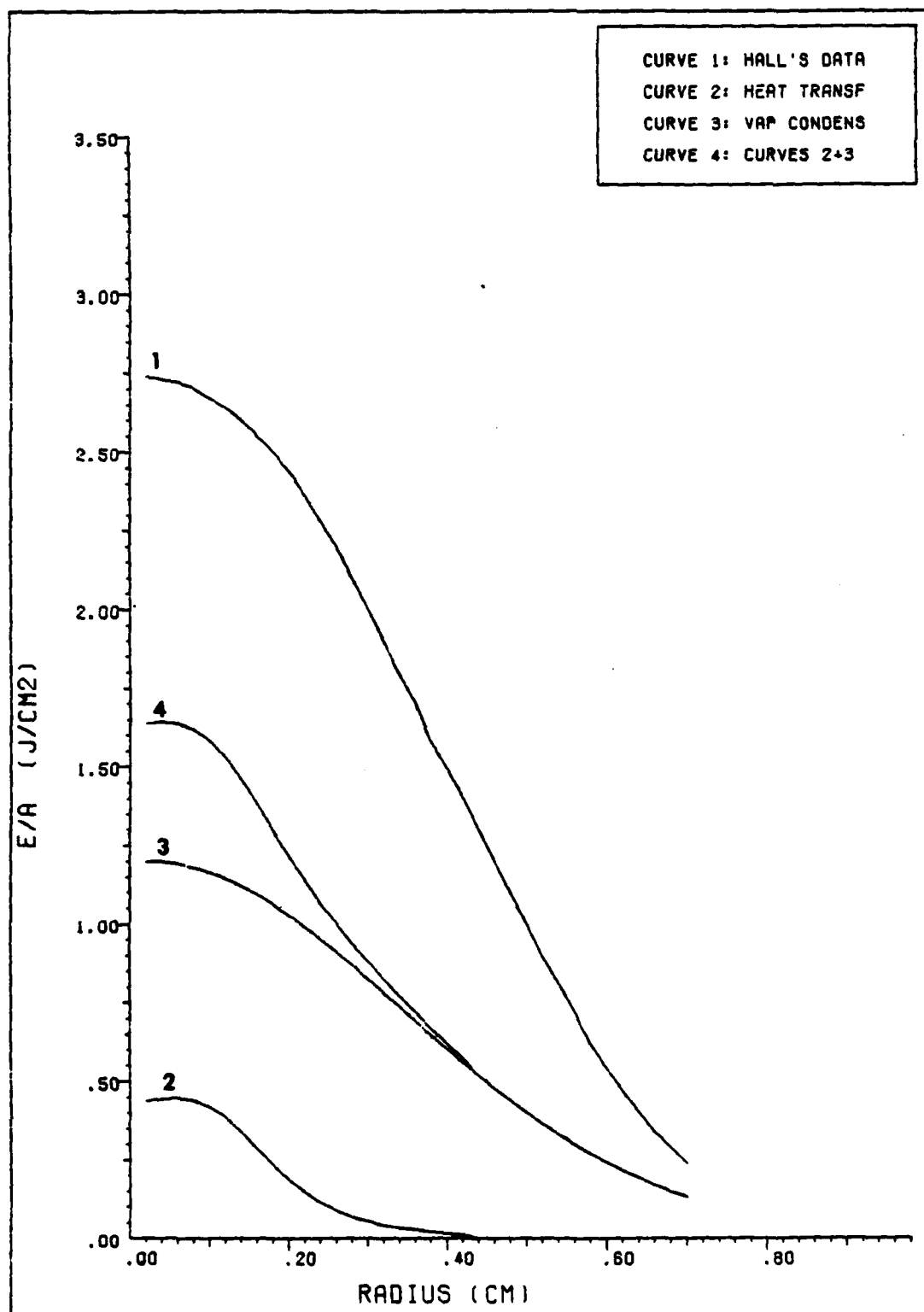


FIG. 13: ENERGY ABSORBED BY TARGET PER UNIT AREA

In order to find the thermal coupling due to vapor condensation, curve 3 was fit to the following expression:

$$E/A = 1.2\exp(-4.76r^2). \quad (109)$$

Integrating equation (112) over the area, the energy residing in the target due to vapor condensation is,

$$E_t \approx 2\pi \int_0^{0.7} E/A \, r dr. \quad (110)$$

Equation (110) gives E_t to be about 0.715J. The energy in the beam at 10 microseconds is about 5 J; therefore, the thermal coupling due to vapor condensation at 10 microseconds is about 0.143. Curve 4 of Fig. 13 shows the additive effect of convection heat transfer and vapor condensation on the energy absorbed by the target.

The radiation heat transfer to the target from the LSD front was estimated from equation (105) of Section VI. If the absorption coefficient defined by equation (37) of Section III is greater than 10, the radiation is blackbody and is neglected according to Dawson's [27] recommendation discussed in Section III. Otherwise, the radiation is bremsstrahlung and equation (105) applies. From the numerical data given by HYDRO, it was observed that, prior to ignition of the LSD, the radiation is bremsstrahlung,

and afterwards, the radiation is blackbody. The calculation of the heat flux into the target due to bremsstrahlung radiation is summarized in Table I.

Table I

Estimate of Bremsstrahlung Plasma Reradiation

$t \times 10^{-6}$ sec	k_{ff} cm^{-1}	T (deg K)	q W-cm^{-2}
1.59	2.31	2942	11.43
2.71	2.24	3747	17.97
3.73	1.95	3767	15.81

From Table I, one sees that the maximum heat flux into the target due to bremsstrahlung radiation is about 18 watts per square centimeter. For reasons discussed in Section VI, it is felt that this number greatly overestimates the true radiation heat flux into the target. Assuming that the radiation heat flux into the target is the maximum value given above and that it is constant through the entire laser pulse, one obtains that the energy absorbed by the target per unit area is only about 4.68×10^{-4} J/cm². Furthermore, if one assumes that this value is constant over the entire laser spot radius, one obtains that the total energy transferred to the target by radiation is about 5.9×10^{-5} J. The beam energy at the end of the pulse is 9.3 J; therefore, the

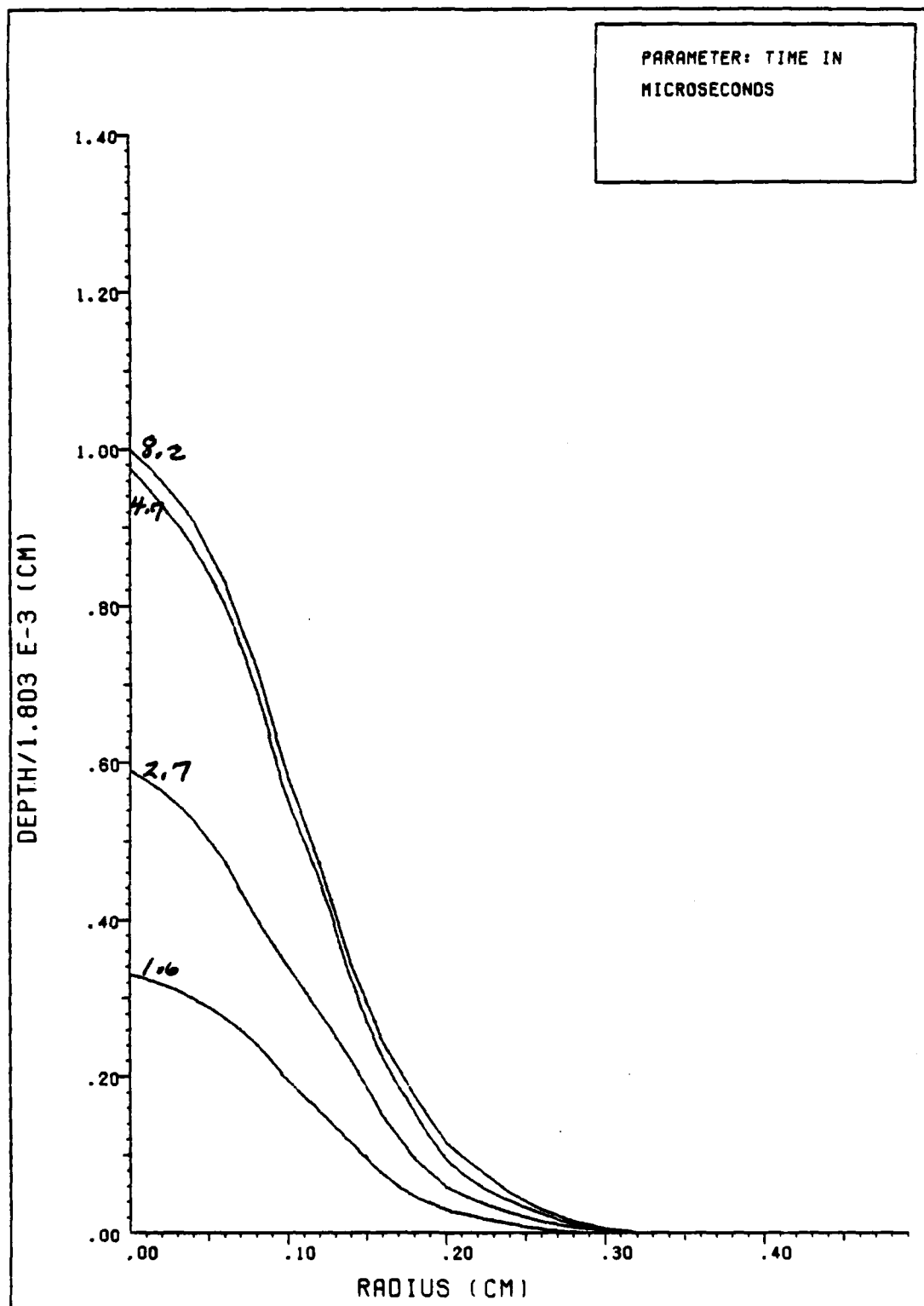


FIG. 14: DEPTH OF LASER-INDUCED VAPORIZATION

thermal coupling due to bremsstrahlung radiation from the LSD front is only 6×10^{-5} percent. This number is extremely small compared to the coupling via convection heat transfer and vapor condensation. Note also that this extremely small number is felt to greatly overestimate the true value. It appears that plasma radiation is an insignificant coupling mechanism for the problem under study. This is consistent with results given by Jumper [28], in which he accurately predicted the propagation speed of a LSD using a global energy balance and completely ignoring radiation away from the LSD.

It was stated above that the time of LSD ignition is about 5 microseconds. Referring to Fig. 14, where the depth of laser-induced target vaporization is plotted, one sees that by about 5 microseconds, laser radiation has practically ceased reaching the target. The reason for the rapid decrease in vaporization is that the surface-shielding LSD has formed, detached from the surface, and is absorbing practically all of the incident radiation. Thus, it is seen that the LSD is formed at about 5 microseconds.

In summary, the energy imparted to the target per unit area by convection heat transfer was calculated with the methods of Section IV. The results of these calculations are presented in Fig. 9 and Fig. 10. The energy imparted to the target per unit area by vapor condensation was

calculated with the methods of Section V. The results of these calculations are presented in Fig. 11 and Fig. 12. The relative magnitudes (and radial distributions) of these calculations are compared both with each other and with Halls experimental profile in Fig. 13. Finally, the radiation heat flux into the target was estimated using Dawson's recommendations discussed in Section VI. The results of these estimations are shown in Table I.

VIII. Conclusions

The conclusions of this study were made based on the results discussed in Section VII. From the results shown in Fig. 9 and Fig. 10, it was concluded that convection heat transfer is only a minor contributor to enhanced coupling observed by Hall for a 9.3 J laser pulse. First of all, convection heat transfer does not give the measured magnitude of energy absorbed by the target; furthermore, it does not give the correct radial distribution of the absorbed energy. From the results shown in Fig. 11 and Fig. 12, it was concluded that vapor condensation could essentially account for most of the enhanced coupling, since the magnitude of energy "returned" to the target is not only higher than that for the heat transfer, but furthermore, the radial distribution of the absorbed energy more closely resembles Hall's measured profile, as shown in Fig. 13. The above results are based on numerical data spanning 10 microseconds of a 25 microsecond pulse. However the author feels that the projected curves shown in Fig. 10 and Fig. 12 will not increase much, if any, for times greater than 10 microseconds due to the fact that the incident laser radiation falls to zero fairly rapidly past this time (see Fig. 2). Therefore, the above conclusions are felt to be justified for the entire pulse. Finally, it was concluded that plasma reradiation plays practically no role in enhanced thermal coupling.

The above conclusions are for a particular problem, that of Hall's 9.3 J pulse. It is recommended that further studies in this area be directed towards examining the effects of laser beam and target material parameters on enhanced thermal coupling.

Appendix A

Thermodynamic and Transport Properties of High Temperature Air

The curve fits presented in this appendix were derived from tabulated data given by reference {29}, using the method of least squares given in reference {13}. All of the fits are polynomials and, though they are somewhat tedious, they accurately match Hansen's {29} tabulated data. Curve fits were obtained for the following properties: compressibility factor (Z), mass specific enthalpy (i) in calories per gram, mass specific heat at constant pressure (c_p) in calories per gram per degree Kelvin, dynamic viscosity (μ) in grams per centimeter per second, thermal conductivity (k) in calories per centimeter per second per degree Kelvin, and Prandtl number. The curves are given as functions of temperature (times 1/1000 degrees Kelvin) with pressure (in atmospheres) as a parameter. With the pressure and temperature given by HYDRO, the properties are found in the following manner: if the pressure is less than one atmosphere, the one atmosphere value is used; if the pressure is greater than ten atmospheres, the ten atmosphere value is used and; if the pressure is between one and ten atmospheres, logarithmic (to base 10) interpolation is used to find the properties.

The actual curve fits are not included here due to the fact that they are quite elementary in nature and very bulky, as some of them are fourth and fifth order polynomials.

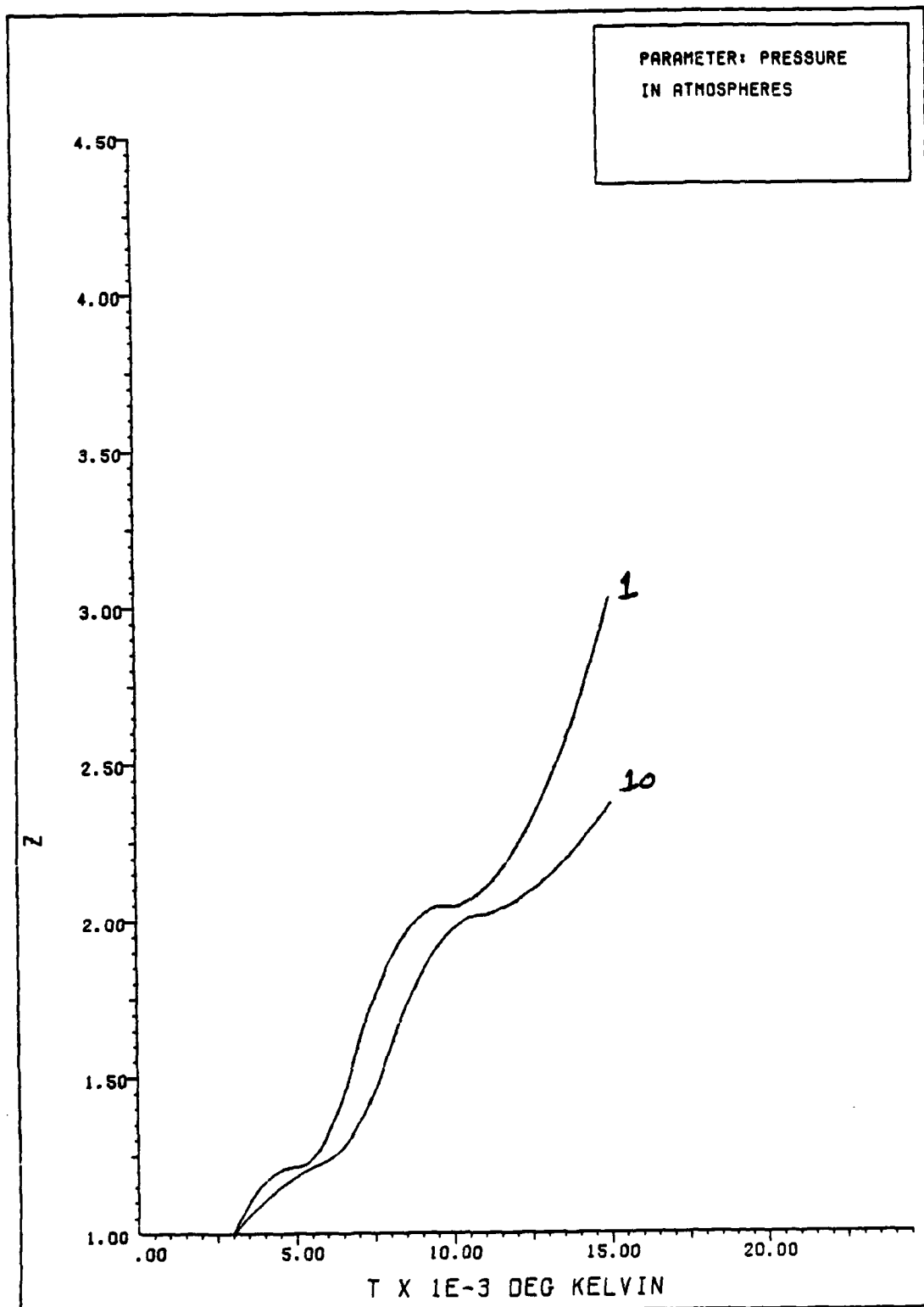


FIG. A.1: COMPRESSIBILITY FACTOR FOR AIR

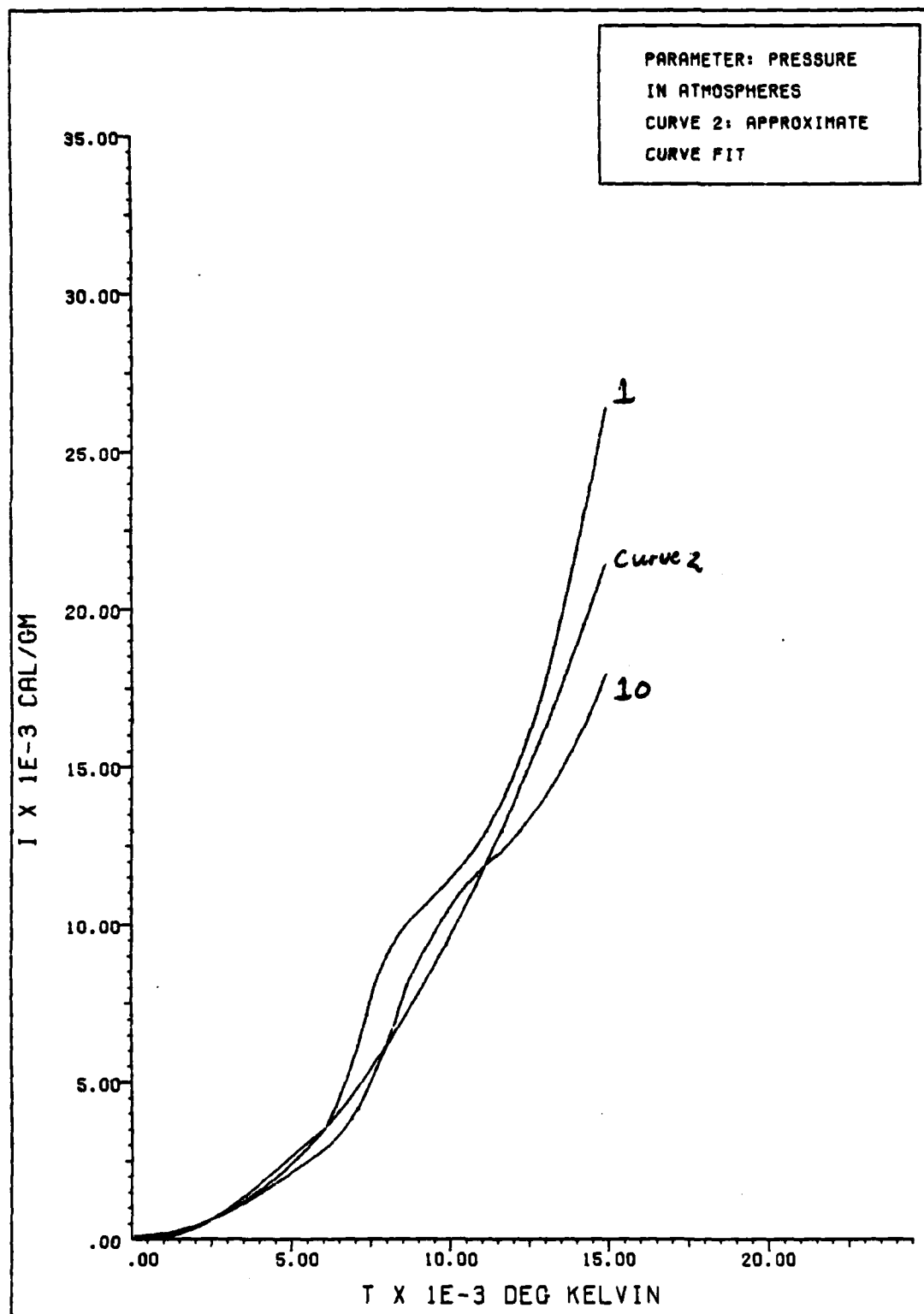


FIG. A.2: MASS SPECIFIC ENTHALPY FOR AIR

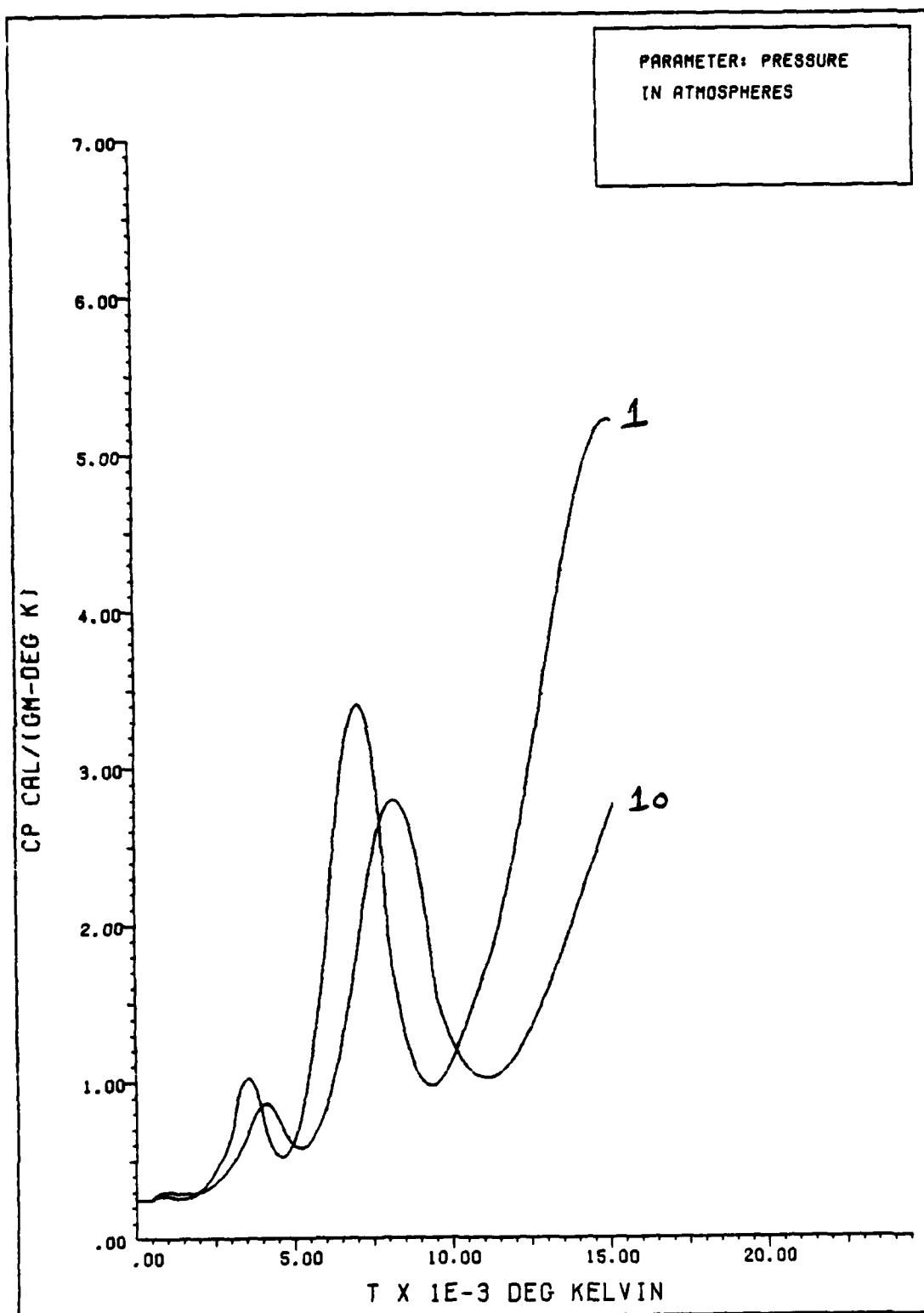


FIG. A.3: SPECIFIC HEAT AT CONSTANT PRESSURE (AIR)

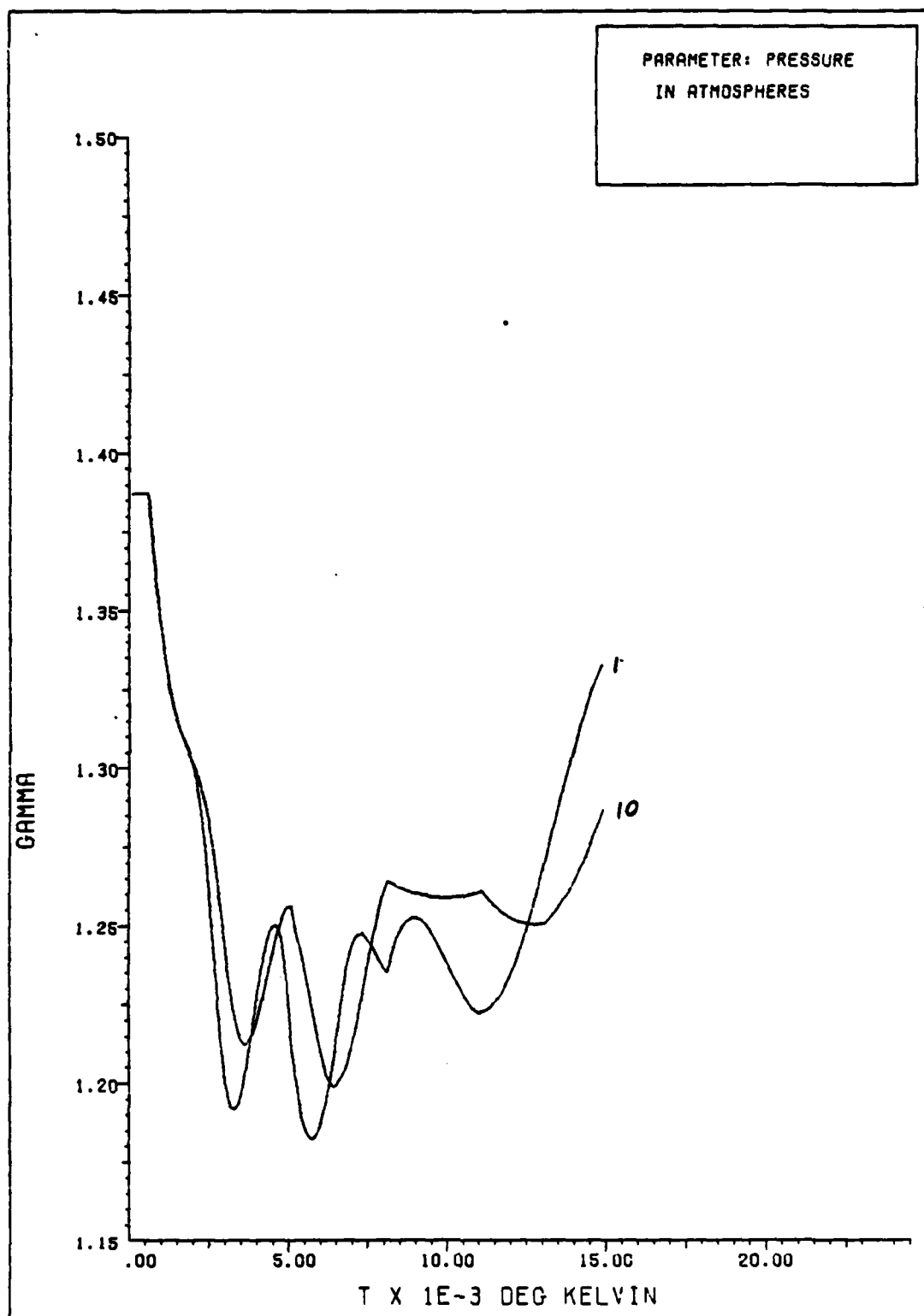


FIG. A.4: RATIO OF SPECIFIC HEATS FOR AIR

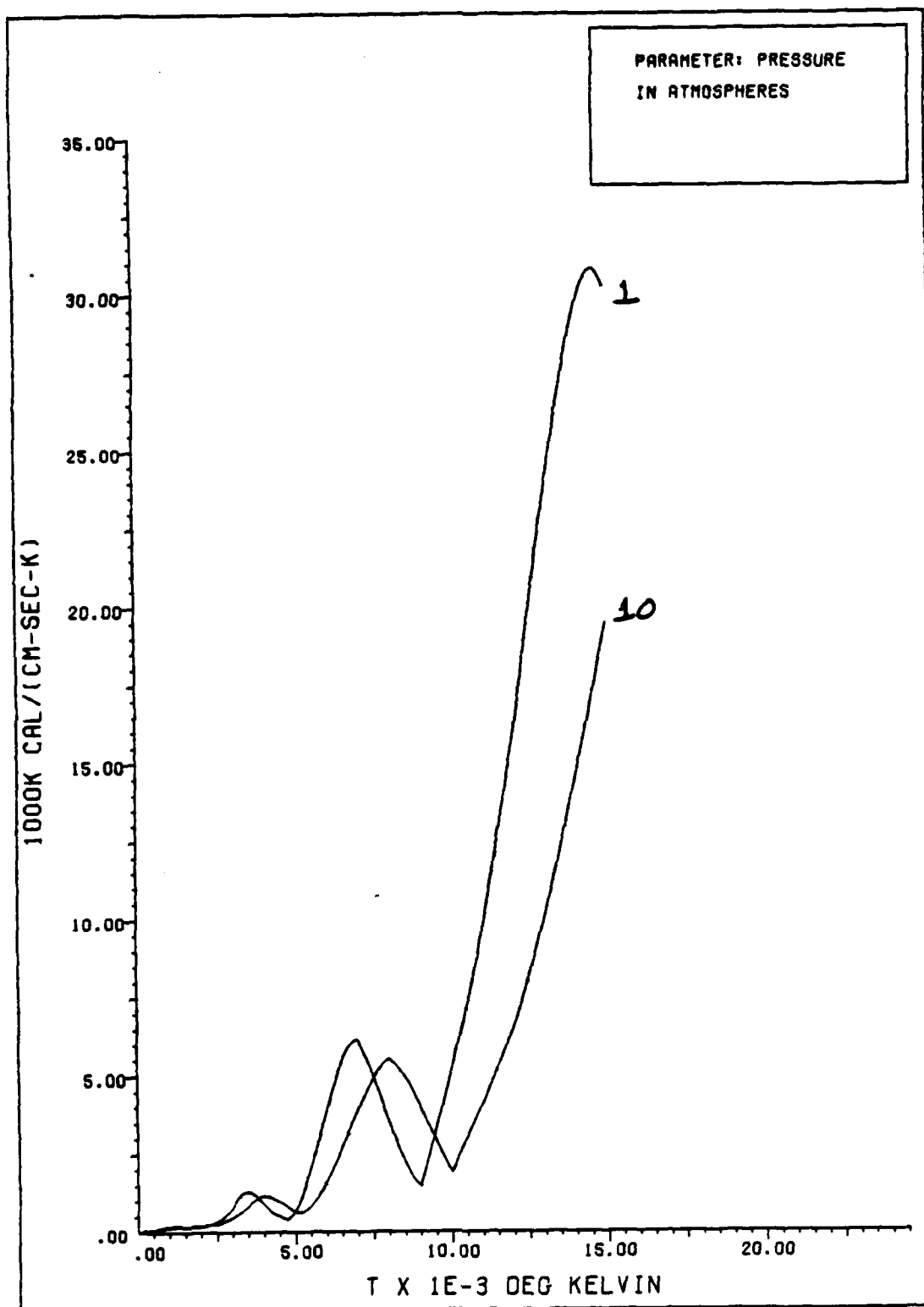


FIG. A.5: THERMAL CONDUCTIVITY OF AIR

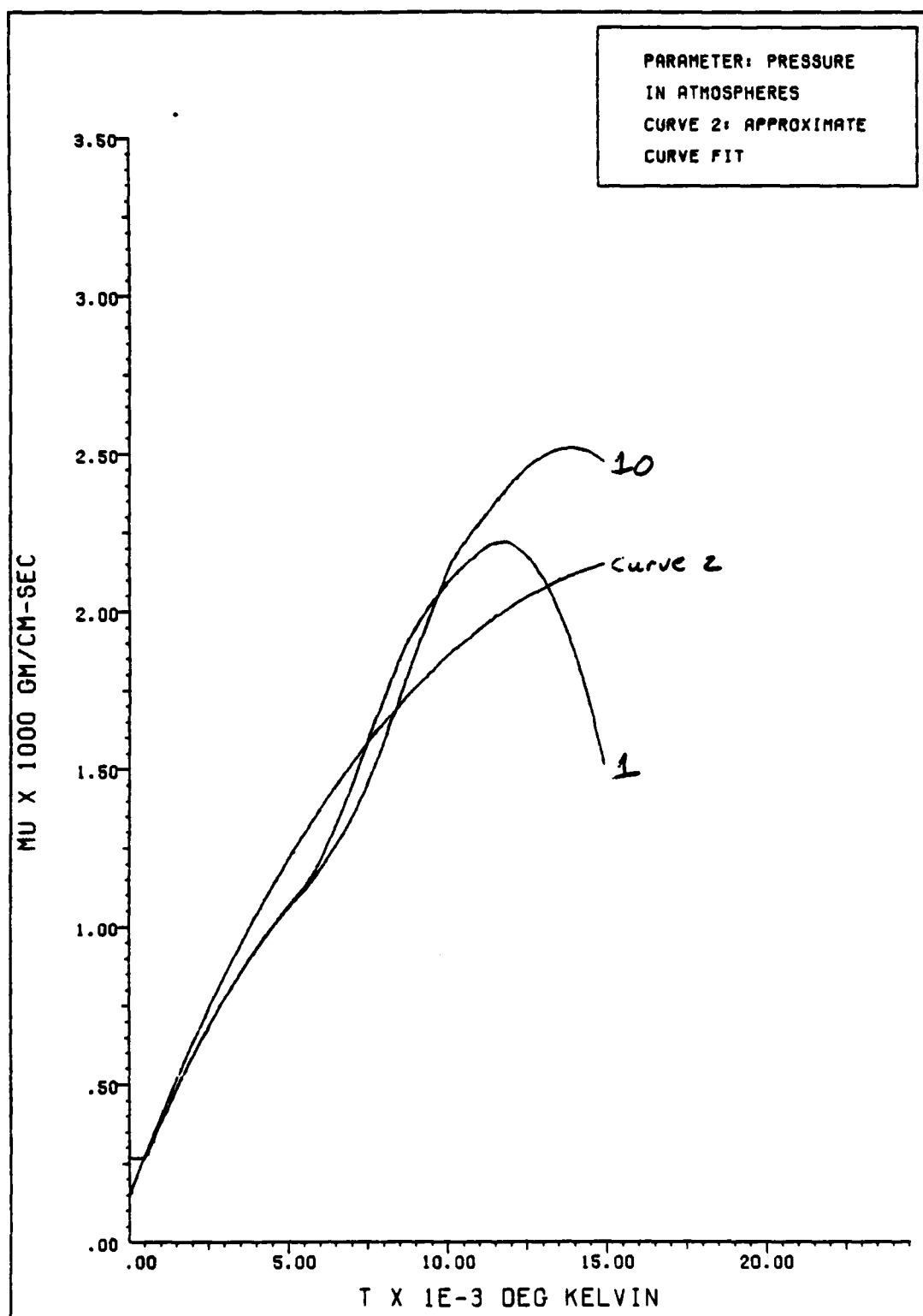


FIG. A.6: DYNAMIC VISCOSITY OF AIR

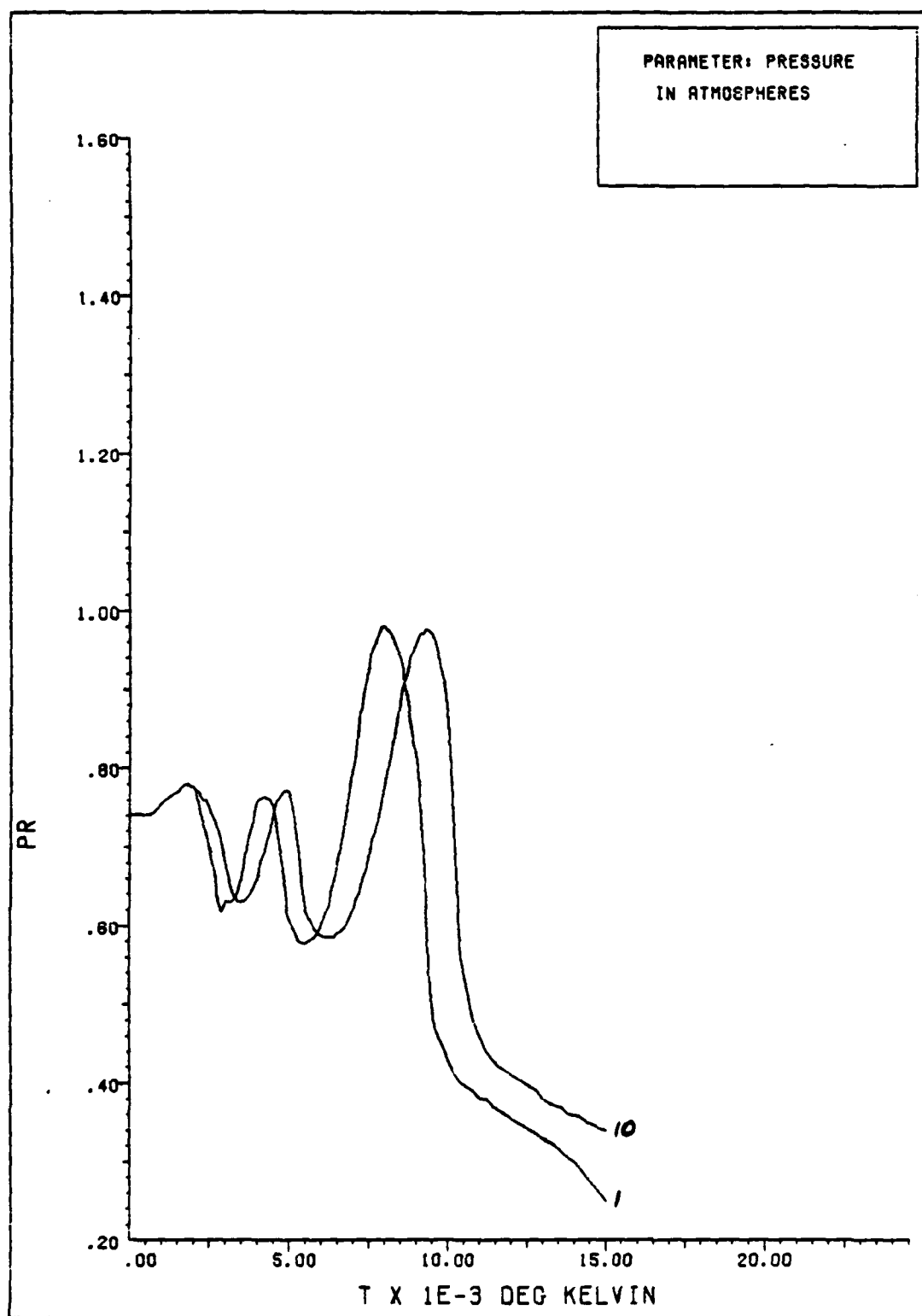


FIG. A.7: PRANDTL NUMBER OF AIR

Appendix B
Listing of Hydrocode


```

PROGRAM HYDRO
IMPLICIT DOUBLE PRECISION(A-H,O-Z)
COMMON/COM1/ DELT(3,3), GAMMO, NM, DELTX, DLT, DELX, ABCM, XULFO
COMMON/COM2/ AN(10000), IM, JM, KM, INMO, JNMO, IQ
COMMON/COM3/ PN(S), PNP(S), PPHH(S), F(S)
COMMON/COM4/ FNP(S), FPHH(S), FB(S), OMEGA(SO), PRES, PRESF, PRESPI,
1 PRESN, NR, NR
COMMON/ASORB/E1, E12, G, THIRD, THRD3, ENDEP, EDEN(100, 100)
COMMON/THERM/EM1, EM2, TN, TNPO
COMMON/DIF/NDIF
COMMON/COM5/PNWIG(S)
COMMON/LOAD/PULSE, SPULSE, SURFP
COMMON/COM6/TIME, NCYCLE, TOTE, CHEV(SO)
COMMON/TEST/XULFX
OPEN(UNIT=7, FILE='DAT2IN')
OPEN(UNIT=8, FILE='ANFILE')
REWIND 8
REWIND 7
READ(7, 300, END=400) TQUIT, IM, JM, KM, NM, NDIF, XULFX, DELX
300 FORMAT(D7.2, 3I3, 2I1, D7.1, P3.2)
400 DO 3 I=1, 50
      OMEGA(I)=8.9D+10
      CHEV(I)=0.
      FB(I)=0.0
3 CONTINUE
DO 17 I=1, 10000
      AN(I)=0.
17 CONTINUE
DO 18 I=1, 5
      PNWIG(I)=0.0
18 CONTINUE
      NAT=0
      PULSE=0.
      SPULSE=0.
      ENDEP=0.
      PI=3.141592654
      THIRD=1./3.
      THRD3=1./27.
      G=2.98D+39
      E1=1.92D-11
      E12=9.56D-12
      EM1=4.81D-23
      EM2=4.48D-23
      RHOO=2.70
      RHOOI=1./RHOO
      GAMMO=.387
      DLT=0.
      ABCM=0.
DO 712 I=1, 3
DO 711 J=1, 3
      DELT(I,J)=0.
711 CONTINUE
      DELT(I,I)=1.
712 CONTINUE
      INMO=IM-1
      JNMO=JM-1
      NQ=8
      ENFAC=1./(1.-GAMMO)*NDIF/GAMMO
      NB=7
      DELX3=DELX**3
C SET INITIAL CONDITIONS IN AMBIENT ATMOSPHERE
EN=1.0128D+6*ENFAC
DO 43 J=1, JM
DO 42 I=1, IM

```

NS=NQ*(I-1)+IN*(J-1)

SET DENSITY

AN(NS+1)=1.28D-3

SET PRESSURE/TOTAL ENERGY

AN(NS+3)=EN

SET MOMENTUM

DO 40 L=1,NA
PN(L)=AN(NS+L)

CONTINUE
CALL HOT(PN,T)
AN(NS+8)=T

40

CONTINUE

42 CONTINUE

43 TIME=0

C*** ENTST=8.D+7*ENFAC

NCYCLE=0

XULFO=0.

TOTE=0.

CALL PRINS

CONTINUE

CALL CRNT

DELTX=DLT/DELX

TIME=TIME+DLT

XULFO=XULFX*SHAPE(TIME-0.8*DLT)

NS=NQ*(IN-1)

IF(AN(NS+3).GE.ENTST) XULFO=0.0

NCYCLE=NCYCLE+1

CALL CALLER

DO 11 J=1,JM

CHEV(J)=CHEV(J)+FB(J)/OMEGA(J)*RH*DDI*DLT

11 CONTINUE

IF(AN(4).LE.0.0) CALL ENDIF(NDIF)

NAT=MOD(NCYCLE,20)

IF(NAT.NE.0) GO TO 98

TOTE=0.

DO 54 I=1,IM

DO 53 J=1,JM

NS=NQ*(I-1)+IN*(J-1)

VSQ=0.

DO 51 L=4,NA

VSQ=VSQ+AN(L+NS)**2

CONTINUE

VOL=DELX*PI*(2+J-2)

IF(J.LE.1) VOL=0.25*DELX3*PI

TOTE=TOTE+(AN(3+NS)/DAMMD+0.8*VSQ/AN(1+NS))*

VOL*(1-NDIF)+AN(3+NS)*VOL*NDIF

51

C

CONTINUE

53 CONTINUE

54 CALL PRINS

98 CONTINUE

IF(TIME.LE.TQUIT) GOTO 99

CLOSE(7)

CLOSE(8)

STOP

END

END MAIN PROGRAM *****

BEGIN SUBROUTINE CRNT *****

SUBROUTINE CRNT

C*****

C

C*****


```

DO 88 L=1,NM
  PN(L)=PN(L)+4.*DELTX*FPMH(L)
  FPMH(L)=FPMH(L)
  AN(L+NS)=PN(L)
CONTINUE
CALL MOT(PN,T)
AN(NS+8)=T
IF(JUNG.LE.1) GOTO 14
DO 13 J=2,JM
  NR=J
  NS=NQ*(I-1)+IN*(J-1)
  DO 88 L=1,NM
    N=L+NS
    FPMH(L)=FPMH(L)
    F(L)=FNP(L)
    PN(L)=PNP(L)
    PNP(L)=AN(N+NQ*IN)
CONTINUE
TN=TNPO
TNPO=AN(NS+8+NQ*IN)
FPMH(3)=FPMH(3)+CF2
F(3)=F(3)+CF1
PNP2=AN(3+NS+2*NQ*IN)
CF1=(PNP(3)+0.5*GAMMA*(PNP(3)+PNP2))/(PNP(3)+0.5*GAMMA
      +
      *PN(3)+PNP(3))
CF1=CF1*(1-NDIF)+NDIF
PRES=PRESP
PRESH=PRESPH
CALL MDO(2)
CF2=PRESPH/(PRESH+0.5*GAMMA*(PRESH+PRESPH))
CF2=CF2*(1-NDIF)+NDIF
DO 89 L=1,NM
  N=L+NS
  AN(N)=PN(L)
CONTINUE
CALL MOT(PN,T)
AN(NS+8)=T
CONTINUE
NR=JM
NS=NQ*(I-1)+IN*(J-1)
DO 90 L=1,NM
  N=L+NS
  FPMH(L)=FPMH(L)
  F(L)=FNP(L)
  PN(L)=AN(N)
  PNP(L)=PN(L)
CONTINUE
TN=TNPO
FPMH(3)=FPMH(3)+CF2
F(3)=F(3)+CF1
PRES=PRESP
PRESH=PRESPH
CALL MDO(2)
DO 91 L=1,NM
  N=L+NS
  AN(N)=PN(L)
CONTINUE
CALL MOT(PN,T)
AN(NS+8)=T
CONTINUE
11

```

C CALCULATE ADVECTION ON THE Z-DIRECTION

100 CONTINUE
DO 9 J=1,JM

```

80 NS=NQ*IN*(J-1)
DO 80 L=1,NM
N=L+NS
PN(L)=AN(N)
PNPO(L)=AN(N+NQ)
CONTINUE
TN=AN(NS+8)
TNPO=AN(NS+8+NQ)
PNP2=AN(3+NS+2*NQ)
CF1=(PNPO(3)+0.5*GAMMO*(PNPO(3)+PNP2))/(PNPO(3)+0.5*GAMMO
*(PN(3)+PNPO(3)))
CF1=CF1*(1-NDIF)+NDIF
CALL PLUSHX(FB(J),OMEGA(J),PRESMH,PRES)
AJ=PI*DELX**2*(2+J-2)
IF(J.LE.1) AJ=.25*PI*DELX**2
DIMP=(SURFP-PO)*AJ*DLT
PULSE=PULSE+DIMP
IF(J.LE.NB) SPULSE=SPULSE+DIMP
CALL MHD(1)
CF2=PRESPH/(PRESPH+0.5*GAMMO*(PRESPH+PRESMH))
CF2=CF2*(1-NDIF)+NDIF
DO 81 L=1,NM
N=L+NS
AN(N)=PN(L)
CONTINUE
CALL HOT(PN,T)
AN(NS+8)=T
IF(IMMO.LE.1) GOTO 17
DO 10 I=2,IMMO
NS=NQ*(I-1)+IM*(J-1)
DO 82 L=1,NM
N=L+NS
FPMH(L)=FPMH(L)
F(L)=FNPO(L)
PN(L)=PNPO(L)
PNPO(L)=AN(N+NQ)
CONTINUE
TN=TNPO
TNPO=AN(NS+8+NQ)
PRESMH=PRESPH
FPMH(3)=FPMH(3)+CF2
F(3)=F(3)+CF1
PNP2=AN(3+NS+2*NQ)
CF1=(PNPO(3)+0.5*GAMMO*(PNPO(3)+PNP2))/(PNPO(3)+0.5*GAMMO
*(PN(3)+PNPO(3)))
CF1=CF1*(1-NDIF)+NDIF
CALL MHD(1)
CF2=PRESPH/(PRESPH+0.5*GAMMO*(PRESPH+PRESMH))
CF2=CF2*(1-NDIF)+NDIF
DO 83 L=1,NM
N=L+NS
AN(N)=PN(L)
CONTINUE
CALL HOT(PN,T)
AN(NS+8)=T
CONTINUE
NS=NQ*(IM-1)+IM*(J-1)
DO 84 L=1,NM
N=L+NS
FPMH(L)=FPMH(L)
F(L)=FNPO(L)
PN(L)=AN(N)
PNPO(L)=PN(L)
CONTINUE
TN=TNPO

```

```

PRESMH=PRESPH
FPHMH(3)=FPHMH(3)*CF2
F(3)=F(3)*CF1
CALL MHD(1)
DO 85 L=1,NM
  N=L+NS
  AN(N)=PN(L)
  CONTINUE
CALL MDT(PN,T)
AN(NS+6)=T
9 CONTINUE
RETURN
END
C***** END CALLER *****
C***** SUBROUTINE PRINS *****
SUBROUTINE PRINS
IMPLICIT DOUBLE PRECISION(A-H,O-Z)
COMMON/COM1/DEL(3,3),GAMMA,NM,DELTX,DLT,DELX,ABCM,XULFO
COMMON/COM2/AN(10000),IM,JM,KM,IMMO,JMMO,NQ
COMMON/COM4/FNPO(5),FPHH(5),FB(50),OMEGA(50),PRES,PRESP,PRESPH,
+ PRESMH,NB,NR
COMMON/DIF/NDIF
COMMON/LOAD/PULSE,SPULSE,SURFP
COMMON/COM6/TIME,NCYCLE,TOTE,CHEW(50)
COMMON/ABSORB/E11,E12,G,THIRD,THROX3,ENDEP,EDEN(100,100)
WRITE(8,250) TIME,NCYCLE,DLT,NDIF
FORMAT(1X,D16.10,1X,I4,D16.10,1X,I1)
250 WRITE(8,251) ABCM,XULFO,PULSE,SPULSE,TOTE,ENDEP
251 FORMAT(1X,8(D16.10,1X))
WRITE(8,252) (FB(I),I=1,NB)
252 WRITE(8,252) (CHEW(I),I=1,NB)
FORMAT(1X,7(D16.10,1X))
DO 63 I=1,IM
  DO 62 J=1,JM
    NS=NQ*(I-1)+IM*(J-1)
    IF(NDIF.EQ.1) THEN
      VSQ=0.
      DO 61 NP=4,NM
        VSQ=VSQ+AN(NP+NS)**2
        CONTINUE
      P=GAMMA*(AN(NS+3)-0.5*VSQ/AN(NS+1))
      ELSE
        P=AN(NS+3)
      ENDIF
      WRITE(8,251) AN(NS+1),AN(NS+2),P,AN(NS+4),AN(NS+5),
+ AN(NS+6)
62 CONTINUE
63 CONTINUE
RETURN
END
C***** END PRINS *****
C***** SUBROUTINE MHD(L) *****
SUBROUTINE MHD(L)
IMPLICIT DOUBLE PRECISION(A-H,O-Z)
COMMON/COM1/ DEL(3,3),GAMMA,NM,DELTX,DLT,DELX,ABCM,XULFO
COMMON/COM2/ AN(10000),IM,JM,KM,IMMO,JMMO,NQ
COMMON/COM3/ PN(5),FNPO(5),FPHH(5),F(5)
COMMON/COM4/ FNPO(5),FPHH(5),FB(50),OMEGA(50),PRES,PRESP,PRESPH,
+ PRESMH,NB,NR
COMMON/THERM/EM1,EM2,TN,TNPO
COMMON/DIF/NDIF
DIMENSION PPHH(5)
SUM=0.0

```

```

DO 10 I=1, NR
SUM=SUM+DABS(PNPO(I)-PN(I))
CONTINUE
10 PC=0.5*(PN(3)+PNPO(3))
CALL FLUX(L, PNPO, FNPO, PRES, PC)
DELP=(PNPO(3)-PN(3))/PN(3)
B=10.*DELT*(DASS(DELP)+PN(3+L)/PN(1))
ALF=1.+DTANH(B)
DO 20 J=1, NR
PPH(J)=ALF*PN(J)+(2.-ALF)*PNPO(J)
PPH(J)=0.5*(PPH(J)-DELT*(1./((1.+0.5*(L-1)/(NR-1))))
*(PNPO(J)+(1.+(L-1)/(NR-1))-F(J)))
20 CONTINUE
PPH(5)=PPH(5)-0.5*DELT*(PRES-PRES)*
DELT(2,L)
DU=SUM/PPH(1)
PC=0.5*(PPH(3)+PRESH)
FPHH(3)=FPHH(3)*((PRESH+GAMMA*PC)*(1-NDIF)/PRESH+NDIF)
CALL FLUX(L, PPH, FPHH, PRES, PC)
CALL HOT(PPH, TPHH, DIFC)
CALL DIFCO(PPH, TPHH, DIFC)
FPHH(3)=FPHH(3)-(DIFC*(TNPO-TN)/DELT)*(NDIF+GAMMA*(1-NDIF))
DO 21 J=1, NR
FPHH(J)=FPHH(J)-DU*(PNPO(J)-PN(J))
PN(J)=PN(J)-DELT*(1./((1.+(L-1)/(2*NR-3)))*(FPHH(J)
*(1.+(L-1)/(NR-1.5))-FPHH(J)))
21 CONTINUE
PN(5)=PN(5)-DELT*(PRESH-PRESH)*DELT(2,L)
RETURN
END

C***** END MID *****
C
C***** BEGIN PLUSW *****
SUBROUTINE PLUSW(L)
IMPLICIT DOUBLE PRECISION(A-H,O-Z)
COMMON/COM1/ DELT(3,3), GAMMA, NR, DELT, DLT, DELX, ABCM, XULFO
COMMON/COM2/ AN(10000), IN, JM, KM, IMMO, JMMO, NQ
COMMON/COM3/ PN(5), PNPO(5), FPHH(5), F(5)
COMMON/COM4/ FNPO(5), FPHH(5), FB(50), OMEGA(50), PRES, PRES, PRES, PRES,
1 PRES, NR, NR
COMMON/DIF/NDIF
COMMON/COM5/PNWIG(5)
COMMON/LOAD/PULSE, SPULSE, SURFP
DIMENSION FWIG(5), PPHH(5)
GO TO (1,2), L
1 CONTINUE
DO 20 J=1, NR
PNWIG(J)=PN(J)
20 CONTINUE
PNWIG(4)=PNWIG(4)
PC=0.5*(PN(3)+PNWIG(3))
CALL FLUX(L, PNWIG, FWIG, PRES, PC)
CALL HOT(PN, TN)
TWIG=TN
TWID=0.5*(TWIG+TN)
CALL DIFCO(PNWIG, TWID, DIFC)
CALL FLUX(L, PN, F, PRES, PC)
SURFP=PRES
DO 21 J=1, NR
PPH(J)=0.5*(PN(J)+PNWIG(J)-DELT*(F(J)-FWIG(J)))
21 CONTINUE
PC=0.
CALL FLUX(L, PPHH, FPHH, PRES, PC)
FPHH(3)=FPHH(3)-(DIFC*(TN-TWIG)/DELT)*(NDIF+GAMMA*(NDIF-1))
RETURN

```

```

2 CONTINUE
SUM=0.0
DO 10 I=4,NM
SUM=SUM+DABS(PMPO(I)-PN(I))
10 CONTINUE
PC=0.5*(PN(3)+PNIG(3))
CALL FLUX(L,PN,F,PRES,PC)
CALL FLUX(L,PMPO,FNPO,PRES,PC)
DO 22 J=1,NM
PPMH(J)=0.5*(PN(J)+PMPO(J)-2.*DELTX*FNPO(J))
22 CONTINUE
PPMH(S)=PPMH(S)-0.5*DELTX*(PRES-PRES)
DU=SUM/PPMH(1)
PC=PPMH(2)
CALL FLUX(L,PPMH,F,PPMH,PRESH,PC)
DO 23 J=1,NM
FPMH(J)=FPPMH(J)-DU*(PMPO(J)-PN(J))
FPMH(J)=FPMH(J)
23 CONTINUE
RETURN
END
C***** END PLUSW *****
C***** BEGIN PLUSX *****
SUBROUTINE PLUSX(FB,OMEGA,PRESH,PRES)
IMPLICIT DOUBLE PRECISION(A-H,O-Z)
COMMON/COM1/ DELT(3,3),GAMM,NM,DELTX,DLT,DELX,ASCH,XULFO
COMMON/COM2/ AN(10000),IN,IM,NM,IMMO,GAMM,NQ
COMMON/COM3/ PN(S),PMPO(S),FPMH(S),F(S)
COMMON/DIF/NDIF
COMMON/LOAD/PULSE,SPULSE,SURFP
DIMENSION PMIG(S),FVIG(S)
IF(FB.LE.1.)GO TO 22
CALL PLUSW(1)
EL=9.9D+10
RHOO=2.70
VO=5.0D+5
CTV=EL/DLOG(RHOO*VO+OMEGA/FB)
OMEGA=EL*CTV
FBO=FB/OMEGA
PMIG(1)=FBO/DSORT(GAMM+CTV)
PMIG(2)=PMIG(1)
PMIG(3)=FBO*DSORT(GAMM+CTV)*(1-NDIF)+0.5*FBO*DSORT(CTV/GAMM)
1*(GAMM+2.)=NDIF
PMIG(4)=FBO
PMIG(S)=0.
SURFP=SURFP+PMIG(S)*(1-NDIF)+GAMM*PMIG(2)*CTV*NDIF
PC=0.
CALL FLUX(1,PMIG,FVIG,PRES,PC)
DO 21 J=1,NM
FPMH(J)=FPMH(J)+FVIG(J)
21 CONTINUE
PRESH=PRESH+PMIG(S)
RETURN
22 CONTINUE
CALL PLUSW(1)
RETURN
END
C***** END PLUSX *****
C***** BEGIN FLUX *****
SUBROUTINE FLUX(L,P,F,PRES,PC)
IMPLICIT DOUBLE PRECISION(A-H,O-Z)
COMMON/COM1/ DELT(3,3),GAMM,NM,DELTX,DLT,DELX,ASCH,XULFO
COMMON/DIF/NDIF

```



```

DIMENSION P(5),F(5)
PINV=1.0/P(1)
ERG=0.
DO 10 J=4,NM
  ERG=ERG+P(J)**2
10 CONTINUE
ERG=0.5*PINV*ERG
PRES=P(3)*(1-NDIF)+GAMMA*(P(3)-ERG)*NDIF
V=P(1+3)*PINV
F(1)=P(3+L)
F(2)=P(2)*V
F(3)=V*(P(3)+GAMMA*PC*(1-NDIF)+PRES*NDIF)
DO 20 J=4,NM
  F(J)=P(J)*V+PRES*DELTA(J-3,L)*(2-L)
20 CONTINUE
RETURN
END

C***** END FLUX *****
C
C***** BEGIN LUX *****
SUBROUTINE LUX(J,K,FB)
IMPLICIT DOUBLE PRECISION(A-H,O-Z)
COMMON/COM1/ DELT(3,3),GAMMA,NM,DELTX,DLT,DELX,ABCM,XULFO
COMMON/COM2/ AN(1000),IM,JM,KM,IMMO,JMNO,NQ
COMMON/ABSORB/E1,E12,G,THIRD,THRD3,ENDEP,EDEN(100,100)
COMMON/THEN/EN1,EN2,TN,TMPO
COMMON/DIF/NDIF
DIMENSION XULF(62),P(5)
ABF=4.05D-53
E=1.05D+23
ABCO=4.35D+2
PI=3.14159264
DELX3=DELX*DELX*DELX
VOL=DELX3*PI*(2+J-2)
IF(J.LE.1)VOL=0.25*DELX3*PI
IMPO=IM+1
XULF(IMPO)=XULFO+ENV(J)
DO 1 I=1,IM
  I=IMPO-I
  NS=NQ*(I-1+IM*(J-1))
  RH0=AN(I+NS)
  RH02=AN(2+NS)
  RH01=DABS(RH0-RH02)
  ABCC=ABCO+RH02
  T=AN(NS+6)
  RH01=RH01/EN1
  RH02=RH02/EN2
  RH0=RH01+RH02
  ANEL=ANE(T,RH01,RH02)
  EDEN(I,J)=ANEL
  IF(T.LE.0.) THEN
    ABCF=0.
  ELSE
    ABCF=ABF+ANEL*(ANEL/(T*DSORT(T)))
  ENDIF
  ABC=ABCC+ABCF
  IF(ABC.GE.ABCM) ABCM=ABC
  TEST=ABC*DELX
  IF(TEST.GE.87.) THEN
    FACTOR=1.6455D-38
  ELSE
    FACTOR=DEXP(-ABC*DELX)
  ENDIF
  XULF(I)=XULF(I+1)+FACTOR
  DE=(XULF(I+1)-XULF(I))/DELX*DLT

```

```

DE=DE-E*ABCFY:Y:DLTY
ENDEP=ENDEP+DE*VOL
AN(3+NS)=AN(3+NS)+DE*(GAMMO*(1-NDIF)+NDIF)
DO 3 L=1,NH
  P(L)=AN(L+NS)
  CONTINUE
CALL HUT(P,T)
AN(NS+8)=T
1 CONTINUE
FB=XULF(1)
RETURN
END

C***** END LUX *****
C
C***** BEGIN ANE *****
FUNCTION ANE(T,RH01,RH02)
IMPLICIT DOUBLE PRECISION(A-H,O-Z)
COMMON/ABSORB/E11,E12,G,THIRD,THRD3,ENDEP,EDEN(100,100)
IF(T.LE.0.) GOTO 2
RH0=RH01+RH02
S1=T*DSQRT(T)*DEXP(-E11/T)*G
S2=T*DSQRT(T)*DEXP(-E12/T)*G
A=S1+S2-RH01*S1-RH02*S2-THRD*(S1+S2)**2
IF(DABS(A)-1.) 3,3,4
4 CONTINUE
B=THRD3*(2*(S1+S2)**3-6*(S1+S2)*(S1+S2-RH01)*S1-RH02*S2)
  + -27.*RH0*S1*S2)
  A=-A
C=DSQRT(THRD3*A)*A
C=-0.5*B/C
IF(C-1.) 5,5,6
5 CONTINUE
CA=DABS(C)
CA=THRD*CA
CB=2.*DSQRT(THRD*A)
R1=CB*DCOS(CA)
ANE=R1-THRD*(S1+S2)
RETURN
3 CONTINUE
ANE=0.
RETURN
8 CONTINUE
C=1
GO TO 5
END

C***** END ANE *****
C
C***** BEGIN DIFCO *****
SUBROUTINE DIFCO(P,T,DIFC)
IMPLICIT DOUBLE PRECISION(A-H,O-Z)
COMMON/DIF/NDIF
DIMENSION P(5)
COMMON/CUM/DELT(3,3),GAMMO,NH,DELTX,DLT,DELX,ABCH,XULFO
IF(T.LE.0.) THEN
  DIFC=0.
ELSE
  RH0=P(1)
  RH02=P(2)
  RH01=DABS(RH0-RH02)
  RH01=1./RH0
  VELSQ=0.
  DO 2 J=1,NH
    VELSQ=VELSQ+P(J)**2
  CONTINUE
  VELSQ=0.5*RH01*VELSQ

```

```

PRES=P(3)*(1-NDIF)+GAMMO*(P(3)-VELSQ)*NDIF
CALL TCOND(PRES,T,DK)
DIFC=DK
ENDIF
RETURN
END
C**** END DIFCO ****
C*****
      BEGIN TCOND *****
      SUBROUTINE TCOND(P,T,DK)
      IMPLICIT DOUBLE PRECISION(A-H,O-Z)
      TP=T/1.38045D-13
      IF(T) 1,1,2
      DK=0.
      RETURN
      IF(TP.LE.3.) THEN
      DK=(-.08935+.19645*TP)*3.0308D+20
      ELSE
      DK=(.5.8226+.8.2413*TP-.4099*TP**3+.02098*TP**5-.16.1749*
      +DSORT(TP))*3.0308D+20
      ENDIF
      RETURN
      END
      C*****
      C**** BEGIN HOT *****
      SUBROUTINE HOT(P,T)
      IMPLICIT DOUBLE PRECISION (A-H,O-Z)
      COMMON/CON1/DELT(3,3),GAMMO,NM,DELT,DLT,DELX,ABCM,XULFO
      COMMON/DIF/NDIF
      DIMENSION P(5)
      RHO=P(1)
      RHO2=P(2)
      RHO1=DABS(RHO-RHO2)
      RHO1=1./RHO
      VELSQ=0.
      DO 2 J=4,NM
      VELSQ=VELSQ+P(J)**2
      CONTINUE
      VELSQ=0.5*NH01*VELSQ
      EN=P(3)*(1-NDIF)+GAMMO*(P(3)-VELSQ)*NDIF
      TG=EN*EN1*EN2/(RHO2*EN1+RHO1*EN2)
      TG=TG/1.38045D-18
      IF(TG.LE.3000.) THEN
      T=TG*1.38045D-18
      ELSE
      PHI=.5878+(RHO2*EN1)/(RHO1*EN2)
      PHI2=PHI**2+.4.D+12*EN*EN1/RHO1
      T=.8.D-13*(DSORT(PHI2)-PHI)
      ENDIF
      CALL GAM(T,EN,GA)
      GAMMO=GA-1.
      RETURN
      END
      C**** END HOT *****
      C*****
      C***** BEGIN GAM *****
      SUBROUTINE GAM(TP,P,Q)
      IMPLICIT DOUBLE PRECISION(A-H,O-Z)
      T=TP/1.38045D-13
      IF(T) 1,1,2
      Q=1.287
      RETURN
      IF(T.LE.3.) THEN

```

G=1.4254-.0783*T

ELSE
G=1.18525+.009917*T
ENDIF
RETURN
END

C***** END GAM *****

C***** BEGIN ENDF *****
SUBROUTINE ENDF(NDIF)
IMPLICIT DOUBLE PRECISION(A-H,O-Z)
COMMON/COM1/ DELT(3,3), GAMMO,NM, DELTX, DLT, DELX, ARCH, XULFO
COMMON/COM2/ AN(1000), IM, JM, KM, LMMO, JMMO, NM
IF(NDIF)1,1,2

1 K=1
DO 3 J=1,IM
DO 5 J=1,JM
NS=NQ*(1-1+IM*(J-1))
VSQ=0.
DO 4 NP=4,NM
VSQ=VSQ+AN(NP+NS)**2
CONTINUE
AN(3+NS)=AN(3+NS)/GAMMO+O.S*VSQ/AN(1+NS)

5 CONTINUE
3 CONTINUE
NDIF=1
2 CONTINUE
RETURN
END

C***** END ENDF *****

C***** BEGIN ENV *****
FUNCTION ENV(J)
IMPLICIT DOUBLE PRECISION (A-H,O-Z)
COMMON/COM1/DELT(3,3), GAMMO,NM, DELTX, DLT, DELX, ARCH, XULFO
COMMON/TEST/XULFX
R=(J-1)*DELT
A=3.2184+XULFX*1.D-13
B=A*R**2
IF(B.GE.100.) THEN
ENV=0.
ELSE
ENV=DEXP(-B)
ENDIF
RETURN
END

C***** END ENV *****

C***** BEGIN SHAPE *****
FUNCTION SHAPE(T)
IMPLICIT DOUBLE PRECISION(A-H,O-Z)
T=T/1.D-8
IF(T.EQ.0.) THEN
S=0.
ELSE
IF(T.GT.0..AND.T.LE.1.5) THEN
S=.07329+1.8879*T-1.2480*T**2+.2845*T**3
ELSE
IF(T.GT.1.5 AND T.LE.3.) THEN
S=.8483+.1785*T-.05188*T**2
ELSE
IF(T.GT.3..AND.T.LE.8.) THEN
S=1.5577-.2599*T+.01508*T**2
ELSE
IF(T.GT.8..AND.T.LE.28.73) THEN

S=8432-0251

```
ELSE  
  S=0.  
  ENDIF  
ENDIF  
ENDIF  
ENDIF  
T-T+1.0-8  
SHAPE=S  
RETURN  
END
```

Listing of Variables in HYDRO

<u>Variable</u>	<u>Definition</u>	<u>Units</u>
A(ANE)	Constant used in finding electron number density	-
A(ENV)	Constant used in defining spatial variation of a Gaussian beam	1/cm ²
ABC	Total absorption coefficient	1/cm
ABCC	"Cold" absorption coefficient	1/cm
ABCF	Free-free absorption coefficient	1/cm
ABCM	Maximum absorption coefficient in mesh	1/cm
ABCO	Constant used in finding ABCC	cm ² /gm
ABF	Constant used in finding ABCF	-
AJ	Area of J th radial cell	cm ²
ALF	Factor used in forward/backward differencing	-
AN	Array of hydrodynamic quantities	-
ANE	Electron number density	1/cm ³
ANEL	Electron number density	1/cm ³
B(MHD)	Factor used in forward/backward differencing	-
B(ANE)	Constant used in finding electron number density	-
B(ENV)	Exponent in exp(B) for a Gaussian beam	-
C	Cosine ϕ , used in finding electron number density	-
CA	Cos ⁻¹ ϕ , as defined above	-
CB	Constant used in finding electron number density	-
CF1	Space-interval pressure correction factor	-

<u>Variable</u>	<u>Definition</u>	<u>Units</u>
CF2	Time-interval pressure correction factor	-
CHEW	Depth of laser-induced target vaporization	cm
CTV	Product of specific heat and vaporization temperature for target material	erg/gm
DE	Energy radiated away from cell during time, Δt	erg
DELP	$(p_{i+1} - p_i)/p_i$, used in forward/backward differencing	-
DELT	Kronecker delta	-
DELTX	$\Delta t / \Delta x$	sec/cm
DELX	Δx	cm
DELX3	$(\Delta x)^3$	cm ³
DIFC	Thermal conductivity	cal/cm/sec/K
DIMP	Impulse over the j^{th} radial cell	dyne-sec
DK	DIFC	
DLT	Δt	sec
DU	Artificial diffusion coefficient	-
E(CRNT)	Mass specific energy	erg/gm
E(LUX)	Constant used in finding DE	cm/sec
EDEN	Electron number density	1/cm ³
EI1	Ionization potential of air	erg
EI2	Ionization potential of target vapor	erg
EL	Latent heat of vaporization of target material	erg/gm
EM	Maximum mass specific energy in mesh	erg/gm

<u>Variable</u>	<u>Definition</u>	<u>Units</u>
EM1	Molecular mass of air	gm
EM2	Molecular mass of target vapor	gm
EN(HYDRO)	Initial energy density/pressure in mesh	erg/cm ³
EN(HOT)	Pressure	erg/cm ³
ENDEP	Energy deposited in mesh	erg
ENFAC	Factor used to determine whether EN(HYDRO) is pressure or energy density	-
ENV	Ratio of laser flux at radius, r, to laser flux at center of beam	-
ERG	$\rho v^2/2$	erg/cm ³
F	Flux of hydrodynamic quantities in cell n,t	-
FACTOR	$\text{Exp}(-ABC \Delta x)$	-
FB	Laser flux incident on surface	erg/cm ² /sec
FBO	$\text{FB}/(\text{EL} + \text{CTV})$	-
FNPO	Flux of hydrodynamic quantities in cell (n + 1),t	-
FPHMH	Flux of hydrodynamic quantities in cell (n-1/2), (t+1/2)	-
FPHPH	Flux of hydrodynamic quantities in cell (n+1/2), (t+1/2)	-
FWIG	Flux of hydrodynamic quantities in "zeroth" cell	-
G	Constant used in finding electron number density	-
GA	Ratio of specific heats, γ	-
GAMMO	$\gamma - 1$	-
I	Index associated with axial direction	-

<u>Variable</u>	<u>Definition</u>	<u>Units</u>
II	Index defining spatial position from front to back of mesh	-
IM	I defining maximum axial position	-
IMMO	IM - 1	-
IMPO	IM + 1	-
J	Index associated with radial direction	-
JM	J defining maximum radial position	-
JMMO	JM - 1	-
NAT	Variable which controls amount of output	-
NB	Index defining radius at which laser radiation is effectively zero	-
NCYCLE	Number of time steps taken	-
NDIF	Variable which determines whether energy density/pressure is differenced	-
NM	Index defining dimensionality of code	-
NQ	Number of hydrodynamic quantities computed	-
NR	Variable defining radial position in the mesh	-
NS	Index defining cell position	-
OMEGA	EL + CTV	erg/gm
P(PRINS)	Energy density/pressure	erg/cm ³
P(LUX)	Hydrodynamic quantities	-
PC	Pressure at cell center	erg/cm ³
PHI	Factor used in iterative process to find temperature	-
PHI2	Factor used in iterative process to find temperature	-

<u>Variable</u>	<u>Definition</u>	<u>Units</u>
PI	π	-
PINV	$1/\rho$	cm ³ /gm
PN	Hydrodynamic quantities in cell n	-
PNPO	Hydrodynamic quantities in cell (n+1)	-
PNP2	Pressure in cell (n+2)	-
PNWIG	Hydrodynamic quantities in "zeroth" cell	-
PO	Ambient pressure	erg/cm ³
PHMH	Hydrodynamic quantities	erg/cm ³
PPHPH	Hydrodynamic quantities in cell (n-1/2), (t+1/2)	erg/cm ³
PRES	Pressure in cell n	erg/cm ³
PRESMH	Pressure in cell (n-1/2), (t+1/2)	erg/cm ³
PRESP	Pressure in cell n+1	erg/cm ³
PRESPH	Pressure in cell (n+1/2), (t+1/2)	erg/cm ³
PULSE	Total impulse over surface	dyne-sec
R	Radius from center of beam	cm
R1	Root in cubic equation for finding electron number density	1/cm ³
RHO	Total density	gm/cm ³
RHOI	1/RHO	cm ³ /gm
RHOO	Target density	gm/cm ³
RHOOI	1/RHOO	cm ³ /gm
RHO1	Density of air	gm/cm ³
RHO2	Density of target vapor	gm/cm ³
S	Ratio of laser flux at time, t, to laser flux at time, zero	-

<u>Variable</u>	<u>Definition</u>	<u>Units</u>
S1	Ratio of ionization rate to recombination rate for air	-
S2	Ratio of ionization rate to recombination rate for target vapor	-
SHAPE	Same as S, given above	
SPULSE	Impulse over irradiated area	dyne-sec
SURFP	Surface pressure	erg/cm ³
T	Temperature	erg
T(GAM)	Temperature/1000	K
TEST	ABC Δx	-
TG	"Guessed" temperature/1000 for iterative process to find temperature	K
THIRD	1/3	-
THRDX3	1/27	-
TIME	Time	sec
TMID	Temperature at cell center	erg
TN	Temperature in cell n	erg
TNPO	Temperature in cell n+1	erg
TOTE	Total energy in mesh	erg
TP	Temperature/1000	K
TPHPH	Temperature in cell (n+1/2), (t+1/2)	erg
TQUIT	Time for calculations to stop	sec
TWIG	Temperature in "zeroth" cell	erg
V	Velocity component	cm/sec
VELSQ	$\rho v^2/2$	erg/cm ³
VO	Speed of sound in target material	cm/sec

<u>Variable</u>	<u>Definition</u>	<u>Units</u>
VSQ	Same as VELSQ	
XULFO	Laser flux at time, t	erg/cm ² /sec
XULFX	Laser flux at time, zero	erg/cm ² /sec

Appendix C

Listing of Convection Heat Transfer Code

```

PROGRAM HEAT
IMPLICIT DOUBLE PRECISION(A-H,O-Z)
DIMENSION QDOT(31,12),AN(10000),FB(50),CHEW(50),R(31)
OPEN(UNIT=7,FILE='DAT2IN')
OPEN(UNIT=8,FILE='HOTFIL')
OPEN(UNIT=9,FILE='QPLT')
OPEN(UNIT=10,FILE='INFILE')
REWIND 7
REWIND 8
REWIND 9
REWIND 10
DATA A1,A2,A3,A4,A5,A6,A7,A8,A9,A10,A11,A12,A13,A14,A15/
+ .121,-.02123,.1003,-.0001123,.36,-.03339,.03363,
+ -.0002449,.15,.2597,-.009815,.00009259,1.9724,
+ -.0001257,3.D-9/
READ(7,100,END=101) TQUIT,IM,JM,KM,NM,NDIF,XULFX,DELX
100 FORMAT(D7.2,3I3,2I1,D7.1,F3.2)
101 NMAX=240
DO 1 J=1,JM
  R(J)=(J-1)*DELX
  FB(J)=0.
  CHEW(J)=0.
1 CONTINUE
ABAR=.95D+5
NQ=6
NB=7
96 NCYCLE=0
NTIME=0
98 NTIME=NTIME+1
IF(NCYCLE.GT.NMAX.OR.NTIME.GT.13) GOTO 99
READ(10,299) IIN,JIN
299 FORMAT(2I2)
READ(8,250) TIME,NCYCLE,DLT,NDIF
250 FORMAT(1X,D16.10,1X,I4,D16.10,1X,I1)
READ(8,251) ABCM,XULFO,PULSE,SPULSE,TOTE,ENDEP
251 FORMAT(1X,6(D16.10,1X))
READ(8,252) (FB(I),I=1,NB)
READ(8,252) (CHEW(I),I=1,NB)
252 FORMAT(1X,7(D16.10,1X))
DO 63 I=1,IM
  DO 62 J=1,JM
    NS=NQ+(I-1+IM*(J-1))
    READ(8,251) AN(NS+1),AN(NS+2),AN(NS+3),
+ AN(NS+4),AN(NS+5),AN(NS+6)
62 CONTINUE
63 CONTINUE
IF(NCYCLE.EQ.0) GOTO 98
L=NTIME-1
DO 61 J=1,JIN
  NS=NQ+(IIN-1+IM*(J-1))
  T=AN(NS+6)/1.38054D-13

```

```

      UE=AN(NS+5)/AN(NS+1)
      VSQ=0.
      DO 60 NP=1,NM
        VSQ=VSQ+AN(NS+NP) **2
60    CONTINUE
      VSQ=.5*VSQ/AN(NS+1)
      IF(T) 5,5,6
5     GAMMA=.387
      GOTO 7
6     IF(T.LE.3.) THEN
          GAMMA=.4254-.0768*T
        ELSE
          GAMMA=.16525+.009917*T
        ENDIF
7     P=AN(NS+3)*(1-NDIF)+GAMMA*NDIF*(AN(NS+3)-VSQ)
      C=A1+A2*T+A3*T**2+A4*T**3
      EREF=.5*(1000.*C+121.)+2200.*R(J)**2
      TREF=A13*EREF+A14*EREF**2+A15*EREF**3
      A=A5+A6*TREF+A7*TREF**2+A8*TREF**3
      B=A9+A10*TREF+A11*TREF**2+A12*TREF**3
      RHOREF=3.484D-7*P/TREF*.001
      QDOT(J,L)=(A)**.6*(B)**-.1*(C-.121)
      QDOT(J,L)=1.01D+5*DSQRT(RHOREF)*QDOT(J,L)
61    CONTINUE
      DO 58 J=JIN+1,JM
        QDOT(J,L)=0.
58    CONTINUE
      GOTO 98
99    NTIME=NTIME-9
      DO 50 J=1,JM
        WRITE(9,*) R(J),QDOT(J,1),I=1,NTIME
50    CONTINUE
      CLOSE(7)
      CLOSE(8)
      CLOSE(9)
      CLOSE(10)
      STOP
      END

```


Appendix D

Listing of Vapor Condensation Code

```

PROGRAM VAP
IMPLICIT DOUBLE PRECISION(A-H,O-Z)
DIMENSION AN(1000), QDOT(31,12), FB(50), CHEW(50), R(31), F1(31,12)
OPEN(UNIT=7, FILE='DAT2IN')
OPEN(UNIT=8, FILE='VAPFIL')
OPEN(UNIT=9, FILE='VAPPLT')
OPEN(UNIT=10, FILE='NASPLT')
REWIND 7
REWIND 8
REWIND 9
REWIND 10
READ(7,100,END=101) TQUIT,IN,UM,KM,MM,NDIF,XULFX,DELX
FORMAT(D7.2,3F3.2,F7.1,D7.1,F3.2)
100 101
NMAX=240
DO 1 J=1,JM
  R(J)=(J-1)*DELX
  FB(J)=0.
  CHEW(J)=0.
1  CONTINUE
  NQ=6
  NB=7
  NCYCLE=0
  NTIME=0
  NTIME=NTIME+1
  IF(NCYCLE.GT.NMAX.ON.NTIME.GT.13) GOTO 99
  READ(8,250) TIME,NCYCLE,DLT,NDIF
  FORMAT(1X,D16.10,1X,D16.10,1X,11)
  READ(8,251) ARCH,XULFO,PULSE,SPULSE,TOTE,ENDEP
  251  FORMAT(1X,8(D16.10,1X))
  READ(8,252) (FB(I),I=1,NB)
  READ(8,252) (CHEW(I),I=1,NB)
  252  FORMAT(1X,7(D16.10,1X))
  DO 63 I=1,IN
    DO 62 J=1,JM
      NS=NQ*(I-1)+IN*(J-1)
      READ(9,251,END=200) AN(NS+1),AN(NS+2),AN(NS+3),AN(NS+4),
        AN(NS+5),AN(NS+6)
      62  CONTINUE
      63  CONTINUE
      200  IF(NCYCLE.EQ.0) GOTO 98
      L=NTIME-1
      DO 61 J=1,JM
        SUM1=0.
        SUM2=0.
        IN=1
        DO 60 I=1,IN
          NS=NQ*(I-1)+IN*(J-1)
          T=AN(NS+6)/1.38045D-16
          RNDV=AN(NS+2)
          P2=4.316D+9*RNDV*T+1.5+6.833D+13*RNDV*DSQRT(T)
          P2=P2+D-12
          PO=700.3*RNDV*DSQRT(T)
          UZ=AN(NS+4)/AN(NS+1)
          TEST=(6.1727D+6*T)/2.
          TEST=DSQRT(TEST)
          IF(UZ.GE.TEST) THEN
            PO=0.
            P2=0.
          ENDIF
          SUM1=SUM1+PO
          SUM2=SUM2+P2
        60  CONTINUE
        QDOT(J,L)=SUM2
        F1(J,L)=SUM1
      98  CONTINUE
    99  CONTINUE
  END

```

```

81 CONTINUE
GOTO 98
NTIME=NTIME-2
DO 50 J=1,JM
  WRITE(9,300) R(J), (QDOT(J,I), I=1,NTIME)
  WRITE(10,300) R(J), (P1(J,I), I=1,NTIME)
  FORMAT(1X,D8.3,1X,12(D8.4,1X))
CONTINUE
CLOSE(7)
CLOSE(8)
CLOSE(9)
CLOSE(10)
STOP
END
300
50

```

Bibliography

1. Hall, R. B. et al. "An Investigation of Laser-Supported Detonation Waves," AFWL-TR-73-28, Air Force Weapons Laboratory, Kirtland AFB, NM, June 1973.
2. Hall, R. B. et al. "Laser Beam Target Interaction, Vol. II, AFWL-TR-75-342, Vol. 2, Air Force Weapons Laboratory, Kirtland AFB, NM, July 1976.
3. Jumper, E. J. "Enhanced Thermal coupling By Repetitively-Pulsed Lasers," Laser Digest, Summer 1976. AFWL-TR-76-229, Air Force Weapons Laboratory, Kirtland AFB, NM, January 1977.
4. Stamm, M. R. and P. E. Nielsen. "Thermal Coupling In Multiply-Pulsed Laser-Target Interactions," Laser Digest. Spring 1974, AFWL-TR-74-100, Air Force Weapons Laboratory, Kirtland AFB, NM, May 1974.
5. Rudder, R. R. and R. L. Carlson. "Material Response to Repetitively Pulsed 10.6-Micron Laser Radiation," Laser Digest, Spring 1974 AFWL-TR-74-100, Air Force Weapons Laboratory, Kirtland AFB, NM, May 1974.
6. Gilbert, R. G. and R. L. Carlson. A Comparative Experimental Study of Material Interaction for Repetitively Pulsed and Continuous Wave CO₂ Lasers, AFWL-TR-72-168, Air Force Weapons Laboratory, Kirtland AFB, NM, November, 1972.
7. Stamm, M. R., et al. "Radiative Coupling in Laser-Target Interactions," Laser Digest, AFWL-TR-74-241, Air Force Weapons Laboratory, Kirtland AFB, NM, Summer 1974.
8. Jumper, E. J. and J. P. Jackson, "Two-Dimensional Calculations of Thermal Enhanced Coupling By a Repetitively-Pulsed Laser," Laser Digest, Fall 1974, AFWL-TR-74-344, Air Force Weapons Laboratory, Kirtland AFB, NM, January 1975.
9. Same as reference 3.
10. Jumper, E. J. and J. P. Jackson, "Two-Dimensional Effects on Enhanced Thermal Coupling by a Repetitively-Pulsed Laser: Vapor Condensation," Laser Digest, Spring 1975, AFWL-TR-75-140, Air Force Weapons Laboratory, Kirtland Air Force Base, NM, May 1975.

11. Nielsen, P. E., AFWL-TR-75-117, Air Force Weapons Laboratory, Kirtland AFB, NM, 1975.
12. Ready, John F. Effects of High-Power Laser Radiation, Academic Press, New York, 1971.
13. Book, Stephen A. Statistics, Basic Techniques for Solving Applied Problems, McGraw-Hill New York 1977.
14. Richtmyer, R. D. and K. W. Morton, Difference Methods for Initial Value Problems, Interscience Publishers, New York, 1967.
15. Vincenti, Walter G. and Charles H. Kruger, Jr., Introduction to Physical Gas Dynamics, Wiley and Sons, New York, 1965.
16. Anisimov, et.al. "Effect of Powerful Light flux on Metals, "Soviet Physics - Technical Physics 11, 945, 1967.
17. Zeldovich, Ya. B. and Yu. P. Raizer, Physics of Shock Waves and High-Temperature Hydrodynamic Phenomena, Academic Press, N.Y., 1966.
18. Shapiro, A. H., The Dynamics and Thermodynamics of Compressible Fluid Flow, Vol. I, Ronald Press, New York, 1953.
19. Schlichting, Dr. Hermann, (Fourth Edition), Boundary Layer Theory, McGraw-Hill, New York, 1960.
20. Hornbeck, Robert W., Numerical Methods, Quantum Publishers, New York 1975.
21. Holman, J. P. (Fifth Edition), Heat Transfer, McGraw-Hill, New York, 1981.
22. Eckert, E. R. G., "Survey of Boundary Layer Heat Transfer at High Velocities and High Temperature," WADC Technical Report 59-624, Wright Air Development Center. April 1960.
23. Schwirzke, F. "Unipolar Arcing, a Basic Laser Damage Mechanism." Naval Postgraduate School, Monterey, CA.
24. Jackson, J. P. Private Communication. KAMAN Sciences Corp., Colorado Springs, CO. September 1984.

25. Jackson, J. P. and E. J. Jumper, "Mechanisms of Enhanced Coupling by a Pulsed Laser," Laser Digest, Summer 1975, AFWL-TR-75-229, Air Force Weapons Laboratory, Kirtland Air Force Base, NM, October 1975.
26. Levine, J.D. and E. P. Gyftopoulos, "Absorbtion Physics of Metals Partially Covered by Metallic Particles. II Desorption Rates of Atoms and Ions," Surface Science 1, 1964.
27. Dawson, John M. "On the Production of Plasma by Giant Pulse Lasers," The Physics of Fluids, Vol. 7, Number 7, July 1964.
28. Jumper, E. J., "Implications of Applying a Global Energy Balance to Laser-Supported and Chemical Detonation Waves." Physics of Fluids, Vol. 27, Number 9, September, 1984.
29. Hansen, Frederich C. "Approximations for the Thermodynamic and Transport Properties of High-Temperature Air," NASA-TR-R-50,
30. Reynolds, William C. and H. C. Perkins, Engineering Thermodynamics, McGraw-Hill, New York, 1977.

Vita

First Lieutenant Jerry R. Couick was born on 7 September 1958 in Monroe, North Carolina. He graduated from High School in Monroe, North Carolina, in 1976 and attended High Point College, High Point, North Carolina, from which he received the degree of Bachelor of Science in Mathematics in May 1980. Upon graduation, he was employed as a computer programmer/analyst at Duke Power Company, Charlotte, North Carolina, until he entered the United States Air Force Officer Training School in May 1982. Upon graduation from Officer Training School, he received a commission in the United States Air Force and entered the Air force Institute of Technology degree conversion program, from which he received the degree of Bachelor of Science in Aeronautical Engineering in March 1984. Upon graduation from this program, he entered the Air Force Institute of Technology graduate school.

Permanent Address: Route 2, Box 223B
Waxhaw, NC 28173

UNCLASSIFIED

SECURITY CLASSIFICATION OF THIS PAGE

REPORT DOCUMENTATION PAGE

1a. REPORT SECURITY CLASSIFICATION UNCLASSIFIED			1b. RESTRICTIVE MARKINGS		
2a. SECURITY CLASSIFICATION AUTHORITY			3. DISTRIBUTION/AVAILABILITY OF REPORT Approved for public release; distribution unlimited		
2b. DECLASSIFICATION/DOWNGRADING SCHEDULE					
4. PERFORMING ORGANIZATION REPORT NUMBER(S) AFIT/GAE/AA/85M-3			5. MONITORING ORGANIZATION REPORT NUMBER(S)		
6a. NAME OF PERFORMING ORGANIZATION School of Engineering		6b. OFFICE SYMBOL (If applicable) AFIT/EN		7a. NAME OF MONITORING ORGANIZATION	
6c. ADDRESS (City, State and ZIP Code) Air Force Institute of Technology Wright-Patterson AFB, Ohio 45433			7b. ADDRESS (City, State and ZIP Code)		
8a. NAME OF FUNDING/SPONSORING ORGANIZATION		8b. OFFICE SYMBOL (If applicable)		9. PROCUREMENT INSTRUMENT IDENTIFICATION NUMBER	
8c. ADDRESS (City, State and ZIP Code)			10. SOURCE OF FUNDING NOS.		
11. TITLE (Include Security Classification) See box 19			PROGRAM ELEMENT NO.		TASK NO.
			PROJECT NO.		WORK UNIT NO.
12. PERSONAL AUTHOR(S) Jerry R. Couick, B.S. 1st Lt, USAF					
13a. TYPE OF REPORT MS Thesis		13b. TIME COVERED FROM _____ TO _____		14. DATE OF REPORT (Yr., Mo., Day) 1985 March	
15. PAGE COUNT 147					
16. SUPPLEMENTARY NOTATION					
17. COSATI CODES			18. SUBJECT TERMS (Continue on reverse if necessary and identify by block number)		
FIELD	GROUP	SUB. GR.	Thermal Coupling, Convection Heat Transfer, Vapor Condensation, Plasma Radiation		
20	13				
19. ABSTRACT (Continue on reverse if necessary and identify by block number)					
<p>Title: ENHANCED THERMAL COUPLING BY A REPETITIVELY PULSED LASER</p> <p>Thesis Advisor: Eric J. Jumper, Lt Col, USAF</p> <p>Approved for public release: IAW AFR 190-1/ 124181 1. For Research and Professional Development Air Force Institute of Technology (AFIT) Wright-Patterson AFB OH 45433</p>					
20. DISTRIBUTION/AVAILABILITY OF ABSTRACT UNCLASSIFIED/UNLIMITED <input checked="" type="checkbox"/> SAME AS RPT. <input type="checkbox"/> DTIC USERS <input type="checkbox"/>			21. ABSTRACT SECURITY CLASSIFICATION UNCLASSIFIED		
22a. NAME OF RESPONSIBLE INDIVIDUAL Eric J. Jumper, Lt Col, USAF			22b. TELEPHONE NUMBER (Include Area Code) 513-255-3517		22c. OFFICE SYMBOL AFIT/ENY

The purpose of this study was to determine the effects of convection heat transfer, target vapor condensation, and radiation heat transfer on the observed enhanced thermal coupling of a pulsed laser to an Aluminum target. The need for this study is to develop a base from which the laser parameters needed to most efficiently couple laser energy to a metal target may be predicted.

An attempt was made to analytically duplicate a set of experimental data in which enhanced thermal coupling was observed. Analytical relations were developed to compute the heat flux, into the surface of an Aluminum species, due to convection heat transfer, target vapor condensation, and plasma reradiation. From these relations, the most significant coupling mechanism was identified to be vapor condensation. Convection heat transfer was found to have a less significant effect on enhanced coupling, and plasma reradiation was found to be negligible. The calculations were performed by a three-dimensional Lagrangian hydrocode. The results of this work are somewhat inconclusive due to the extensive computer resources used by the hydrocode; however, the relations presented here do seem to give promising results. The work should be continued to investigate the effects of laser and target parameters on enhanced thermal coupling.

END

FILMED

6-85

DTIC